THE HONG KONG
POLYTECHNIC UNIVERSITY
香港理工大學
Pao Yue-kong Library
包玉剛圖書館

Copyright Undertaking

This thesis is protected by copyright, with all rights reserved.

By reading and using the thesis, the reader understands and agrees to the following terms:

1. The reader will abide by the rules and legal ordinances governing copyright regarding the use of the thesis.
2. The reader will use the thesis for the purpose of research or private study only and not for distribution or further reproduction or any other purpose.
3. The reader agrees to indemnify and hold the University harmless from and against any loss, damage, cost, liability or expenses arising from copyright infringement or unauthorized usage.

If you have reasons to believe that any materials in this thesis are deemed not suitable to be distributed in this form, or a copyright owner having difficulty with the material being included in our database, please contact lbsys@polyu.edu.hk providing details. The Library will look into your claim and consider taking remedial action upon receipt of the written requests.

Pao Yue-kong Library, The Hong Kong Polytechnic University, Hung Hom, Kowloon, Hong Kong

http://www.lib.polyu.edu.hk

Effects of Ultrasound Field on the Catalytic Kinetics of Stem Bromelain

Sze Chui Ling

M. Phil.

The Hong Kong Polytechnic University
2002

Pao Yue-kong Library
PolyU • Hong Kong

Abstract of thesis entitled

Effects of Ultrasound Field on the Catalytic Kinetics of Stem Bromelain

submitted by

Sze Chui Ling

for the degree of Master of Philosophy

at the Hong Kong Polytechnic University in October 2001.

Abstract

Previous researches have revealed that the catalytic ability of a protease appeared to be the best if it is in its native state as presented in the plant cells of origin. However, when the protease is extracted and applied to industrial uses, its proteolytic activity is much lower than that in the plant cells. This may be explained by two major aspects. First, the conformation of the enzyme including active site may be altered during extraction and hence the kinetic parameters are changed. Second, the environment for the optimum activity of the enzyme may be disturbed by the changes in type of substrates, pH and existence of other chemical substances.

The purpose of this research is to study the effects of ultrasound field on the conformation and the catalytic activity of a typical protease, the stem bromelain (SB). The objectives include (1) to ascertain the influence of ultrasound field on the conformation and the catalytic efficiency of SB; (2) to study the effective mechanisms of ultrasound field based on the experimental findings; (3) to propose a hypothesis model for incorporating the effect of ultrasound into the enzyme kinetics.

The experimental results show that the SB activity was first promoted at low ultrasound power (amplitude setting <5%) and then gradually decreased at a higher power level (amplitude setting >20%). When the treatment time was less than 5min, the effect of ultrasound on SB activities were similar for the power level at amplitude settings of 30% and 40%. It was also found that at amplitude setting of 5% for 5min, the maximum catalytic activity of SB was about 25% higher than that without treatment, while its activity reduced by about 40% at amplitude setting of 40%. At low ultrasound power, acoustic microstreaming was favored that facilitates the diffusion of substrate to or product away from the active site of the enzyme. It also enhances the 'lock and key' mechanism during enzyme and substrate binding. Thus, the increase in the catalytic efficiency was double at amplitude range of 5% to 10%. At higher ultrasound power,

vigorous cavitation was created in the sonicated medium that caused enzyme denaturation resulting in a 50% decrease in the catalytic efficiency at amplitude setting of 40%.

The analytic results indicated that ultrasound induced only a minor conformational change of SB without varying its secondary structures. The major change was caused by the interaction between exposed aromatic residues, which were originally buried in the inner zone of the protein, and their surrounding environments. That altered only the tertiary structure. Moreover, ultrasound also reduced the surface hydrophobicity of SB. These effects were more severe at high ultrasound amplitude (40%). As a result, the activity and catalytic efficiency was dramatically decreased.

A hypothesis model for incorporating the effect of ultrasound into the enzyme kinetics was proposed by introducing the concept of activation power. This kinetic model suggested that the activation energy for the catalytic reaction could be replaced by the activation power and treatment time. A critical power zone should exist for a given system. Ultrasound activation and inactivation may occur before and after this zone respectively.

Table of Content

Acknowledgement	i
Abbreviation	ii
List of Figures	iv
List of Tables	vi
Chapter 1. Introduction	**1**
Chapter 2. Literature Reviews	**4**
2.1 Ultrasound	4
2.1.1 Background	4
2.1.2 Mechanisms	5
2.1.2.1 Cavitation	5
(a) Stable cavitation	6
(b) Transient cavitation	6
2.1.2.2 Mass transfer	7
2.1.3 Biological Effects	7
2.1.3.1 Enzyme Activation	8
2.1.3.2 Enzyme Inactivation	9
2.1.4 Application	10
2.2 Stem Bromelain	10
2.2.1 Background	10
2.2.2. Categorization	11
2.2.3 Forms	12
2.2.4 Physical Properties	13
2.2.5 Chemical Properties	14
2.2.6 Kinetic Properties	17
2.2.6.1 Kinetic Parameters	19
2.2.7 Inhibition	22
2.2.8 Thermal Denaturation	22
2.3 Protein Conformation	23
2.3.1 Background	23
2.3.2 Types of Forces	24
2.3.3 Three-dimensional Structures	24
2.3.4 Protein Denaturation	25

2.3.5 Analytical Methods of Protein Conformation 25
2.3.5.1 Gel Electrophoresis 26
2.3.5.2 Spectroscopy Methods 28
(a) UV Absorption Spectrum 28
(b) Fluorescence Emission Spectrum 29
(c) CD Spectrum 31
2.3.5.3 Surface Hydrophobicity Test 33
2.4 Kinetic Model 34

Chapter 3. Materials and Methods **37**
3.1 Materials 37
3.1.1 SB Preparation 37
3.1.2 CLN Preparation 38
3.1.3 Assay Buffer Preparation 38
3.1.4 Ultrasonic Equipment 38
3.2 Methods 39
3.2.1 Determination of Ultrasound Power in the Experimental Media 39
3.2.2 Ultrasound Treatment on SB-catalyzed Reaction 42
3.2.3 Effect of Mechanical Stirring on SB-catalyzed Reaction 43
3.2.4 Effect of Ultrasound Pretreated SB or CLN on SB Activity 44
3.2.5 Ultrasound, Thermal and Chemical Treatment on SB 45
3.2.6 Analysis of SB Conformation 46
3.2.6.1 Ultraviolet Absorption Spectrometry 46
3.2.6.2 Fluorescence Emission Spectrometry 47
3.2.6.3 Circular Dichroism Spectrometry 47
3.2.6.4 Surface Hydrophobicity Test 48
3.2.7 Data Analysis 49

Chapter 4. Results and Interpretation **50**
4.1 Ultrasound Power in the Experimental Media 50
4.2 Ultrasound Treatment on SB-catalyzed Reaction 54
4.2.1 Effect of ultrasound power and treatment time on SB-catalyzed reaction at various CLN concentrations 54
4.2.1.1 Effect of Ultrasound Power 54
4.2.1.2 Effect of Treatment Time 55
4.2.2 Effect of CLN concentration on SB-catalyzed reaction at various ultrasound settings 58
4.2.3 Effect of ultrasound on the kinetic parameters of SB 60

4.3 Effect of Mechanical Stirring on SB-catalyzed Reaction 62
4.4 Effect of Ultrasound Pretreated SB or CLN on SB Activity 63
4.5 Analysis of SB Conformation 64
4.5.1 Ultraviolet Absorption Spectrometry 64
4.5.2 Fluorescence Emission Spectrometry 67
4.5.3 Circular Dichroism Spectrometry 70
4.5.4 Surface Hydrophobicity Test 75

Chapter 5. Discussion **78**
5.1 Ultrasound Mechanisms 78
5.1.1 Chemical Effect 78
5.1.2 Effect of Mechanical Mixing 80
5.1.3 Effect of Cavitation 80
5.1.3.1 Low Ultrasound Power 81
5.1.3.2 High Ultrasound Power 82
5.2 Conformational Change of SB under Ultrasound Treatment 83
5.2.1 Ultraviolet Absorption Spectrometry 83
5.2.2 Fluorescence Emission Spectrometry 84
5.2.3 Circular Dichroism Spectrometry 85
5.2.4 Surface Hydrophobicity Test 86
5.3 Kinetic Model 86

Chapter 6. Conclusion and Recommendation **92**
6.1 Conclusion 92
6.2 Recommendation 94

References **95**

Appendix A **100**
Calculation of Ultrasound Power in the Experimental Media

Appendix B **102**
Calculation of Proteolytic Activity of SB

Appendix C **103**
Calculation of CD Spectrum

Appendix D 106

Calculation of Surface Hydrophobicity (SH)

Appendix D 107

Calculation of Kinetic Parameters of SB

Acknowledgment

I am extremely grateful to my chief supervisor Dr. H. H. Liang for his invaluable advice and professional criticism on this research. He discusses with me patiently and provides meaningful suggestions for changes. From the bottom of my heart, I would like to say that I have ever met such a good teacher before.

I am greatly indebted to the following individuals in the laboratory: Carrie Chau, Christine Kwok, Edith Lai, Hongbing Liu, Huihua Huang, Kong Wong, Litong Lin, Michael Ng, Phoeby Wong, Reiko Cheung and Shiyi Ou. Their advice and encouragement help me to carry out the experiments more smoothly.

I would like to express my gratitude to those technicians in both biological and chemical laboratories especially Cecilia Chan, Mabel Yau, Manlong Wong, Mr. Au, Mr. Cheung, and Yuiwah Shiu for their assistances and advice in the laboratory.

I must thank my parents, my family members, my best friend Christina Chu and her husband, and my fiancé Neil Yam for their endless love, patience, support and encouragement.

Abbreviation

A	A	activity at time t_r
	A_a	activity with ultrasound treatment
	A_o	activity at time t_r=0 or activity without ultrasound treatment
	ANS	1-anilinonaphthalene-8-sulphonate
C	CD	circular dichroism
	CLN	*p*-nitrophenyl N^{α}-benzyloxycarbonyl-L-lysinate
	c_p	heat capacity
	L-Cys	L-cysteine
	CYS	cysteine residues
D	$[\theta]$	molar ellipticity
	DTNB	5,5'-dithiobis-(2-nitrobenzoic acid)
E	E	free enzyme
	E_a	activation energy
	E_t	total enzyme
	E_1	energy absorbed by the media
	E_2	energy lost from the media
	E_3	energy delivered from the probe
	E-64	trans-epoxysuccinyl-L-leucylamido-(4-guanidino)butane
	EDTA	ethylenediamine tetraacetic acid
	ES_1	enzyme-substrate complex
	ES_2	acylated enzyme intermediate
F	FB	fruit bromelain
	FI	fluorescent intensity
G	GmHCl	guanidine hydrochloride
H	H_o	hydrophobicity index
K	k	rate constant at a given temperature
	k_o	rate constant at a reference temperature
	k_{cat}	catalytic constant or turnover number

	k_i	inactivation rate constant
	K_m	Michaelis-Menten constant or dissociation constant
	k_{cat}/K_m	catalytic efficiency
	KCl	potassium chloride
M	m	mass of the substance
P	p	pressure
	pI	isoelectric point
	P_a	alcohol or ammonium ion
	P_b	acylamino acid
	P_t	activation power of the system
	$P_{t,ac}$	activation power of the system during activation
	$P_{t,in}$	activation power of the system during inactivation
	Phe	phenylalanine
	PAGE	Polyacrylamide gel electrophoresis
R	R	gas constant
S	S	substrate
	S-S	disulfide bridge or linkage
	SB	stem bromelain
	SDS	sodium dodecyl sulfate
	S.E.	standard error
	SH	surface hydrophobicity
T	T	temperature
	t or t_t	treatment time
	t_r	reaction time
	TCA	trichloroacetic acid
	TNB	5-thiobis-(2-nitrobenzoic acid)
	Trp	tryptophan
	Tyr	tyrosine
U	UV	ultraviolet
V	ΔV^*	activation volume
	V_o	initial velocity
	V_{max}	maximum initial velocity

W	w/v	weight/volume
	WL	wavelength

List of Figures

Figure 2.1 The CD spectra of stem bromelain, SB1 (—) and SB2 (---).

Figure 2.2 The amino acid sequence of SB.

Figure 2.3 The oxidized and reduced states of SB.

Figure 2.4 The amino acid sequence of SB near the reactive cysteine residues (CYS).

Figure 2.5 The hydrolytic mechanism of SB.

Figure 2.6 Native gel electrophoresis of bovine pancreatic trypsin inhibitior: (a) native form; (b) reduced and unfolded form.

Figure 2.7 UV absorption spectra of native (—) and unfolded (---) RNase T1.

Figure 2.8 Fluorescence emission spectra of native (–) and unfolded (--) RNase T1 at the excitation wavelength of 295nm (copied from Schmid, 1997).

Figure 2.9 The classes of protein secondary structures and their associated CD spectra: α-helix (—), antiparallel β-sheet (–––), parallel β-sheet (···), turn type (---), and left-handed extended 3_1-helix (+++).

Figure 2.10 CD spectra of native (—) and unfolded (---) RNase A (a) in the aromatic region; (b) in the amide region (copied from Schmid, 1997).

Figure 3.1 The experimental set up of ultrasound treatment.

Figure 4.1 Different energy in the experimental media (a) energy absorbed, E_1; (b) energy lost, E_2; (c) energy delivered, E_3.

Figure 4.2 Effect of ultrasound power on SB activity at different CLN concentrations (a) 60μM; (b) 480μM and (c) 960μM.

Figure 4.3 Effect of treatment time on SB activity in different CLN concentrations (a) 60μM; (b) 480μM and (c) 960μM.

Figure 4.4 Effect of CLN concentration on SB activity in various ultrasound power at different treatment times (a) 1min; (b) 5min and (c) 10min.

Figure 4.5 Effect of mechanical stirring speed on SB activity for 5min of stirring time.

Figure 4.6 The SB activities when SB or CLN (480μM) were pretreated with ultrasound for various times.

Figure 4.7 UV absorption spectra of SB for different amplitude settings and treatment time at (a) 5min and (b) 10min.

Figure 4.8 Fluorescence emission spectra of SB for different amplitude settings and treatment time at (a) 5min and (b) 10min.

Figure 4.9 CD spectra of SB in near-UV region for different amplitude settings and treatment time at (a) 5min and (b) 10min.

Figure 4.10 CD spectra of SB in far-UV region for different amplitude settings and treatment time at (a) 5min and (b) 10min.

Figure 4.11 Change in surface hydrophobicity of SB for different amplitude settings and treatment time at (a) 5min and (b) 10min.

Figure 5.1 Product of the activation power (P_t) and treatment time (Δt_t) found during ultrasound treatment.

List of Tables

Table 2.1 Amino acid composition of stem bromelain.

Table 4.1 Ultrasound power delivered at different amplitude settings.

Table 4.2 Kinetic parameters of SB at different amplitudes settings and treatment times.

Table 4.3 Peak absorbance and corresponding wavelength for UV absorption.

Table 4.4 Peak FI and corresponding wavelength for fluorescence emission

Table 4.5 Contents of secondary structures of SB in the far-UV regions of CD spectra.

Table 5.1 Activation power (P_t) found during ultrasound treatment at 960μM CLN.

Table 5.2 Product of the Activation power (P_t) and treatment time (Δt_t) found during ultrasound treatment.

Chapter 1. Introduction

Stem bromelain (SB, EC 3.4.22.4) is a proteolytic enzyme originating in pineapple, *Ananas comosus*, which is particularly abundant in the stem tissue. This protease can catalyze the hydrolysis of protein peptide linkages. With its catalysis, protein molecule can be hydrolyzed to peptone, proteose and peptide rapidly, and converted into amino acid eventually. It has been widely applied in the food industry including chill-proofing of beer, tenderizing of meat, and production of protein hydrolysates (Budavari *et al.*, 1989; Burdock, 1997). In cheese production, proteases are usually added to accelerate ripening that accompanies with casein hydrolysis; however, bitterness is evolved under such circumstance. The addition of SB can improve the flavor of cheese because the hydrophobic hydrolysate was produced together with a lot of high molecular weight peptides, which are not involved in flavor production (Gallagher *et al.*, 1994).

In the past decades, researches have revealed that the catalytic ability of a protease appeared to be the best if it is in its native state as presented in the plant cells. However, when the protease is extracted and applied to industrial uses, its proteolytic activity is much lower than that in the plant cells. This may be explained by two major aspects. First, the conformation of the enzyme including active site may be altered during

extraction and hence the kinetic parameters are changed. Second, the environment needed for achieving the optimum activity of the enzyme may be disturbed by the changes of substrates in terms of types and concentrations, pH of the media, concentration of the metallic ions, and existence of other chemical substances.

Ultrasound is a kind of radiation with dual properties of wave and energy. Cavitation and vibration induced by ultrasound can facilitate a number of chemical and biochemical reactions. Ultrasound alters the structural and functional properties of both viable cells and enzymes (Mason *et al.*, 1996). The change in the activity of enzyme is in dual direction either activation or inactivation. It depends on a number of factors such as the characters of the ultrasound field (intensity and frequency), the processing parameters (temperature, pH, ionic concentration and presence of other chemicals), and the nature of enzyme and substrate.

SB as a typical plant protease was used to ascertain the influence of ultrasound field on its proteolytic properties. Two approaches are employed in the study: (1) the effect on enzyme-catalyzed reaction; and (2) the effect on enzyme only. Both the reaction rate and the conformational change of the enzyme are compared with those without ultrasound treatment.

The wide spread in the application of such a novel technology is still pending for the development of effective mechanism and modification of kinetic theory. The study can enrich the effect mechanism of ultrasound to enzyme kinetics. That will enhance the understanding on the conformational changes of enzyme molecules caused by ultrasound. Consequently, it will lead to a new, high efficient and economic way for strengthening the enzyme catalysis with foreign field, promote the development of enzyme theory, and give a new leap in the production industry with enzyme.

The purpose of this research is to study the effects of ultrasound field on the conformation and the catalytic activity of SB. The objectives include (1) to ascertain the influence of ultrasound field on the conformation and the catalytic efficiency of SB; (2) to study the effective mechanisms of ultrasound field based on the experimental findings; (3) to propose a hypothesis model for incorporating the effect of ultrasound into the enzyme kinetics.

Chapter 2. Literature Reviews

2.1 Ultrasound

2.1.1 Background

It is well known that ultrasound is widely adopted by most of the animals such as bats, dolphins and whales for probing location in the dark. Although humans are unable to hear ultrasound, they can still utilize it properly even in ice-age times. In ancient time, wolves with their inborn ultrasound hearing were tamed by human beings for hunting purpose. Nowadays, the application of ultrasound is more diverse, especially in the fields of engineering, physics, chemistry, medicine, microscopy and underwater detection, etc. (Wade, 2000).

In the late 1800s, Lord Rayleigh was the first to propose the basic theory of wave propagation in acoustics and optics. Later, Paul Langevin and his colleagues observed the phenomenon of cavitation under acoustic field. Besides, they also used piezoelectric transducers at resonance to obtain high ultrasonic intensity. This technique could be applied in submarine detection. In the 1920s, S.J. Sokolov changed the format of ultrasound application, from a large scale to a small scale, in which, some trivial structural inhomogeneities could be probed by ultrasound. On the whole, intensity was the major factor concerned by Langevin while Sokolov investigated both phase and amplitude (Atchley & Crum, 1988; Wade, 2000).

2.1.2 Mechanisms

Ultrasound consists of high-frequency acoustic waves of pressure and particle displacement which propagate through a medium (Miller *et al.*, 1996). The ultrasound in the megahertz range refers to the sound wave that is in high frequency and low energy form. The energy of low frequency ultrasound in the kilohertz range is high. There are two types of mechanisms: thermal and non-thermal. Although temperature is an important parameter in biotechnology, its increase is not the main determinant causing the positive effect of ultrasound. It is suggested to carry out the biotechnological processes in isothermal condition (Sinisterra, 1992). The non-thermal mechanisms include cavitation, acoustically induced streaming and radiation forces (Thomenius, 1993).

2.1.2.1 Cavitation

Cavitation is a typical phenomenon in non-thermal mechanisms of the ultrasound. According to Miller *et al.* (1996), it is defined as 'the interaction between an ultrasonic field in a liquid and a gaseous inclusion in the insonated medium'. It is evoked in the compression and expansion zones that are formed by transmitting the longitudinal waves from ultrasonic source into the liquid medium (Sala *et al.*, 1995). The other author, Suslick (1988) defined cavitation as the formation of gas bubbles (or cavities) in a liquid and occurs when the pressure within the liquid drops sufficiently lower than the vapor pressure of the liquid. There are two types of cavitation including transient and stable cavitation. Both of them have their unique characteristics on the behavior of gas bubbles.

(a) Stable cavitation

Stable cavitation involves regular oscillation of small bubbles without any collapsing. It always occurs in low ultrasound intensity. It can be developed to transient cavitation and vice versa. Under an ultrasonic field, those bubbles vibrate to induce the attachment of other bubbles that induce strong currents in the nearby region. This is called 'acoustic microstreaming'. It exerts shear stress to any objects in the medium. High shear forces cause lethal effect on living cells and enzymes (Frizzell, 1988; Sinisterra, 1992; Sala *et al.*, 1995).

(b) Transient cavitation

Transient cavitation refers to the stage that the size of bubbles varies rapidly and collapses eventually to generate very high pressures and temperatures to surroundings. These sudden rises in pressures and temperatures cause mechanical injury and free radicals formation respectively. Free radicals can induce carcinogen to animal cells and denature proteins. These bubbles are adhered and separated alternately in the compression and expansion cycles. If the liquid tensile strength is greater than the negative pressures, small bubbles are formed and hence become the nuclei of cavitation. This phenomenon occurs in high intensity of the ultrasound (Frizzell, 1988; Sinisterra, 1992; Sala *et al.*, 1995; Miller *et al.*, 1996).

2.1.2.2 Mass transfer

Low intensity ultrasound promotes liquid movement and hence mass transfer. This effect can be observed in 3 different zonal areas: the boundary layer, the cellular wall and membrane, and the cytosol. Acoustic microstreaming is a common phenomenon occurring near the boundary layer. It enhances transportation of substrate into or product away from the active site of the enzyme, so the turnover number of the enzyme is increased. Ultrasound can increase the diffusion rate through the artificial and biological membranes without damaging them. In cytosol, ultrasonic-induced intracellular microstreaming causes the rotation of organelles in both animal and plant cells, and eddying motions in the vacuoles of the plant cells. As a result, cell metabolism is increased (Sinisterra, 1992).

2.1.3 Biological Effects

Ultrasound alters the structural and functional properties of both viable cells and enzymes (Mason *et al.*, 1996). In living cells, cavitation causes cell disruption through breakdown of the cell membrane. Moreover, it also induces a change of the genetic materials inside cells such as breakdown of DNA strands and chromosomes, cell transformation, and mutation (Miller *et al.*, 1996). Since this study focuses on the effect of ultrasound on the enzyme, only the mechanisms of enzymes will be discussed here.

2.1.3.1 Enzyme Activation

Many researchers have reported that ultrasound can increase the rate of enzyme reaction when both enzyme and substrate were subjected to sonication. The increase is more favorable in immobilized enzymes. Ishimori *et al.* (1981) found that the proteolytic activity of the immobilized α-chymotrysin on agarose gel was increased at 20kHz and 10-15W ultrasound treatments. The activity was double in comparison with that without ultrasound. Vulfson *et al.* (1991) demonstrated that ultrasound irradiation could enhance the reaction rate of subtilisin-catalyzed interesterifiation in organic solvent about 50%. It was believed that ultrasound prevented water molecules accumulating on the enzyme surface that allows more active sites available for substrate binding. In 1996, Sakakibara *et al.* pointed out that the activation or inhibition of the enzyme reaction by ultrasound depended on substrate concentration. In low sucrose concentration (0.005 to 0.05M), the rate of invertase hydrolysis increased after ultrasound treatment. The value of V_{max} remained unchanged, but the value of K_m reduced to the half value of the one without any treatment (Sakakibara *et al.*, 1996). Similar results were reported by Barton *et al.* in the same year. Invertase activity is enhanced at lower sucrose concentration with ultrasound treatment. This phenomenon is held for starch hydrolysis either by α-amylase or glucoamylase.

There are limited studies focusing on the effect of ultrasound on enzyme itself. The enzymatic activity cannot be enhanced by ultrasound in the absence of substrate. The activity was determined by pre-treating the enzyme first and then substrate was added. After treating β-amylase itself by ultrasound, its activity was similar to that without any treatment (Azhar & Hamdy, 1979). Sakakibara *et al.* (1996) reported that invertase was

stable under ultrasound for 2-hour irradiation as the relative activity was kept at 100%. Their results also showed that enzyme was relatively stable under ultrasound rather than thermal treatment.

2.1.3.2 Enzyme Inactivation

Ultrasound is widely used to terminate enzymatic reaction or inhibit enzyme activity. The goal seems to be achieved more easily by ultrasound and heat treatment synergistically. The heat-resistant pectinmethylesterase of orange was effectively inactivated by manothermosonication. The inactivation rates were 25-fold increase in buffer and over 400-fold increase in orange juice (Vercent *et al*, 1999). Lopez *et al.* (1994) also demonstrated the inactivation of peroxidase, lipoxygenase, and polyphenol oxidase by manothermosonication. The effect was more pronounced in large ultrasonic wave amplitude but no effect was found for different pressures. The inactivation of peroxidase diminished with increasing ultrasonic power, but it decreased faster at low ultrasonic frequency (De Gennaro *et al.*, 1999). The soybean trypsin inhibitors were significantly inactivated by treatment temperature and ultrasonic power at 80°C and 150W respectively. In such treatment, about 73% reduction of trypsin activity was observed (Liang *et al.*, 1998). At high substrate concentration (0.02 to 1.0M), the rate of sucrose hydrolysis by invertase decreased after ultrasound treatment. The rate was reduced as ultrasonic intensity increased (Sakakibara *et al.*, 1996).

2.1.4 Application

Enzyme activation or inactivation by ultrasound can be applied for different purposes. This strongly depends on the role of a particular enzyme whether it is useful in this process or not. For example, hydrolase is commonly added in hydrolysis of starch, glycogen and sucrose. Ultrasound irradiation can be introduced to accelerate the enzymatic reaction rate and hence the production of sugar syrups is increased. Moreover, the activity of immobilized enzymes such as α-chymotrysin and subtilisin can also be enhanced by ultrasound treatment. On the other hand, it is appreciable to inactivate those enzymes that produce off-color and off-flavor in fresh vegetable and fruit juices. Peroxidases, lipoxygenases and polyphenol oxidases are easily deactivated by manothermosonication. The effect of inactivation is more obvious for those heat-resistant enzymes such as pectinmethylesterase in orange. In soymilk, soybean trypsin inhibitors exert undesirable effects including growth depression and adenoma to the experimental animals after ingestion. The effects can be minimized by ultrasonic inactivation of the inhibitors.

2.2 Stem Bromelain

2.2.1 Background

In 1891, Marcano, a Venezuelan pharmacist, discovered the digestive function of pineapple fruit juice. That is the first digesting enzyme obtained from the pineapple plant. The term 'bromelin' is used to describe it according to the family name of the

pineapple plant '*Bromeliaceae*'. In 1953, Heinicke and Gortner found similar enzymes from the stem tissue of pineapple plants (Murachi, 1976). They found the stele (the central part) contained more enzymes than the cortex (the outer part). Since then, the term 'bromelain' has been defined as any protease from any member of *Bromeliaceae* (Omar *et al.*, 1978).

Bromelain is present in the stem, fruit, skin, stalk and leaves. It is mainly divided into SB and fruit bromelain (FB) based on their presences in the different organs of pineapple. SB, FB, ananain and comosain are four distinct cysteine proteinases found in the stem, while only SB and FB can be detected in pineapple fruits. SB and FB are present most abundantly in stem and fruit respectively (Rowan *et al.*, 1990).

2.2.2. Categorization

Both SB and FB are categorized as EC 3.4.22 by the International Enzyme Commission. They are considered to be endopeptidases or cysteine peptidases with cysteine in the active site. They are highly sensitive to oxidizing agents and can be inactivated by the later, as well as by metal ions or alkylating reagents. Therefore, they must be used in the presence of reducing agent (L-cysteine, L-Cys) and a chelating agent (ethylenediamine tetraacetic acid, EDTA) (Belitz & Grosch, 1999). A detailed comparison of the two appears in Yamada *et al.* (1976).

2.2.3 Forms

SB is a single enzyme that constructed by a single polypeptide chain. It exists in several forms that are called isoenzymes of SB. Some researchers reported that there are totally six different forms, but only the most abundant two have been studied. During purification, the one eluted first is designated as SB1, while the second is called SB2. More SB1 can be obtained from the crude stem extracts. Both of them are identical in molecular weight and catalytic properties. Moreover, their amino-terminal sequence (Val-Pro-Gln-), carboxyl end-group (glycine) and active site sequence (-Asn-Gln-Asn-Pro-Cys-Gly-Ala-CYS-) are identical. The similarity in their circular dichroism (CD) spectra indicates that there is little structural difference between them.

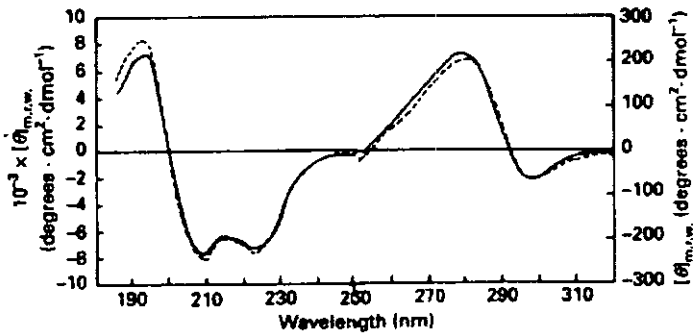

Figure 2.1 CD spectra of stem bromelain, SB1 (—) and SB2 (---) (Copied from Arroyo-Reyna *et al.*, 1994).

However, SB1 contains more glycine and alanine, and less tyrosine than SB2. In native gel electrophoresis, SB2 shows more basic character because it migrates slightly more towards the cathode than SB1 (Minami *et al.*, 1971; Takahashi *et al.*, 1973; Rowan *et al.*, 1990; Arroyo-Reyna *et al.*, 1994).

2.2.4 Physical Properties

SB is a basic protein with its isoelectric point (pI) at 9.55. Its absorption coefficient is 20.1, i.e. the absorbance of a 1% (w/v) solution of pure SB in a 1-cm cell at 280nm is 20.1 (Murachi, 1976). Such a high absorption coefficient is attributed to the high content of aromatic amino acid. Ritonja *et al.* (1989) reported that SB contains 14 tyrosyl and 5 tryptophyl residues per molecule. The ratio of tyrosine to tryptophan is 2.8.

Murachi (1976) reported that there were 19 tyrosyl residues in each SB molecule. These residues exist either in 'exposed' form or 'buried' form. The former refers to those residues that are freely accessible to the solvent; while the latter represents to others that can be accessible if they become ionizable or after denaturation. The researchers found that there are 9 exposed tyrosyl residues in the native SB. From the spectrophotometric titration curve, 4 different ionization stages can be observed in the process of increasing the pH of the solvent. In stage 1, nine exposed tyrosyl residues become ionizable at the pH range of 7 to10.3. The next stage involves ionization of 7 buried tyrosyl groups from pH 10.3 to pH 12. The degree of ionization in this stage is time-dependent. One more buried tyrosyl group is ionized rapidly in stage 3 which the

pH value is higher than 12. At the last stage, at pH 13.6 or higher, the remaining two residues are slowly ionized.

Different molecular weights of SB have been reported by different authors. The reported molecular weights are 28000 (Takahashi *et al.*, 1973), 33000 (Murachi, 1976), 23800 (Ritonja *et al.*, 1989) and 25400 (Arroyo-Reyna *et al.*, 1994), respectively. The variation may be attributed to various pineapple varieties, analytical methods and the abundance of isoenzymes existed.

Murachi (1976) found that the molar ellipticity [θ] of SB was –4200 and the α-helix content nearly 10%. However, different results were reported by Arroyo-Reyna *et al.* (1994). From the CD spectrum, the major secondary structure was α-helix, about 23%. The content of antiparallel β-sheet and turns were similar, about 18%. The lowest content was parallel β-sheet, about 5%. As a result, the spectrum is classified in the $\alpha + \beta$ protein class. Although the contents of all secondary structures are similar to those of papain and proteinase Ω, the CD spectrum of SB is predominantly different from either of them.

2.2.5 Chemical Properties

SB is a single polypeptide with 211 or 212 residues. Being a glycoprotein, it consists of D-mannose, L-fructose, D-xylose and two *N*-acetylglucosamine molecules, and 2.1% neutral sugars (Murachi, 1976). The carbohydrate is attached at residue 117 (aspartic acid) at which a glycosylated asparaginyl residue was detected (Ritonja *et al.*, 1989).

Table 2.1 Amino acid composition of stem bromelain (Ritonja *et al.*, 1989).

Amino acid	**No. of residues**	**Amino acid**	**No. of residues**
Ala	25	Leu	6
Arg	6	Lys	15
Asn	10	Met	3
Asp	8	Phe	6
Cys	7	Pro	11
Gln	7	Ser	17
Glu	9	Thr	9
Gly	22	Trp	5
His	1	Tyr	14
Ile	17	Val	14
		Total no. of residues	**212**

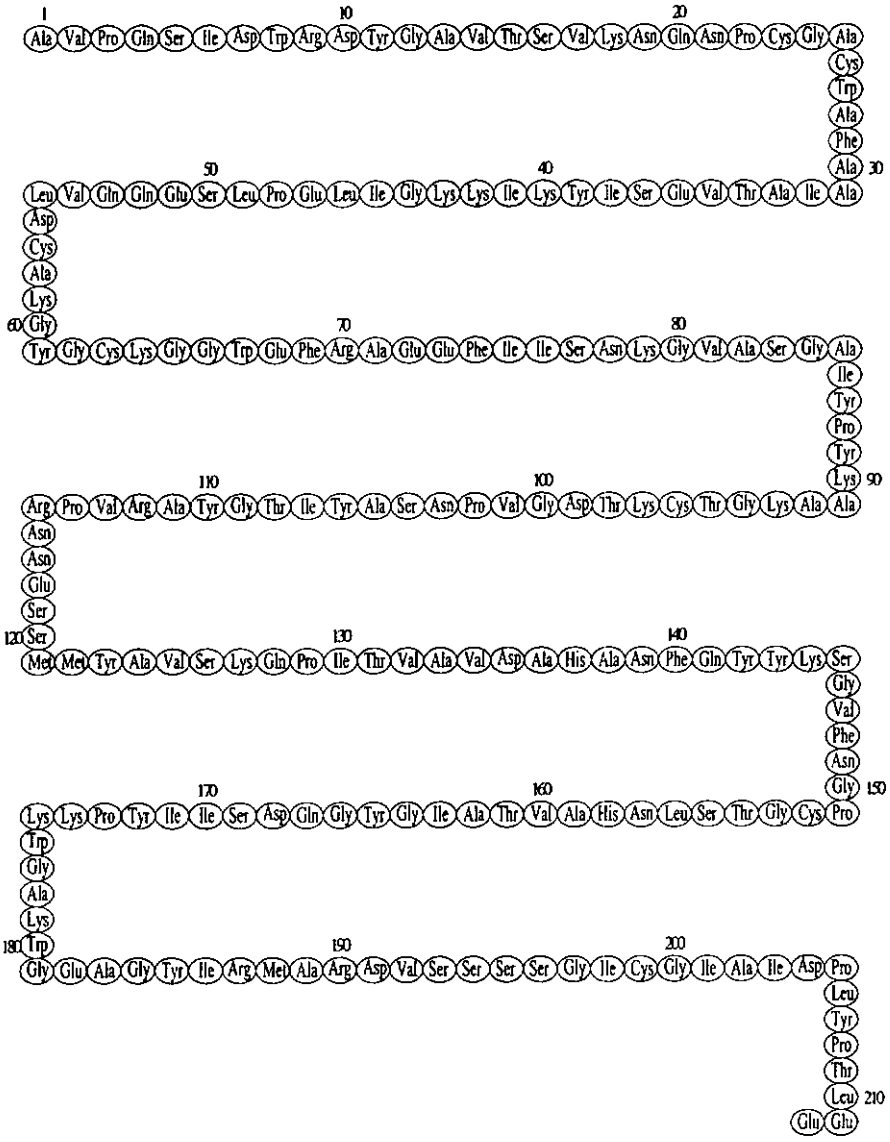

Figure 2.2 The amino acid sequence of SB (Ritonja *et al.*, 1989).

Seven cysteine residues are found in each SB molecule (Ritonja *et al.*, 1989). Takahashi *et al.* (1973) reported that there was a disulfide bond between the cysteine residues of serine chain. It also contains one sulfhydryl group and five disulfide linkages. The sulfhydryl group is essential for the proteolytic activity of SB (Murachi, 1976). Similar to other cysteine proteases, SB is inactivated when its sulfhydryl group is oxidized to form disulfide linkage (-S-S-). It is suggested that SB usually

interchanges within the oxidized and reduced states as shown in Figure 2.3. Rowan *et al.* (1990) found that the amino acid sequence around the active site is similar to papain (Figure 2.4).

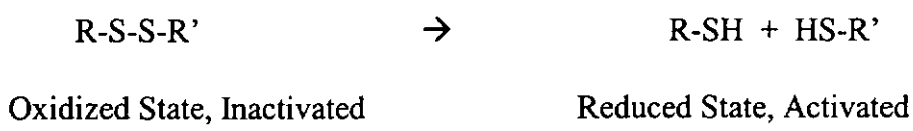

Figure 2.3 The oxidized and reduced states of SB.

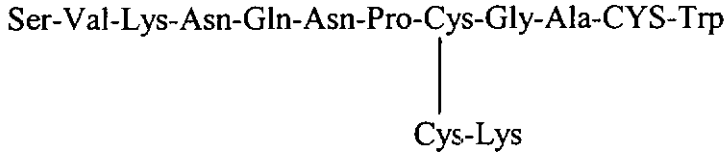

Figure 2.4 The amino acid sequence of SB near the reactive cysteine residues (CYS) (Copied from Takahashi *et al.*, 1973).

2.2.6 Kinetic Properties

SB is a protease which catalyses protein hydrolysis. Benzoylarginine esters, the artificial substrates, are more susceptible to hydrolysated by SB (Murachi, 1976). SB hydrolyzed the substrate with specific peptide chain of Lys-, Arg-, Phe-, Tyr-COOH (Jens, 1986).

Casein is commonly used as a substrate to test the effectiveness of proteolytic enzymes. When casein is used as a substrate, SB shows a quite broad range in the pH optima, ranging from pH 6 to 8 (Murachi, 1976).

Murachi (1976) assumed a three-step hydrolytic mechanism for SB (Figure 2.5). First, a free enzyme (E) binds with a substrate (S) molecule to form an initial enzyme-substrate complex (ES_1). The carbonyl carbon located at the scissile bond of the substrate acts as a nucleophile that attacks the thiolate anion of the Cys25. Then the complex is transformed into the acylated enzyme intermediate (ES_2), accompanied by the release of an alcohol or ammonium ion (P_a). The leaving group is evolved due to the protonation by the His159 imidazolium. Eventually, the intermediate is deacylated to yield acylamino acid (P_b) and free enzyme. The deacylation is initiated due to the nucleophilic attack of a water molecule assisted by His159 acting as base catalyst.

$$E + S \leftrightarrow ES_1 \rightarrow ES_2 \rightarrow E + P_b$$
$$+$$
$$P_a$$

Figure 2.5 The hydrolytic mechanism of SB (Zeffren & Hall, 1973; Murachi, 1976; Whitaker & Bender, 1965).

In the case of SB, the rate-determining step depends strongly on the type of the substrate being hydrolyzed. During the hydrolysis of ester, the second step is rate determining because the rate of acylation is greater than that of deacylation. The rate of deacylation is greater than that of acylation for amide or peptide, thus the last step becomes the rate-determining step.

2.2.6.1 Kinetic Parameters

The Michaelis-Menten equation states the quantitative relationship between the initial velocity V_o, the maximum initial velocity V_{max} and the initial substrate concentration [S]. The equation is shown as follows:

$$V_o = \frac{V_{max}[S]}{K_m + [S]}$$

where K_m is Michaelis-Menten constant.

When V_o is equal to the half of V_{max}, then the equation becomes

$$\frac{V_{max}}{2} = \frac{V_{max}[S]}{K_m + [S]}$$

By dividing to V_{max}, the equation becomes

$$\frac{1}{2} = \frac{[S]}{K_m + [S]}$$

All parameters V_o, V_{max} and [S] are related to the Michaelis-Menten constant or dissociation constant K_m which is equivalent to that substrate concentration at which V_o is equal to the half of V_{max}. It also represents the substrate affinity of an enzyme in the enzyme-substrate complex.

The Michaelis-Menten equation can be algebraically transformed into the Lineweave-Burk equation which is useful in practical determination of K_m and V_{max}. The

transformation is derived by taking the reciprocal of both sides of the Michaelis-Menten equation to give

$$\frac{1}{V_o} = \frac{K_m + [S]}{V_{\max}[S]}$$

Separating the components of the numerator on the right side of the equation gives

$$\frac{1}{V_o} = \frac{K_m}{V_{\max}[S]} + \frac{[S]}{V_{\max}[S]}$$

The above equation is then simplified to yield the Lineweaver-Burk equation:

$$\frac{1}{V_o} = \frac{K_m}{V_{\max}} \cdot \frac{1}{[S]} + \frac{1}{V_{\max}}$$

For enzymes obeying the Michaelis-Menten relationship, a plot of $1/V_o$ versus $1/[S]$ yields a straight line which will have a slope of K_m/V_{max}, a y-intercept of $1/V_{max}$, and a x-intercept of $-1/K_m$. The plot is called a Lineweaver-Burk plot that can determine V_{max} more precisely.

When the enzyme is saturated with substrate, the number of substrate molecules that can be converted to products by one enzyme molecule in a given period of time is defined as turnover number or catalytic constant, k_{cat}.

$$k_{cat} = \frac{V_{max}}{[E_t]}$$

The Michaelis-Menten equation becomes

$$V_o = \frac{k_{cat}[E_t][S]}{K_m + [S]}$$

Neither k_{cat} nor K_m is suitable to determine the catalytic efficiency of different enzymes. The constant k_{cat} is only useful to explain the properties of an enzyme when it is saturated with substrate. Moreover, it is not unique for an enzyme because two enzymes catalyzing different reactions may have the same turnover number. Without k_{cat}, the constant K_m is unsatisfied to explain the properties of an enzyme. When an enzyme is subjected to a very low concentration of the substrate, a lower value of K_m will be found in comparison to an enzyme surrounding by normally abundant of the substrate. Therefore, both constants of k_{cat} and K_m is useful to determine the catalytic efficiency of an enzyme. When $[S] << K_m$, the equation reduces to the form of

$$V_o = \frac{k_{cat}}{K_m}[E_t][S]$$

In that case, V_o depends on the concentration of $[E_t]$ and [S]. It follows a second-order rate law and the constant k_{cat}/K_m is a second-order rate constant. The constant is useful as it shows the properties and the reactions of free substrate and enzyme (Fersht, 1985; Lehninger *et al.*, 1993).

Yamada *et al.* (1976) reported that SB showed higher activity (K_m = 0.17M) than fruit bromelain in the hydrolysis of casein, but its specific activity was slightly lower about 6.86-units/mg proteins. Similar results were demonstrated by Omar *et al.* (1978) who tested SB activity on the basis of milk clotting property. The optimum pH for milk clotting activity of SB was about 3.8. This activity was inhibited by the presence of sodium chloride. Among those proteases obtained from the pineapple plant, only SB could hydrolyze the dibasic substrate Z-Arg-Arg-NH-Mec with K_m of 15.4μM and k_{cat} of 27.26s^{-1}. The ratio of k_{cat}/K_m was 1770 $mM^{-1} \cdot s^{-1}$ (Rowan *et al.*, 1990).

2.2.7 Inhibition

According to the similarity in amino acid sequence, SB is a member of the cysteine proteinase superfamily. Most of them in the superfamily are quickly irreversibly inhibited by trans-epoxysuccinyl-L-leucylamido-(4-guanidino)butane (E-64), and they are strongly inhibited by chicken cystatin and L-kininogen. On the other hand, SB is slowly inactivated by E-64 with inhibition constant of 678 $M^{-1} \cdot s^{-1}$ but it is difficult to inhibit with cystatin. Therefore, E-64 can be used as an active-site titrant for SB (Rowan *et al.*, 1988; Rowan *et al.*, 1990).

2.2.8 Thermal Denaturation

Arroyo-Reyna and Hernandez-Arana (1995) demonstrated that thermal denaturation of SB underwent a single two-state irreversible mechanism with first-order kinetics. The process that has involved transferring the unfolding state to the denatured state was the rate-determining step:

Native ↔ Unfolded → Denatured

This irreversibility can be accounted for the metastable characteristic of its native state. Hence, the unfolded state is unable to refold. The formation of the transition state is due to the breakdown of the stabilizing bonding in the native state.

2.3 Protein Conformation

2.3.1 Background

A conformation refers to the spatial arrangement of atoms in a protein. It also involves interconverting a structural state with other structural states by the covalent bonds. A protein contains numerous single bonds of which changing any one will alter the protein conformation. Proteins contain functional conformations in their native states (Lehninger *et al.*, 1993).

An enzyme is a kind of protein that acts as a reaction catalyst in the biological system. The functional property of the enzyme is tremendously determined by its three-dimensional structure in the native state. It is important to retain the native conformation of the enzyme as any alteration of it can either promote or inhibit the catalytic activity.

2.3.2 Types of Forces

There are two types of molecular forces governing the structural arrangement within a protein, namely covalent bonds and non-covalent forces.

The major covalent bond is the peptide bond which is formed by the condensation of the carboxyl group of an amino acid and the amino group of another, and eventually a water molecule is eliminated. Amino acid residues are attached to form polypeptide chains through the peptide bonds. Two adjacent cysteine residues, no matter their locations in the same or different polypeptide chains, can be oxidized to form a disulfide bridge (S-S). This linkage is useful to maintain the three-dimensional structure of a protein (Branden & Tooze, 1999).

The hydrophobic effect, ionic interactions, hydrogen bonds and van der Waals forces are four non-covalent forces found in a protein molecule. The forces interact with each other. They are participated in the processes of polypeptide folding, polypeptide association, and substrate or other molecule binding.

2.3.3 Three-dimensional Structures

In general, the three-dimensional structure of a protein can be categorized into four levels. Primary structure refers to the amino acid sequence in a polypeptide chain. It includes all the covalent peptide bonds such as disulfide bonds. Secondary structure is developed by regular spatial arrangement of adjacent amino acid residues in the polypeptide chain. The α-helix and β-strands are the most abundant structures found in

this level. They are stable due to the maximum of hydrogen bonding and the minimum of steric repulsion. The arrangement of all amino acid residues in the spaces within the chain forms the tertiary structure. A domain that is created in the folding chain provides specific substrate binding site in an enzyme. The quaternary structure contains several polypeptide chains or globular subunits joining together (Lehninger *et al.*, 1993; Branden & Tooze, 1999).

2.3.4 Protein Denaturation

Protein denaturation is a process that a protein totally losses its native three-dimensional structure. It is caused by heat, change of pH, and exposure to detergent, miscible organic solvents (e.g acetone or alcohol) and certain solutes (e.g. urea and guanidine hydrochloride). Different denaturing sources alter the different portions of the protein structure. It should be pointed out that no covalent bonds in the polypeptide chain are disrupted during this process. Heating breaks down the weak interaction such as ionic interaction. A change of the net charge on the protein can occur in extremely high or low pH, in which electrostatic repulsion was arisen and some hydrogen bonds was broken. The hydrophobic interactions stabilizing the core of globular protein can be disrupted by exposure to those denaturing agents including detergent, organic solvents and solutes (Lehninger *et al.*, 1993; Fersht, 1998).

2.3.5 Analytical Methods of Protein Conformation

X-ray crystallography is a powerful tool to determine the three-dimensional structure of a protein molecule because a strong and unique diffraction pattern evolves from a well-

ordered crystal. However, it is difficult to yield such well-ordered crystal from a large globular protein with irregular surface. Many large holes and channels are formed during crystallization that disturbs the diffraction pattern (Branden & Tooze, 1999). Therefore, other analytical methods should be adopted and their results should be combined in order to get a clear picture of conformational change in a protein molecule.

The analytical methods can be divided into several trends namely gel electrophoresis, optical spectroscopy, and immunochemical analysis etc. Each of them holds their own advantages and limitations. The one to be used is merely dependent on the degree of structural resolution required and the amount of protein obtained.

2.3.5.1 Gel Electrophoresis

Polyacrylamide gel electrophoresis (PAGE) with the detergent sodium dodecyl sulfate (SDS) is a common technique to estimate the molecular weight and the peptide pattern of a protein. On the other hand, the native gel without any denaturing agent can be used to determine the protein conformation. Moreover, the folding-unfolding mechanism of a protein can be studied by the gel with transverse gradients of denaturants.

Under an electric field, the mobility of a molecule through a gel is monitored by its net charge, size and shape. Greater in the net charge will let more electrostatic force exert on the molecule and hence its velocity increases. The native protein has greater net charge and size, so it moves faster. When the protein is reduced and unfolded, its electrophoretic mobility is decreased because of smaller net charge and size. The

method is simple and inexpensive. Only small amount of protein is needed (Goldenberg, 1997).

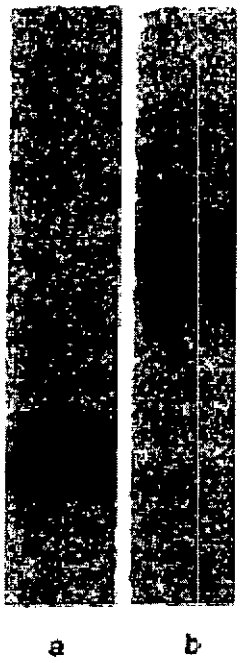

Figure 2.6 Native gel electrophoresis of bovine pancreatic trypsin inhibitor: (a) native form; (b) reduced and unfolded form (copied from Goldenberg, 1997).

SDS denatures the protein by coating it with uniform negative charges and constant charge-to-mass ratio. It also dissociates multimeric proteins into its subunits that can be identified through SDS-PAGE with reducing agent such as β-mercaptoethanol (Lodish *et al.*, 2000). According to Froment *et al.* (1998), they confirmed that ultrasound did not break the inter-monomeric disulphide bridge in dimmer and no monomer was produced. SB is a single polypeptide chain without any subunit; therefore, SB with minor conformational change under ultrasound is difficult to access via denaturing SDS-PAGE.

2.3.5.2 Spectroscopy Methods

Proteins possess inherent optical characteristics of light absorption and fluorescence emission in the ultraviolet (UV) region of the spectrum. In a protein molecule, peptide bonds, aromatic amino acids and disulfide bonds can absorb light, while merely the aromatic amino acids emit fluorescence (Schmid, 1997). The spectrums of UV absorption, fluorescence and near-UV CD provide information about the degree of exposure of the amino acid side-chain to solvent. On the other side, far-UV CD spectrum shows the folding and unfolding pattern of the peptide backbone (Owusu, 1992). The major advantage of these methods is non-destructive that the protein sample can be recovered for further analysis.

(a) UV Absorption Spectrum

Absorption is a process that energy from a photon transfers to a molecule. During absorption, the electrons of the molecule are boosted to higher energy level by light, i.e. from the ground state to an excited state. The absorbance of a protein molecule is contributed to light absorption of the electrons in the delocalized aromatic systems.

There are 3 types of aromatic residues participating in light absorption, namely tyrosine (Tyr), tryptophan (Trp) and phenylalanine (Phe). They have different absorption maxima, such as Trp at 280nm, Tyr at 275nm and Phe at 258nm. Disulfide bonds show little absorbance around 250nm.

In UV absorption spectrum, any change in protein structure can shift the absorption wavelength, alter the intensity of absorbance, and the width of the absorption band. Some of the aromatic residues that are originally buried in the hydrophobic core of the folded native protein will be exposed to the solvent during unfolding. A blue shift of the absorption spectrum can be observed (Schmid, 1997).

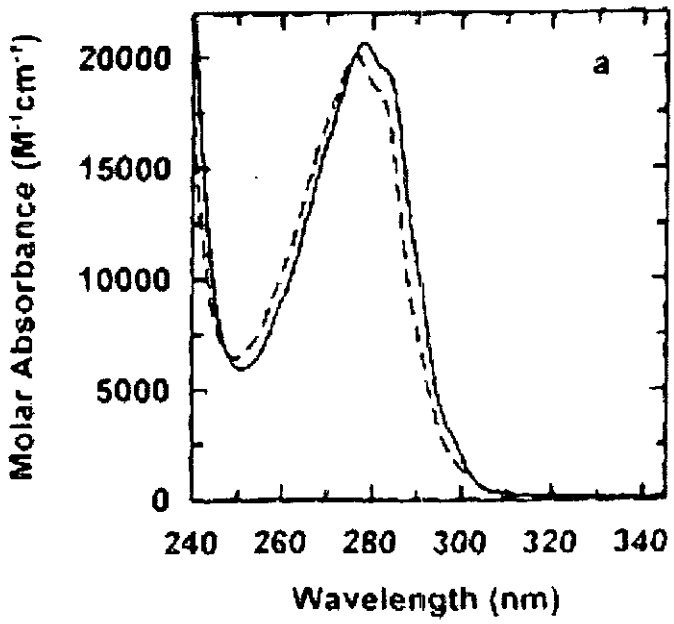

Figure 2.7 UV absorption spectra of native (—) and unfolded (---) RNase T1 (copied from Schmid, 1997).

(b) Fluorescence Emission Spectrum

After light absorption, an electron is excited and then returns to its ground state with fluorescence emission. Since non-radiative energy is lost during the excited state, the energy of light emission is less than of light absorption. That is the reason why fluorescence emission is observed in longer wavelength.

Unlike other biopolymers such as lipids and saccharides, proteins display their typical intrinsic fluorescence emission spectrum after light absorption. Phe, Tyr and Trp are three aromatic residues emitting fluorescence. Among them, Trp shows a strong emission spectrum because it shows higher quantum yield. As a result, the change of protein conformation can be easily detected by the emission spectrum of Trp (Lakowicz, 1999). Protein unfolding can be indicated by the shift of wavelength and the change of fluorescent intensity no matter it is increased or decreased. Trp residues, which are not freely accessible in a folded protein, usually show the maximum intensity at 320nm. When the protein is denatured by GmHCl, the fluorescent intensity is decreased obviously and the emission maximum is red-shifted to around 350nm (Schmid, 1997).

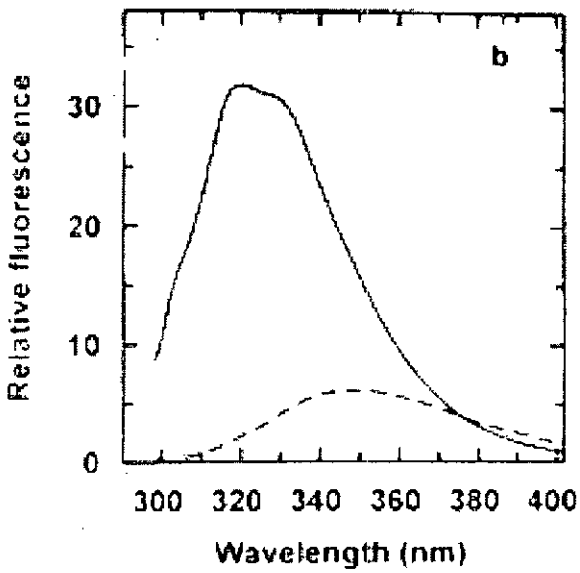

Figure 2.8 Fluorescence emission spectra of native (–) and unfolded (--) RNase T1 at the excitation wavelength of 295nm (copied from Schmid, 1997).

(c) CD Spectrum

Circular dichroism refers to a phenomenon of the absorption difference of left and right circularly polarized light by an optically active molecule. Similar to UV absorption and fluorescence emission spectra, Phe, Tyr and Trp are participating in light absorption. The positive CD value is the result of protein interacting with left circularly polarized light; while the negative value is due to the interaction between protein and right circularly light (Drake, 1994).

In amide or far-UV region (170-250nm), the peptide bonds of proteins absorb light that provides the information of protein secondary structures, especially α-helix. The α-helix structure displays a typical CD spectrum with a negative band from 210nm to 230nm. There are two negative maxima located at 222nm and 208nm within the band. The CD spectrum of β-sheet is characterized by a negative band at 216nm and a positive band at 195nm. The β-turn structure shows a weak negative band near 225nm, a strong positive band between 200nm and 205nm, and a strong negative band between 180nm and 190nm.

The CD signal in the aromatic or near-UV region (250-300nm) is contributed to majority of the aromatic side chains and minority of the disulfide bonds. It monitors the tertiary structure of a protein by giving the information of changing environment to the protein. Since the sign, magnitude and wavelength of the signal are strongly affected by the structure interacting with the electronic surrounding environment, it is difficult to interpret the results. But, the spectrum is useful as the native folded conformation can be distinguished correctly. In general, the number of aromatic residue increase will lead

a reduction in CD band (Bloemendal & Johnson, 1995; Schmid, 1997; Rodger & Ismail, 2000).

Conformational change of a protein can be precisely determined by the CD spectrum. It is because the unfolded protein shows zero magnitude in the aromatic region. Besides, the change in the contents of secondary structures can be calculated by the signal in the amide region (Schmid, 1997).

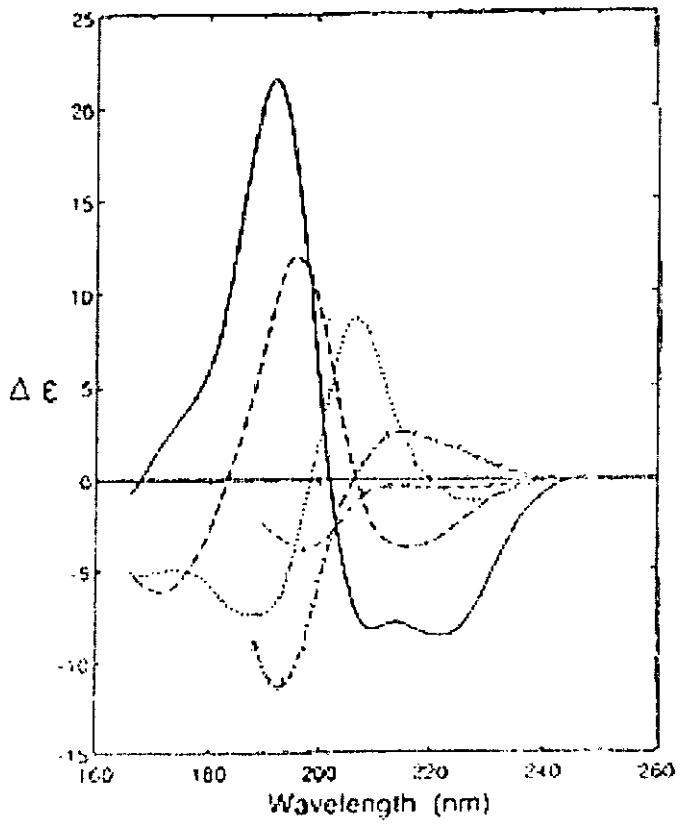

Figure 2.9 The classes of protein secondary structures and their associated CD spectra: α-helix (—), antiparallel β-sheet (– – –), parallel β-sheet (···), turn type (---), and left-handed extended 3_1-helix (+++)(copied from Drake, 1994).

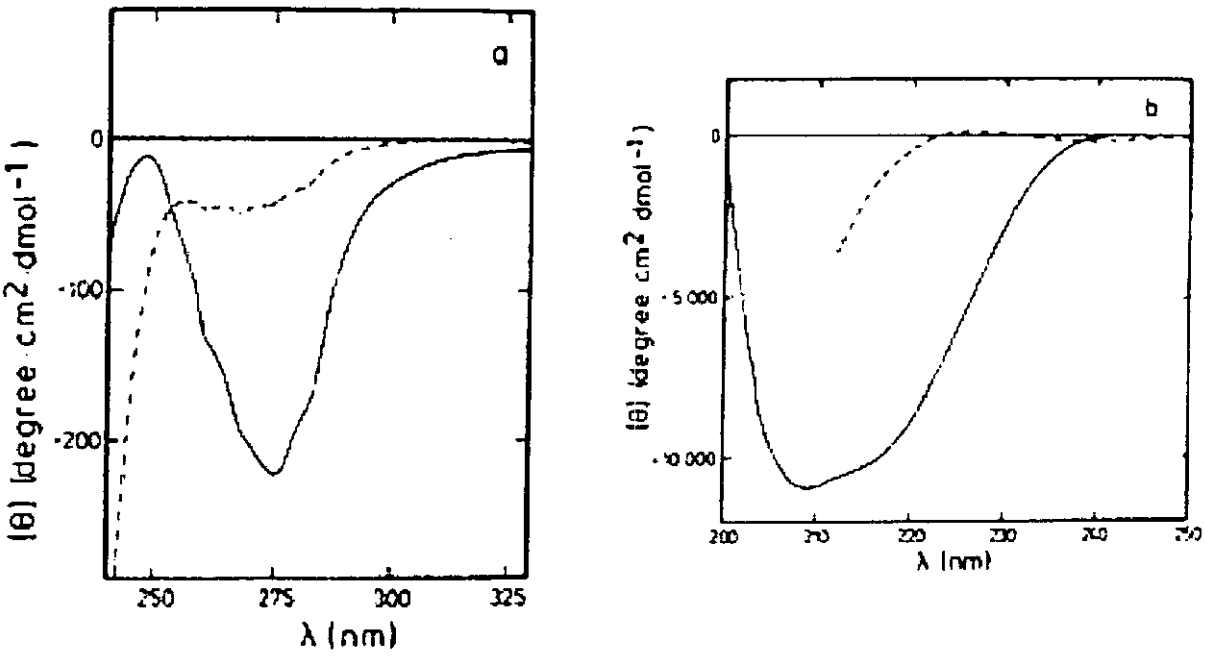

Figure 2.10 CD spectra of native (—) and unfolded (---) RNase A (a) in the aromatic region; (b) in the amide region (copied from Schmid, 1997).

2.3.5.3 Surface Hydrophobicity Test

Hydrophobic interaction is an important weak force stabilizing a protein conformation. The non-polar parts of the protein are adhering to one another. In the native state, most of the hydrophobic aromatic side chains are buried in the interior of a protein. They are exposed to the surface and become freely accessible upon unfolding. Consequently, the measurement of surface hydrophobicity is useful to assess the conformational change of a protein. The hydrophobicity index (H_o) is the sum of free energy of each amino acid residue transferring from aqueous to organic medium (Cardamone and Puri, 1992).

A hydrophobic probe called 1-anilinonaphthalene-8-sulphonate (ANS) can be used for this test. It is fluorescent with the emission maximum at 519nm. After binding with the hydrophobic groups, its quantum yield is increased with a blue shift in the peak wavelength from 519nm to 480nm. The magnitude of the quantum yield and the

emission maximum depends on the number of ANS-binding sites. A denaturing agent can disrupt the hydrophobic portions and expose from the core of a protein to the surface. Cardamone and Puri (1992) reported that bacteriorhodopsin has the shortest wavelength at the emission maximum, the largest value in ANS quantum yield and the most abundant hydrophobic groups in ANS binding sites. So, its surface hydrophobicity is the greatest. Rumbo *et al.* (1996) found that surface hydrophobicity of heat-treated ovalbumin increased markedly. In general, higher in surface hydrophobicity will be in turn lowering the solubility of the protein (Wagner & Anon, 1990).

2.4 Kinetic Model

No publication was found in the kinetic modeling of ultrasound activation or inactivation of enzymes. However, models for the effect of hydrostatic pressure on the enzyme inactivation kinetics were developed. According to Laidler (1951), activation volume (ΔV^*), which is defined as the volume increase as the enzyme-substrate complex becomes an activated complex, is an important parameter in the system of hydrostatic pressure. The value of the volume is positive in the enzyme reaction. Ludwig and Greulich (1978) pointed out that an increase in volume of the enzyme molecule was caused by a substrate induced conformational change. The change in the volume is determined by the volume change of substrate and enzyme, interaction between enzyme and solvent, and the conformational change of enzyme.

The inactivation was assumed to follow the first-order kinetic model. According to the *Le Chatelier's* principle, the chemical reaction can be accelerated or delayed by the

hydrostatic pressure depending on a positive activation volume. Raabe and Knorr (1996) showed that the starch hydrolysis with *Bacillus amyloliquefaciens* α-amylase was retarded with increasing pressure and the resulting activation volume was positive. Ludikhuyze *et al.* (1996) found the similar result in inactivation of *Bacillus subtilis* α-amylase.

As referred to the first-order reaction, the inactivation rate constant is described by the following equation (Raabe and Knorr, 1996):

$$\frac{dA}{dt_r} = -k_i * A \qquad (1)$$

After rearranging the variables and integrating the left side of the resulted equation, the following equation is yielded:

$$\ln \frac{A}{A_o} = -\int_0^t k_i * dt_r \qquad (2)$$

where A is the activity at time t_r; A_o is the activity at time t_r=0; k_i is the inactivation rate constant (min^{-1}); t_r is the reaction time (min).

Based on the Arrhenius equation, the inactivation rate constant affecting by the activation energy and temperature change can be showed by the following equation:

$$\ln k = \ln k_o - \frac{E_a}{RT} \qquad (3)$$

where k is the rate constant at a given temperature (min^{-1}); k_o is the rate constant at a reference temperature (min^{-1}); E_a is the activation energy (kJ/mol); R is gas constant (8.314 J/mol·K); T is the temperature change during the reaction (K).

According to Ludikhuyze *et al.* (1996), the activation energy could also be calculated by pressure and volume in the case of the hydrostatic pressure.

$$E_a = p * \Delta V^* \qquad (4)$$

where p is the pressure (Pa); ΔV^* is the activation volume at constant temperature T (ml/mol).

The change in the activation volume is important to explain the enzyme-inhibitor system. When the enzyme reaction is free of inhibitor, the enzyme unfolds in order to reveal its active site for substrate binding. After formation of product, the enzyme is restored to its original configuration, and is then ready to react with another substrate molecule. Competitive inhibitor shows similar phenomenon during binding as the inhibitor reacts with the enzyme at the active site. The activation volume is increased in the above cases. On the other hand, in the case of non-competitive inhibitor, the formation of the enzyme-inhibitor complex is associated with little change in shape or volume of the enzyme as this inhibitor reacts with the enzyme at a point other than the active site (Laidler, 1951).

Chapter 3. Materials and Methods

3.1 Materials

Stem bromelain from pineapple stem, *p*-nitrophenyl N^{α}-benzyloxycarbonyl-L-lysinate (CLN), L-cysteine, trichloroacetic acid (TCA), 1-anilinonaphthalene-8-sulphonate (ANS), and guanidine hydrochloride (GmHCl) were purchased from Sigma Chemical Co. (USA). Sodium acetate trihydrate was purchased from Junsei Chemical Co., Ltd (Japan). Potassium chloride (KCl) was purchased from China National Chemicals Import & Export Corporation (China). Acetic acid was purchased from Riedel-de Haën (Germany). Acetonitrile was purchased from Lab-Scan (Ireland). All reagents were of analytical grade.

3.1.1 SB Preparation

Fifty milligrams of SB was suspended in 100ml of 10mM sodium acetate-acetic acid buffer with pH 4.6. It was then diluted to the desired concentrations by the same buffer.

3.1.2 CLN Preparation

A 150mM CLN was prepared by suspending 0.06g in 800µl of acetonitrile at first and then 200µl of dH_2O was added to make up the final volume of 1ml. It was then diluted to the desired concentrations by the same solvent.

3.1.3 Assay Buffer Preparation

Assay buffer was prepared by adding 0.0606g L-cysteine and 3.7275g KCl into 500ml of 10mM sodium acetate-acetic acid buffer. The final concentrations of L-cysteine and KCl were 1mM and 100mM respectively. The solution should be freshly prepared.

3.1.4 Ultrasonic Equipment

The ultrasound treatment was carried out by a high intensity ultrasonic processor (Model CPX600; Cole-Parmer Instrument Co.; Vernon Hills; USA) with a fixed frequency of 20kHz and a maximum power output of 600W. The amount of power output delivered from the processor to the titanium-alloy probe could be adjusted by the percentage of

amplitude (0-100%). Its amplitude was only allowed up to 40% when a tapered microtip with 3mm tip diameter was used.

3.2 Methods

3.2.1 Determination of Ultrasound Power in the Experimental Media

Actual energy delivered into the sonicated media was determined by a calorimetric method that was to measure the rate of temperature change throughout ultrasound treatment (De Gennaro *et al.*, 1999). Energy delivered from the probe (E_3) can be divided into energy absorbed by the media (E_1) and energy lost from the media (E_2).

Energy absorbed by the media (E_1) was calculated by the following equation:

$$E_1 = c_p \cdot m \cdot \Delta T$$

where c_p was the specific heat capacity of the substance ($Jg^{-1}{}^{o}C^{-1}$), m was the mass of the substance (g^{-1}) and ΔT was the change of temperature (^{o}C).

Energy lost from the media (E_2) was calculated by the following equation:

$$E_2 = k \cdot A \cdot \frac{\Delta T}{\Delta x} \cdot \Delta t$$

where k was the thermal conductivity of the Pyrex glass (W/m.K), ΔT was the temperature difference (K), Δx was the thickness of the Pyrex glass (m), A was the surface area of the sample container (m^2) and Δt was the treatment time (s).

Energy delivered from the probe (E_3) was equal to the summation of energy absorbed by the media (E_1) and energy lost from the media (E_2). Power delivered from the ultrasound system was calculated by dividing E_3 to Δt.

As shown in Figure 3.1, the experimental set up consisted of 4 units: the ultrasonic processor with the tapered microtip (3mm in diameter), a sonicated chamber, a peristaltic pump (MasterFlex®, Model#7518-12, Cole Parmer, USA) and a thermostatic bath (Model#F10, Julabo Labortechnik GMBH, Germany). The sonicated chamber was made of 2 layers of Pyrex glass (1mm in thickness). The inner cavity was a sample container with 28mm in diameter and 54mm in height. The microtip was immersed into the medium two centimeters in depth. The outer cavity was a cooling cell (75mm in diameter;

135mm in height) with water inlet and outlet at both sides. The temperature of the thermostatic bath was kept at 10°C throughout the experiment.

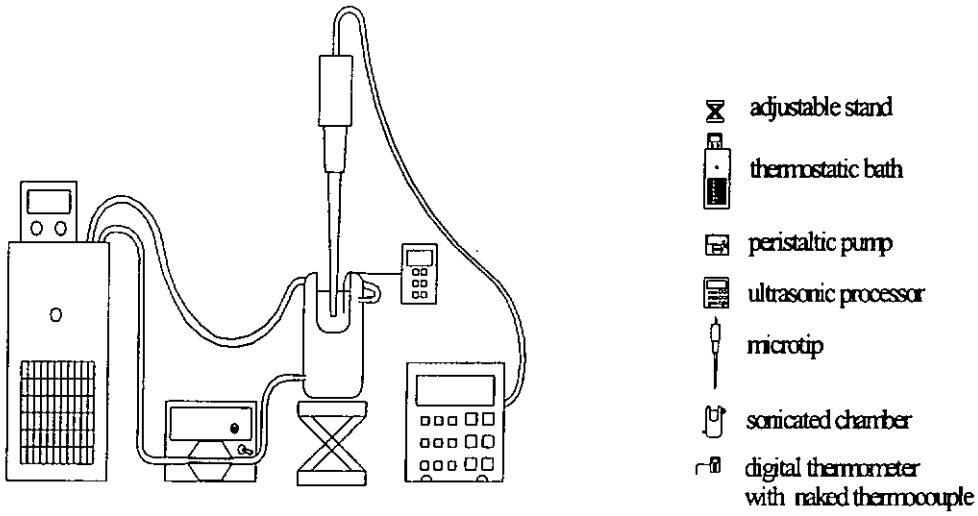

Figure 3.1 The experimental set up of ultrasound treatment.

During energy measurement, 25ml of water was poured into a Pyrex beaker (28mm in diameter; 54mm in height; 1mm in thickness). A naked thermocouple (Type K, Cole Parmer, USA) was dipped into half height of the volume of water inside the beaker. The speed of the pump was adjusted to the maximum. Six hundreds milliliters of water was pumped into the cooling bath. The microtip connected to the ultrasonic processor was dipped into the water in 2cm. The amplitude of the processor was adjusted to the desired percentages (5-40%) and 10min of treatment time was entered. The whole system was stabilized for 5 minutes in order to maintain constant temperature. After 5 minutes, the

ultrasound processor was turned on. The change of temperature was recorded every minute. All measurements were carried out in triplicate. The specific heat capacity of water is 4.184 $Jg^{-1}°C^{-1}$ and the thermal conductivity of the Pyrex glass is 1.123W/m. K (Perry & Chilton, 1973). The detailed calculations of energy measurement were shown in Appendix A.

3.2.2 Ultrasound Treatment on SB-catalyzed Reaction

The proteolytic activity of SB was determined by a stopped assay of CLN hydrolysis similar to that previously described by Heinrikson and Kézdy (1976) with some modification. SB could catalyze the reaction of converting the chromogenic substrate CLN to the product *p*-nitrophenol. The change in molar absorptivity of CLN was $6320M^{-1}cm^{-1}$. One unit of SB activity was defined as 1μmol of *p*-nitrophenol released per min per mg of SB at 25°C and pH4.6.

The experimental set up was the same as in Figure 3.1. The total volume of SB-catalyzed reaction mixture was 25ml. A 250μl of SB solution (0.5mg/ml) was activated by adding to a desired amount of assay buffer for 1min. Certain amount of CLN was added to the reaction mixture to yield the final concentrations ranging from 60μM to 960μM. The

ultrasonic processor was turned on immediately. The amplitudes applied were 5%, 10%, 20% and 40%. The speed of the pump was adjusted to pump water into and out from the cooling cell in order to maintain constant reaction temperature. The treatment temperature was monitored by the thermocouple in order to maintain it at 25°C±1°C. After 1min, 3min, 5min and 10min of treatment, 1ml of reaction mixture was transferred to 1ml of 5% (w/v) TCA for termination of the reaction. The mixtures were blended for 5s and incubated at room temperature for 30min. The absorbance was measured at 340nm with a double beam spectrophotometer (Model#U-2000, HP, USA). All treatments were carried out in triplicate. The reaction mixture without any ultrasound treatment was used as a control. The detailed calculations of the proteolytic activity of SB were shown in Appendix B.

3.2.3 Effect of Mechanical Stirring on SB-catalyzed Reaction

The total volume of SB-catalyzed reaction mixture was 25ml. A 250µl of SB solution (0.5mg/ml) was activated by adding to a desired amount of assay buffer for 1min. Certain amount of CLN was added to the reaction mixture to yield the final concentrations of 60µM, 480µM and 960µM. The conventional stirrer (Thermolyne Cimarec® I, Model#SP46510-26, USA) was turned on immediately. The stirring speed was adjusted

to 100rpm, 500rpm and 1000rpm. The temperature was kept at 25°C±1°C. After 1min, 3min, 5min and 10min of stirring, 1ml of reaction mixture was transferred to 1ml of 5% (w/v) TCA for termination of the reaction. The mixtures were blended for 5s and incubated at room temperature for 30min. The absorbance was measured at 340nm with a double beam spectrophotometer (Model#U-2000, HP, USA). All treatments were carried out in triplicate. The reaction mixture without stirring acted as a control. The detailed calculations of the proteolytic activity of SB were shown in Appendix B.

3.2.4 Effect of Ultrasound Pretreated SB or CLN on SB Activity

The total volume of SB-catalyzed reaction mixture was 25ml. A 250µl of SB solution (0.5mg/ml) was activated by adding to a desired amount of assay buffer for 1min. The ultrasonic processor was turned on immediately. The amplitudes used were 5% and 40%. The treatment temperature was monitored by the thermocouple in order to maintain it at 25°C±1°C. After 5min or 10min treatment, certain amount of untreated CLN was added to the reaction mixture to yield the final concentrations of 480µM. After 5min of reaction time, 1ml of reaction mixture was transferred to 1ml of 5% (w/v) TCA for termination of the reaction. The mixtures were blended for 5s and incubated at room temperature for 30min.

The above procedures were repeated by sonicating 480μM of CLN at first, and followed by adding untreated SB to test the effect of ultrasound pretreated CLN.

The absorbance was measured at 340nm with a double beam spectrophotometer (Model#U-2000, HP, USA). All treatments were carried out in triplicate. The reaction mixture with untreated SB or CLN acted as control. The detailed calculations of the esteolytic activity of SB were shown in Appendix B.

3.2.5 Ultrasound, Thermal and Chemical Treatment on SB

In ultrasound treatment, a 25ml of SB solution (0.5mg/ml) was treated by ultrasound with amplitudes of 5%, 10%, 20% and 40% for 5min and 10min. The treatment temperature was monitored by the thermocouple in order to maintain it at 25°C±1°C. In thermal treatment, a 25ml of SB solution (0.5mg/ml) was incubated at 95°C for 60min. In chemical treatment, a 25ml of SB solution (0.5mg/ml) was incubated in 6M GmHCl with mechanical stirring for 60min. After all treatments, SB solution was transferred to ice bath and subjected to conformational analysis.

3.2.6 Analysis of SB Conformation

After ultrasound, thermal and chemical treatments, SB solution was subjected to various conformational analyses including ultraviolet absorption spectrometry, fluorescence emission spectrometry, circular dichroism spectrometry and surface hydrophobicity test.

3.2.6.1 Ultraviolet Absorption Spectrometry

Ultraviolet (UV) absorption spectrum was measured by using a double beam spectrophotometer (Perkin Elmer, Model#LamdaBio20). One ml of 10mM sodium acetate-acetic acid buffer (pH 4.6) was pipetted into a quartz cuvette with 1cm path length and the solution was scanned over the wavelength range of 240-350nm. That spectrum measured was used as the baseline for sample measurement. One ml of SB solution (0.5mg/ml) was pipetted into another quartz cuvette with 1cm path-length. The spectrum of the solution could be found by scanning over the same wavelength range. All measurements were performed at 25°C and they were carried out in triplicate.

3.2.6.2 Fluorescence Emission Spectrometry

Fluorescence emission spectrum was measured by using a fluorescence spectrophotometer (Perkin Elmer, Model#LS50B). The excitation wavelength was 295nm and the emission wavelength range was 300-500nm for each measurement (Mendoza-Hernandez *et al.*, 2000). Both slit width of excitation and emission were set to 5nm. The SB solution (0.5mg/ml) was diluted to 0.25mg/ml by mixing 500µl of SB solution (0.5mg/ml) and 500µl of 10mM sodium acetate-acetic acid buffer in a quartz cuvette with 1cm path-length. The spectrum of the solution was then measured under the conditions described above. All measurements were performed at 25°C and carried out in triplicate.

3.2.6.3 Circular Dichroism Spectrometry

Circular dichroism (CD) spectrum was recorded by a CD spectropolarimeter (JASCO, Model#J810) at 25°C. Before measurement, SB solution (0.5mg/ml) was diluted to 0.25mg/ml by mixing 500µl of SB solution (0.5mg/ml) and 500µl of 10mM sodium acetate-acetic acid buffer. In the far UV region (185-250nm), 0.25mg/ml SB solution was

transferred in a cylindrical quartz cell with 1mm path-length. Measurements in the near UV region (250-320nm) were made on 0.5mg/ml SB solution in a cylindrical quartz cell with 10mm path-length. That spectrum of 10mM sodium acetate-acetic acid buffer (pH 4.6) was used as the baseline for sample measurement in each wavelength region. The accumulation of each CD spectrum was 2.

All spectra were expressed as mean residue ellipticities $[\theta]_{MRW.}$, which were calculated using the molecular mass of a mean residue, as 108 (Arroyo-Reyna & Hernandez-Arana, 1995). The content of the secondary structure was estimated according to Compton and Johnson (1986). The detailed calculations of secondary structure contents are shown in Appendix C.

3.2.6.4 Surface Hydrophobicity Test

Surface hydrophobicity was determined by using a hydrophobic fluorescence probe, 1-anillino-8-naphthalene sulfonate (ANS) (Wagner & Anon, 1990; Rumbo *et al.*, 1996). Before the analysis, the reading of fluorescence intensity (FI) was standardized by using a solution of 5µl ANS in 1ml of methanol, and then the FI was adjusted to 800. One ml of 10mM sodium acetate-acetic acid buffer was used as a blank solution. A 25µl ANS

solution (8mM) was added to 1ml of SB solution. The mixture was excited at 374nm and the relative emission intensity was recorded at 485nm with a fluorescence spectrophotometer (Perkin Elmer, Model#LS50B). All measurements were carried out in triplicate. The detailed calculations are shown in Appendix D.

3.2.7 Data Analysis

The standard error (S.E.) of ultrasound power, SB activity, kinetic parameters and contents of secondary structures was determined. Linear and quadratic regressions were used to fit the data of energy absorbed in the experimental media. The statistical analysis and model fitting were performed by using SPSS 10.0 (SPSS Inc., 1989).

Chapter 4. Results and Interpretation

4.1 Ultrasound Power in the Experimental Media

During the experiment, energy was delivered from the probe to the medium in which part of it would be absorbed by the medium and the others would be lost to surroundings. Since the size of sample medium was small (about 25ml), it was assumed that the ultrasound field was evenly distributed in the medium.

Figures 4.1a, 4.1b and 4.1c show the results of energy absorbed, energy lost and energy delivered to the media respectively. The level of energy was controlled by the amplitude settings that the former increased as the setting was adjusted to a higher value. Larger amplitude represented that ultrasound wave oscillated more vigorously and hence transmitted more mechanical energy to the medium. The amount of energy could be found by measuring the change in temperature.

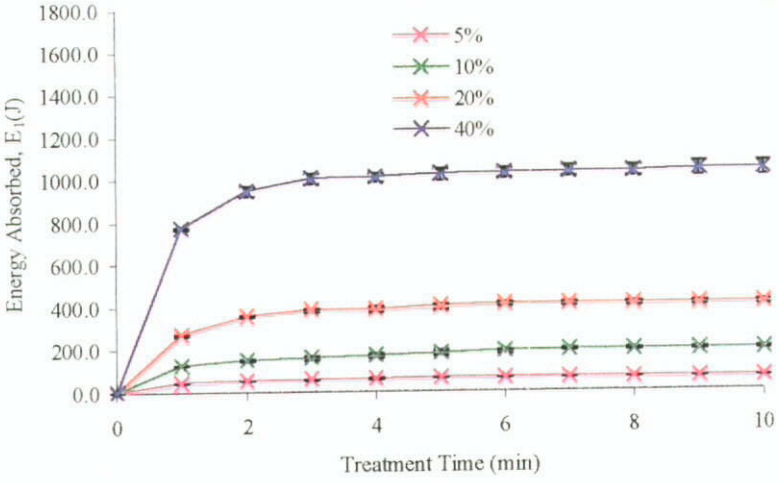

(a)

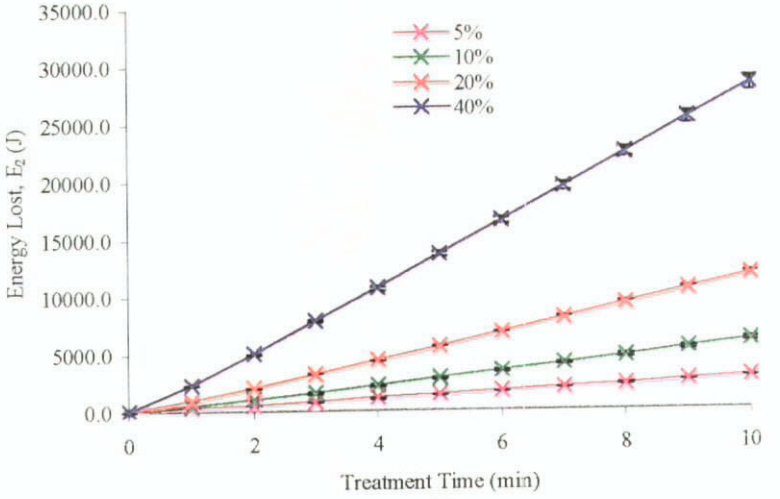

(b)

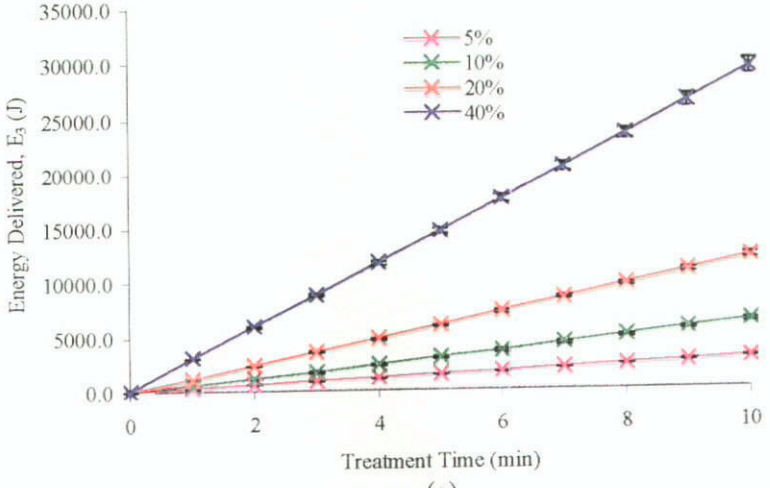

(c)

Figure 4.1 Different energy in the experimental media (a) energy absorbed, E_1; (b) energy lost, E_2; (c) energy delivered, E_3.

The energy absorbed increased vigorously as the treatment time increased up to 3min and then flattened afterwards. Most energy was absorbed at the first 3min of treatment time in each amplitude setting. Moreover, the amount of energy absorbed increased with the increase in amplitude setting. Apart from ultrasound amplitude, energy lost depended on the treatment time and increased as the time prolonged. More energy lost as the amplitude setting was increased. The change of energy delivered was similar to that of energy lost. However, energy absorbed by the medium did not follow the same trend as others. There were several factors affecting energy absorption, namely ultrasound frequency, ultrasound amplitude, treatment time and viscosity of the medium. Since the frequency was fixed throughout the experiment and the sample was largely diluted with buffer, amplitude setting and treatment time were the main factors affecting energy absorption.

After statistical fitting, it was found that energy absorbed by the medium could be fitted to a second order polynomial equation of the form:

$$Y = b_0 + b_1X_1 + b_2X_2 + b_3X_1X_2 + b_4X_1X_1 + b_5X_2X_2$$

where Y was the response or energy absorbed by the medium; b_0, b_1, b_2, b_3, b_4 and b_5 were the coefficients; X_1 was ultrasound amplitude and X_2 was treatment time.

The resulting equation with $R^2 = 0.992$ was:

$$Y = -80.27 + 12.86X_1 + 29.66X_2 + 0.49X_1X_2 + 0.24X_1X_1 - 2.62X_2X_2$$

Energy delivered was calculated by summation of energy absorbed and lost. It increased as amplitude setting and treatment time increased. However, ultrasound power was constantly delivered from the probe to the medium in each time period. Within 10-min treatment, the average power delivered was about 4.67W for 5%, 10.23W for 10%, 20.19W for 20% and 48.89W for 40% of amplitude setting. The results were summarized in Table 4.1. Ultrasound amplitude could be used to present the power delivered from the probe, thus it will be used in the rest of the thesis to present the results.

Table 4.1 Ultrasound power delivered at different amplitude settings.

Ultrasound Amplitude	Power Delivered (W)
5%	4.67 ± 0.00
10%	10.23 ± 0.38
20%	20.19 ± 0.37
40%	48.89 ± 0.39

**The mean value of data in 10 replicates ± S.E.*

4.2 Ultrasound Treatment on SB-catalyzed Reaction

4.2.1 Effect of ultrasound power and treatment time on SB-catalyzed reaction at various CLN concentrations

Ultrasound exerted different effect on SB-catalyzed reaction at various CLN concentrations. Three typical CLN concentrations were chosen for data interpretation. They were low (60μM), medium (480μM) and high (960μM) concentration of the substrate.

4.2.1.1 Effect of Ultrasound Power

Figure 4.2 shows the effect of ultrasound on SB activity at various CLN concentrations and different amplitude settings and treatment times. SB activity was promoted at low amplitude setting of not more than 10% with maximum activation at 5% setting; while inactivation was observed for settings of higher than 10%. The same phenomena were observed for cases with the 4 different treatment periods (1min, 3min, 5min and 10min). As compared to those without ultrasound, SB activity was promoted at low amplitude level (5% and 10%) and inhibited at high amplitude level (20% and 40%). It was also found that at amplitude setting of 5% for 5min, the maximum catalytic activity of SB was

about 25% higher than that without treatment, while its activity reduced by about 40% at the amplitude setting of 40%. Similar results were obtained at 1min and 10min of treatment. Similar changes in the catalytic activity were found at all CLN concentrations investigated (Figure 4.2). The main difference was notified at 10min of treatment time.

4.2.1.2 Effect of Treatment Time

Figure 4.3 shows the effect of treatment time on SB activity at different CLN concentrations. No change in the activity over the first 5min of treatment was observed no matter what ultrasound amplitude was set. The activity was significantly decreased at treatment time of 10min for low CLN concentration (60μM). It was because 60μM CLN was too diluted that was only sufficient for the reaction to proceed for up to 5min. As the time was prolonged, CLN was no longer enough for the reaction. When the CLN concentration increased up to 480μM and 960μM, effect of treatment time on the activity was gradually diminished as there was enough substrate for the complete reaction within 10min.

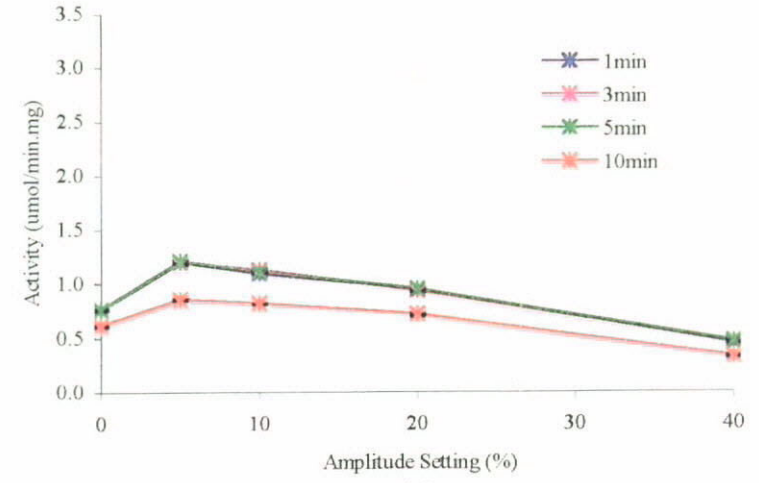

(a)

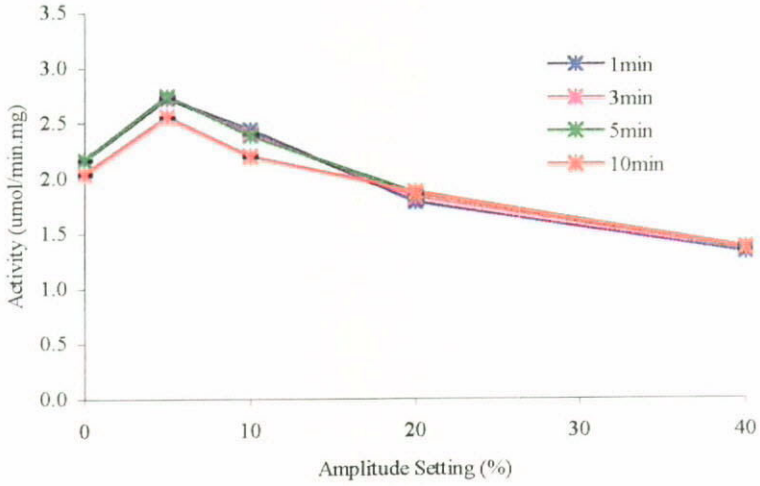

(b)

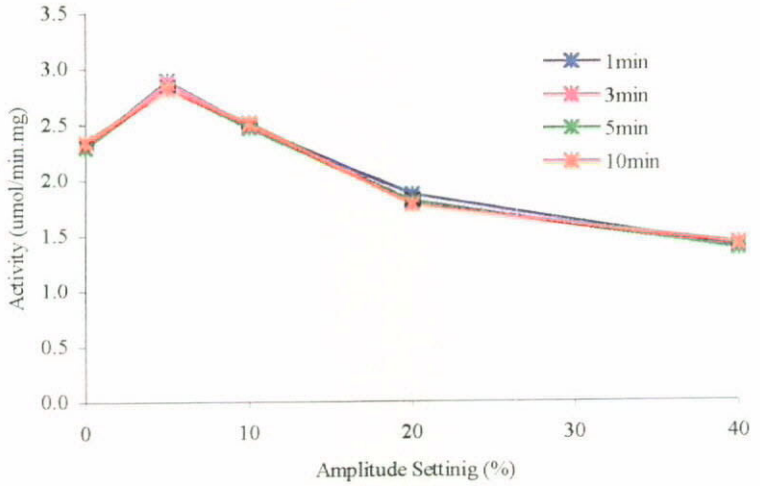

(c)

Figure 4.2 Effect of ultrasound power on SB activity at different CLN concentrations (a) 60μM; (b) 480μM and (c) 960μM.

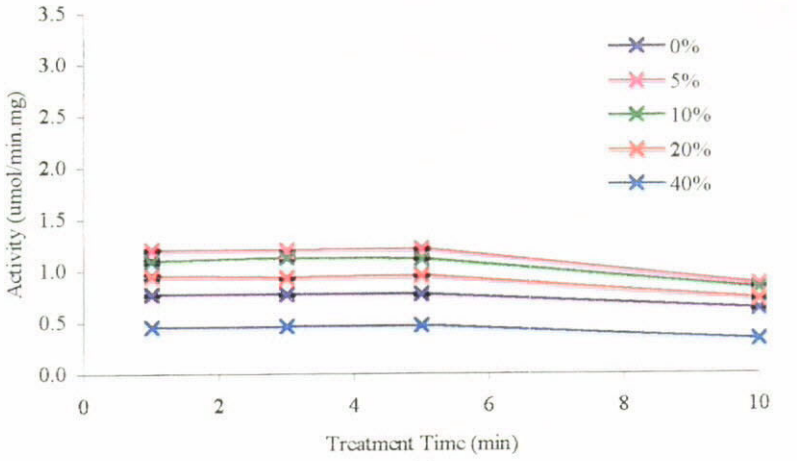

(a)

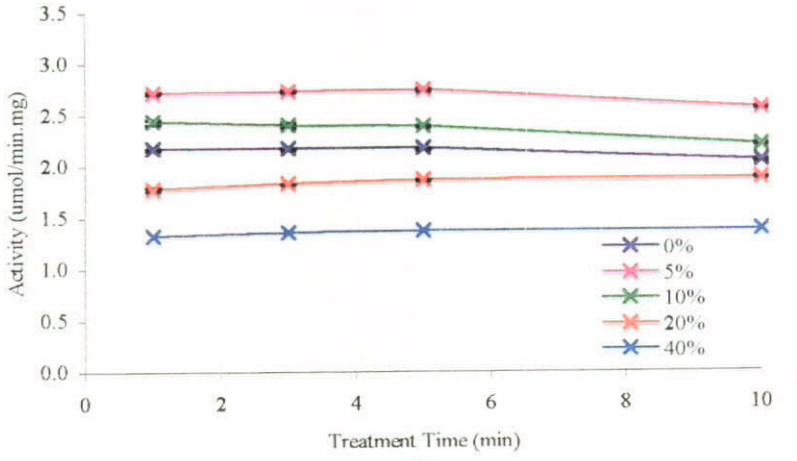

(b)

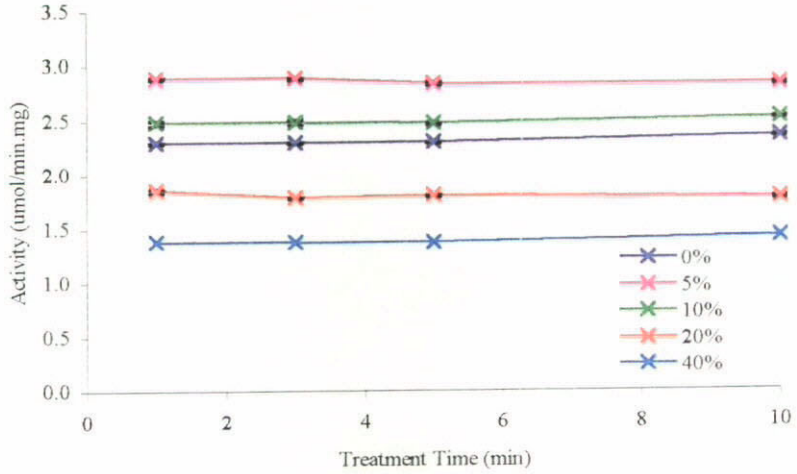

(c)

Figure 4.3 Effect of treatment time on SB activity in different CLN concentrations (a) 60μM; (b) 480μM and (c) 960μM.

4.2.2 Effect of CLN concentration on SB-catalyzed reaction at various ultrasound settings

The effect of CLN concentration on SB-catalyzed reaction at various ultrasound settings was investigated by using CLN from 60μM to 960μM. For each amplitude settings, SB activity increased as the concentration of CLN increased and reached the "steady" level in the CLN range of 480μM to 960μM (Figure 4.4). At low CLN concentrations (below 240μM), SB activity was strongly correlated to the substrate concentration. The active sites of SB were not fully occupied by substrate; the increase in substrate concentration favored the binding of substrate to the sites and hence the activity was apparently increased. At high CLN concentrations (above 480μM), its activity was independent on the substrate concentration due to the active sites were saturated with the substrate, thus any increase in substrate concentration would not bring in any increase in the activity (Lehninger *et al.*, 1993).

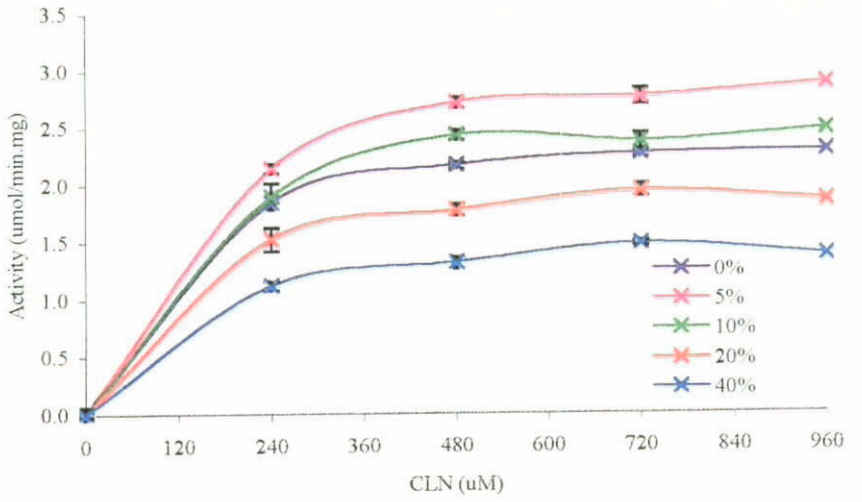

(a)

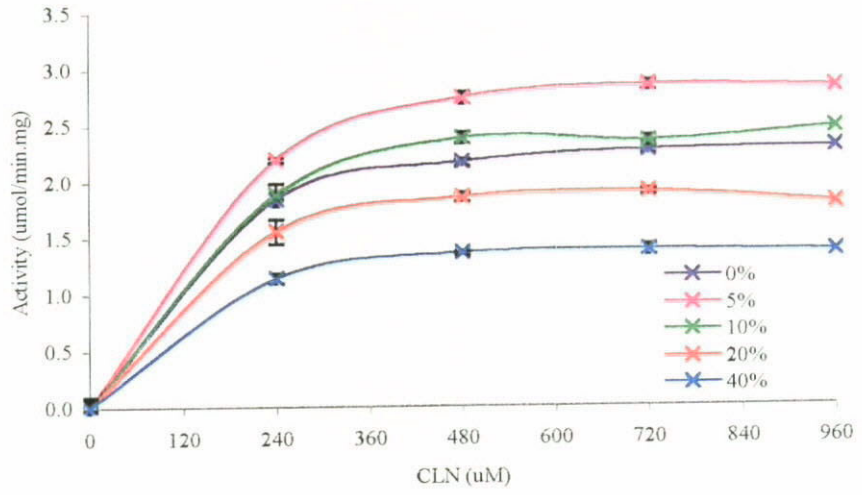

(b)

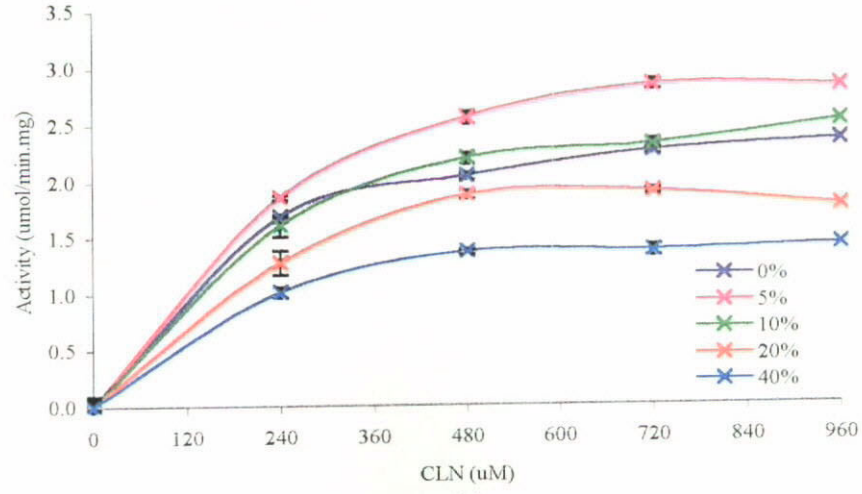

(c)

Figure 4.4 Effect of CLN concentration on SB-catalyzed reaction in various ultrasound settings at different treatment times (a) 1min; (b) 5min and (c) 10min.

4.2.3 Effect of ultrasound on the kinetic parameters of SB

In order to understand the effect of ultrasound on the catalytic efficiency of SB, more related kinetic parameters should be determined. They were calculated at low CLN concentrations (60μM to 480μM). Two constants including the Michaelis constant (K_m) and the catalytic constant (k_{cat}) were useful to notify the effect. The Lineweaver-Burk plots of SB activities at various amplitude settings for different treatment times were plotted to obtain the parameters: K_m and the maximum reaction velocity (V_{max}) that was used to calculate k_{cat}. The detailed derivations of the Michaelis-Menten model and the Lineweaver-Burk plot were shown in Section 2.2.6.1 (Kinetic Parameters). The effect of ultrasound on kinetic parameters of SB are calculated (Appendix E) and summarized in Table 4.2.

As referred to Table 4.2, V_{max} and k_{cat} at amplitude setting of 0% (without ultrasound) and 5% were similar, while K_m was reduced by about 50% at the amplitude setting of 5%. The results showed that the apparent affinity between SB and CLN molecules was increased. In comparison with those without ultrasound, V_{max} and k_{cat} decreased as amplitude increased from 10% to 40%, while the values of K_m reduced at amplitude settings of 10% and 20%, then increased significantly at amplitude setting of 40%.

Table 4.2 Kinetic parameters of SB at different amplitudes settings and treatment times.

Kinetic Parameters*	Amplitude Setting				
	0%	5%	10%	20%	40%
Treatment Time 1min					
V_{max}	3.13±0.01	3.09±0.02	2.66±0.08	2.04±0.18	2.09±0.08
k_{cat}	71.43±0.20	70.45±0.37	60.75±1.74	46.52±4.13	47.66±1.81
K_m	184.70±1.43	101.95±1.67	95.20±1.96	75.16±13.57	220.29±16.72
k_{cat}/K_m	0.39±0.00	0.69±0.01	0.638±0.01	0.64±0.06	0.22±0.01
Treatment Time 5min					
V_{max}	3.13±0.01	3.13±0.03	2.64±0.14	2.00±0.19	2.08±0.00
k_{cat}	71.43±0.20	71.36±0.75	60.15±3.28	45.74±4.42	47.38±0.09
K_m	184.70±1.43	104.33±2.28	90.46±7.03	72.47±11.58	210.50±5.80
k_{cat}/K_m	0.39±0.00	0.68±0.01	0.67±0.02	0.64±0.04	0.23±0.01
Treatment Time 10min					
V_{max}	3.50±0.15	3.41±0.04	2.68±0.03	2.14±0.09	4.21±0.73
k_{cat}	79.88±3.30	77.91±0.80	61.07±0.66	48.92±2.08	96.18±16.56
K_m	280.74±19.39	185.68±4.29	143.56±2.43	125.11±9.33	732.99±159.60
k_{cat}/K_m	0.29±0.01	0.42±0.01	0.43±0.01	0.39±0.01	0.13±0.01

**The mean value of data in triplicates ± S.E.*

The unit of V_{max} was μmol/min/mg, K_m was μM, k_{cat} was min^{-1} and k_{cat}/K_m was $min^{-1}\mu M^{-1}$.

In that case, neither the decrease in k_{cat} nor in K_m could be accounted for the effect of ultrasound. Consequently, the catalytic efficiency (k_{cat}/K_m) was calculated to explain the effect. The detailed explanations were shown in Section 2.2.6.1 (Kinetic Parameters)

In comparison to that without ultrasound treatment, the catalytic efficiency (k_{cat}/K_m) of SB was doubled at ultrasound amplitude settings of 5% and 20%. There was also a 50% reduction in the catalytic efficiency at the amplitude setting of 40%. The same situation could be held for each treatment time. An abnormal observation was found at 40% for 10min that V_{max}, K_m and k_{cat} increased quantitatively with a reduction in k_{cat}/K_m.

4.3 Effect of Mechanical Stirring on SB-catalyzed Reaction

It was suggested that ultrasound might exert a mixing effect on the SB-catalyzed reaction, which in turn enhanced the SB activity. Therefore, a series of experiments were conducted in order to find out that such enhancement was due to the mixing effect or other mechanism induced by ultrasound. Figure 4.5 shows the outcomes of 5min mechanical stirring on SB-catalyzed reaction. Experimental results indicated that mechanical stirring at low speed or high speed could not induce significant increase on SB activity at various CLN concentrations and stirring times. Stirring on SB-catalyzed reaction at 60μM and 480μM CLN concentration, SB activity maintained at the same

level up to 1000rpm. Little enhancement of the activity was found at high CLN concentration (960μM) and high stirring speed (1000rpm).

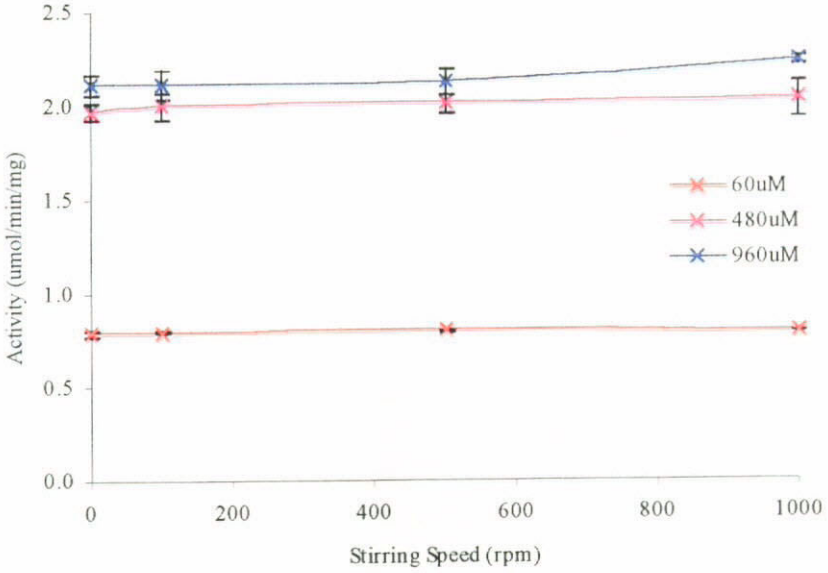

Figure 4.5 Effect of mechanical stirring speed on SB activity for 5min of stirring time.

4.4 Effect of Ultrasound Pretreated SB or CLN on SB Activity

Figure 4.6 shows the SB activity when SB or CLN was pretreated by ultrasound separately. The results indicated that SB activity was promoted at amplitude setting 5% and reduced when amplitude was adjusted up to 40% when pretreated SB was used. The activity at high power level (40%) and short treatment time (5min) was the same as that without ultrasound. Extension of the treatment time decreased the activity in each amplitude setting. However, when pretreated CLN (480μM) was used, the increase in activity was directly proportional to the ultrasound power. Treatment time only exerted little effect on the activity at that case.

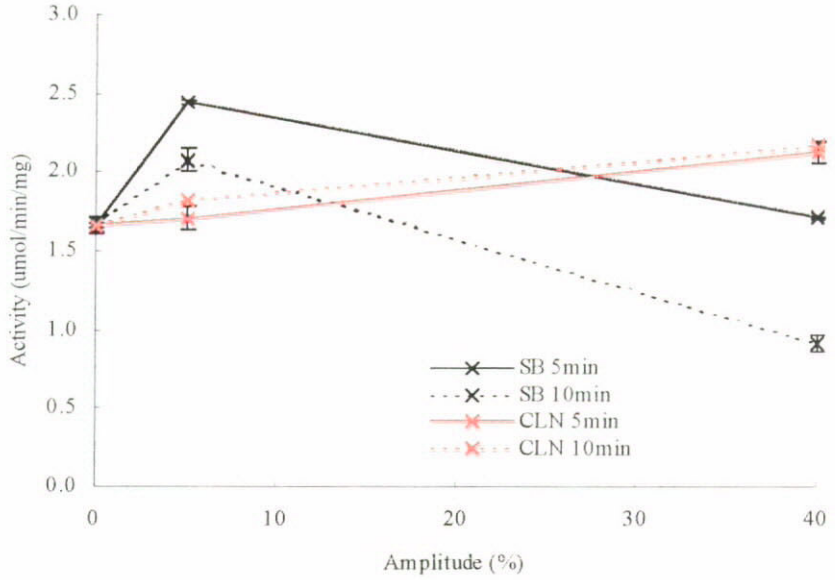

Figure 4.6 The SB activities when SB or CLN (480μM) were pretreated with ultrasound for various times.

4.5 Analysis of SB Conformation

Apart from efficient mass transfer, ultrasound altered both conformations of SB and CLN molecules. But, ultrasound field induced greater changes in the conformation of SB than that of CLN (refer to Section 4.4 and Figure 4.6). Therefore, only the conformation of SB molecule was analyzed in this study.

4.5.1 Ultraviolet Absorption Spectrometry

The results of the UV absorption spectra are shown in Figure 4.7a and 4.7b. The trends of all spectra were similar; there was a peak near 280nm in each spectrum. The absorbance in each spectrum increased as the ultrasound power level increased. A reduction of

absorbance was found in chemical treatment. The change in the absorbance of thermal treatment could be divided into two portions. The absorbance was higher than that of without ultrasound before 280nm and became lower after 280nm. The results were not affected by the treatment times.

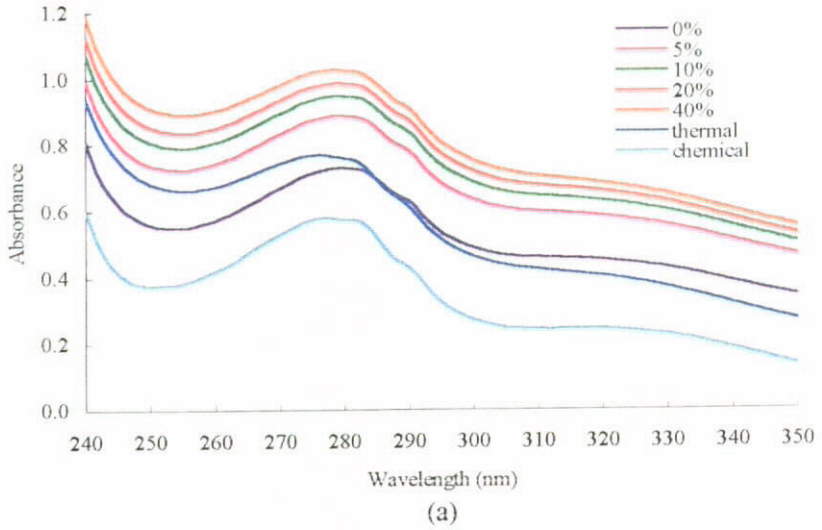

(a)

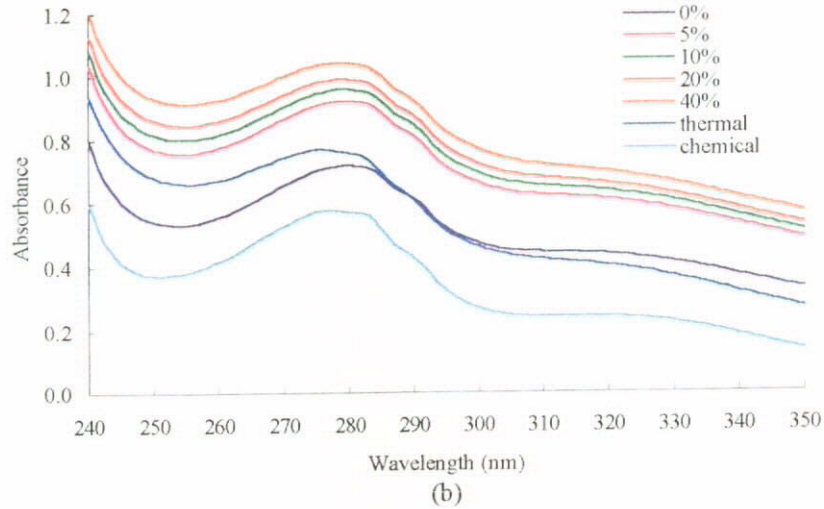

(b)

Figure 4.7 UV absorption spectra of SB for different amplitude settings and treatment time at (a) 5min and (b) 10min.

The peak absorbance and corresponding wavelengths in the UV absorption spectra are shown in Table 4.3. A slightly shift in wavelengths (279.21nm to 278.58nm) could be observed from amplitude setting of 5% to 40% in comparison with SB without ultrasound (279.32nm). Such shifts were more pronounced for SB with either thermal (275.83nm) or chemical treatment (276.69). The peak absorbance increased as the ultrasound power increased, i.e. 0.883 to 1.024 for amplitude setting from 5% to 40%. The same phenomenon was found for 10min of treatment time. The absorbance of thermal treatment (0.766) was higher than that of without any treatment (0.726). The reduction was predominantly in the chemical treatment (0.575).

Table 4.3 Peak absorbance and corresponding wavelength for UV absorption.

Peak	Amplitude Setting					Thermal	Chemical
	0%	5%	10%	20%	40%	Treatment	Treatment
Treatment Time 5min							
Abs.	0.726	0.883	0.944	0.983	1.024	0.766	0.575
WL (nm)	279.32	279.21	279.13	278.93	278.58	275.83	276.69
Treatment Time 10min							
Abs.	0.715	0.919	0.955	0.988	1.041	~	~
WL (nm)	279.34	279.07	278.95	278.74	278.42	~	~

One SB molecule contains 14 Tyr residues, 5 Trp residues and 6 Phe residues (Murachi, 1976). Since the absorption of Phe is weak, the spectrum of SB is dominated by Tyr and Trp residues. In comparison with native SB, the peak absorbance increased at ultrasound amplitude settings from 5% to 40% and the corresponding wavelength underwent blue shift. The blue shift in wavelength was more favored in thermal and chemical treatments. The results indicated that some of the aromatic residues that were originally buried in the hydrophobic core would be exposed to the solvent. The enzyme molecule was unfolded under such an extreme condition.

4.5.2 Fluorescence Emission Spectrometry

The intrinsic fluorescence of a protein can show the exposed environment of the chromophores. It is useful to investigate the conformational changes of SB especially in tertiary structures. The excitation wavelength of 295nm was chosen for Trp residue. The emission spectrum displayed maximum near 340nm.

Figures 4.8a and 4.8b show the change in fluorescence intensity (FI) with the range of wavelength from 300 to 500nm. A peak was established in each spectrum. Obviously, the change in FI of SB with ultrasound treatment was similar to that without treatment. The FI reduced at first and increased with a maximum at near 340nm and then gradually

decreased. The shape of the spectrum for thermally denatured SB was the same as native SB but its peak FI and corresponding wavelength were different. The spectrum of chemically denatured SB was totally different. The FI increased from 300nm to 340nm and flattened up to 380nm, then decreased from 380nm to 500nm. The similar results were found for those with 10min of treatment time.

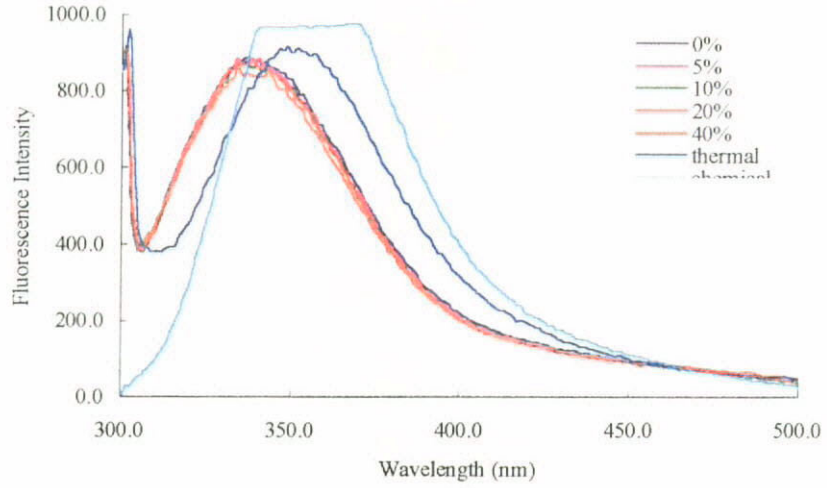

(a)

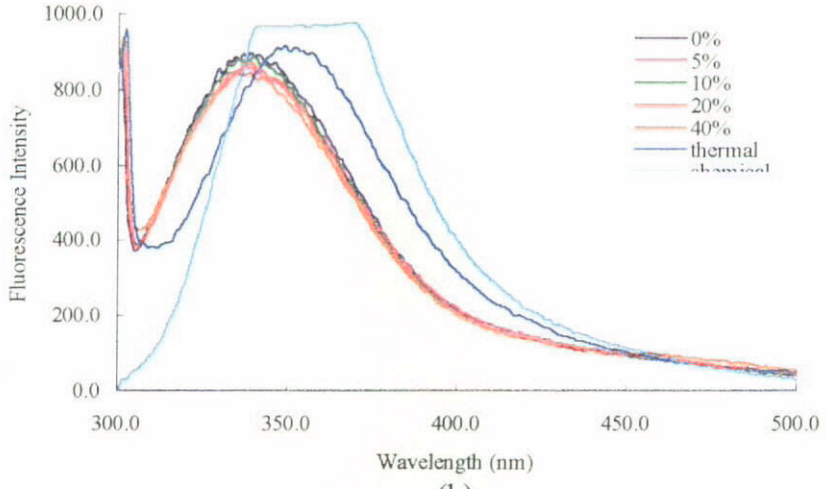

(b)

Figure 4.8 Fluorescence emission spectra of SB for different amplitude settings and treatment time at (a) 5min and (b) 10min.

For thermally and chemically treated SB, both FI and wavelengths were higher than that without any treatment. For most ultrasound treatments, the peak FI and corresponding wavelengths were similar and independent on the treatment time. The results were summarized in Table 4.4. A slightly decrease in FI was found at amplitude setting of 40%. The red shift in wavelength and increase in FI could be observed for SB either in thermally or chemically denatured. Such a shift indicated that the Trp residues were more approached to the hydrogen bonding groups and more exposed to water.

Table 4.4 Peak FI and corresponding wavelength for fluorescence emission

Peak	Amplitude Setting					Thermal	Chemical
	0%	5%	10%	20%	40%	Treatment	Treatment
Treatment Time 5min							
FI	893.8	887.6	875.8	880.1	865.0	917.1	975.1
WL (nm)	336.2	337.0	336.0	336.0	334.2	346.8	369.3
Treatment Time 10min							
FI	898.5	864.3	891.2	877.4	849.9	~	~
WL (nm)	338.0	336.8	339.7	337.7	337.3	~	~

4.5.3 Circular Dichroism Spectrometry

The CD spectra of SB in near-UV regions are shown in Figures 4.9a and 4.9b. The spectra of SB with or without ultrasound treatment could be divided into two portions for explanation. Before 290nm, the residue ellipticity increased as the wavelength increased with a positive peak at near 280nm. The ellipticity decreased after 290nm to form a negative peak near 300nm and then rose up to 320nm. The levels of the spectra dropped when more ultrasound powers were applied. Similar results could be found at 10min of treatment time. The change of the spectrum was similar in thermal and chemical treatments. At the beginning, the ellipticity decreased to form a negative peak near 280nm and then increased up to 320nm. The spectrum in the near-UV region indicated the asymmetrical environment surrounding the aromatic residues. In general, weak residue ellipticity of the CD spectrum in near-UV region was due to the lack of ordered structure such as short peptides. The positive CD bands decreased as ultrasound power increased due to the increase in the number of aromatic residue. However, the CD bands became in negative values for thermally and chemically treated SB. The results indicated that chromophores were subjected to a different surrounding environment.

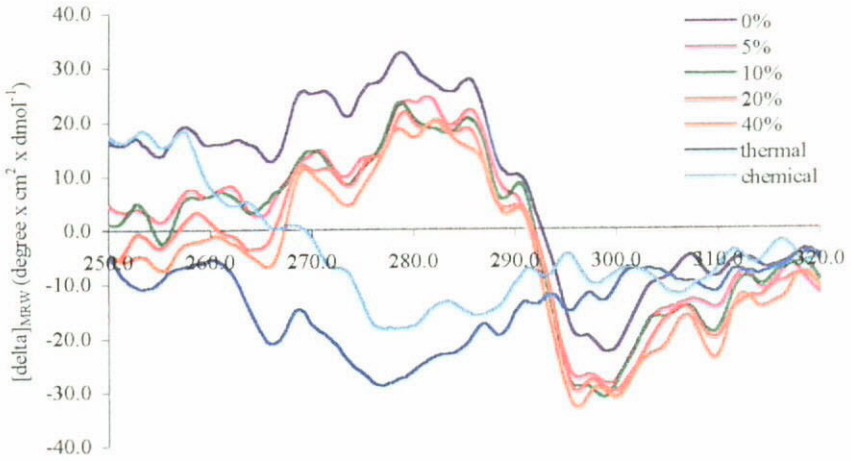

(a)

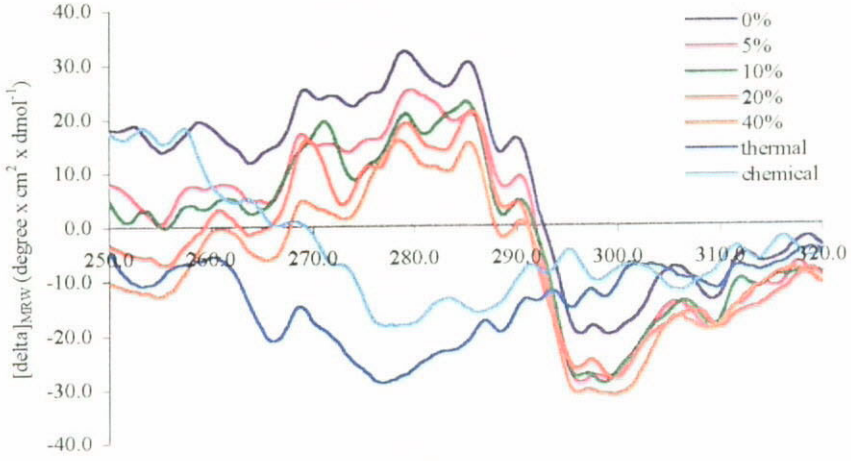

(b)

Figure 4.9 CD spectra of SB in near-UV region for different amplitude settings and treatment time at (a) 5min and (b) 10min.

The secondary structures of a protein are estimated from the residue ellipticity of the amide region. The particular characteristics of α-helix are two negative maxima at 208nm and 222nm. In the far-UV region of the native SB, it showed a positive band from 185-196nm and a negative band from 200-240nm (Figure 4.10). SB was categorized to the class of α+β protein that native SB contained abundant α-helix and antiparallel β-sheet structures.

The CD spectra of SB in far-UV region with different treatments are shown in Figures 4.10a and 4.10b. At 5min treatment time, the spectra for SB with or without ultrasound treatment were similar. There were a positive peak near 190nm and a negative peak near 210nm. At 10min of treatment time, a similar pattern of the spectra was found. The spectrum of thermally denatured SB had a similar pattern with a left shift and diminishment of both peaks. The ellipticity was more approached to zero value in all wavelengths expect from 190 to 200nm. The spectrum of chemically denatured SB could only be showed up to 220nm because GmHCl absorbed strongly in the far-UV region (Bloemendal & Johnson, 1995). The ellipticity of that spectrum was more approached to zero point.

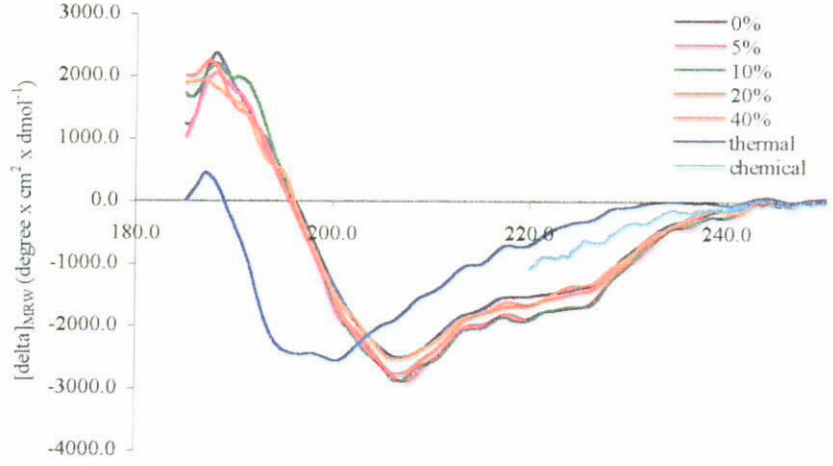

(a)

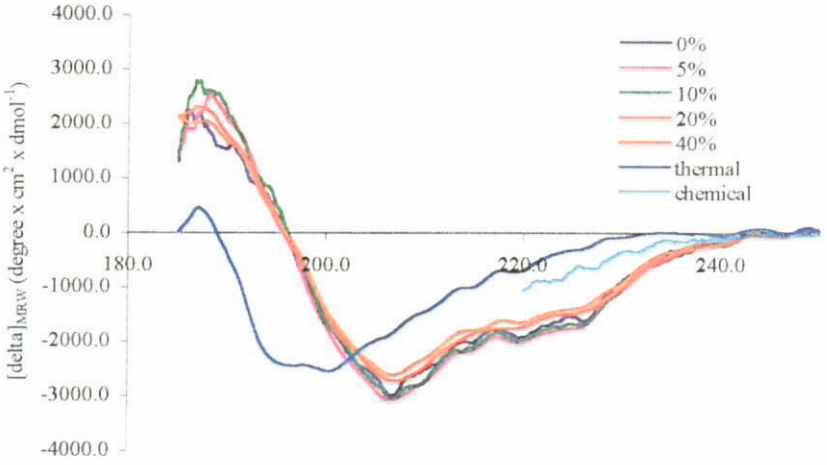

(b)

Figure 4.10 CD spectra of SB in far-UV region for different amplitude settings and treatment time at (a) 5min and (b) 10min.

Table 4.5 Contents of secondary structures of SB in the far-UV regions of CD spectra.

Secondary Structure*	Amplitude Setting					Thermal Treatment
	0%	5%	10%	20%	40%	
Treatment Time 5min						
α-helix	18.02±0.58	18.47±0.09	18.41±0.42	18.21±0.69	18.28±0.84	6.93±0.76
Anti-parallel β-sheet	25.97±1.16	24.08±0.34	24.61±0.19	24.59±1.04	25.20±0.66	31.23±1.15
Parallel β-sheet	1.83±0.33	1.71±0.20	2.04±0.28	2.17±0.59	1.42±0.63	0.00±0.00
β-turn	22.35±0.32	22.03±0.17	21.96±0.20	21.83±0.46	22.37±0.48	25.50±0.39
others	31.83±0.86	33.71±0.27	32.98±0.49	33.21±0.50	32.73±0.81	35.67±1.38
Treatment Time 10min						
α-helix	18.55±0.04	17.92±0.27	18.29±0.41	18.30±0.62	18.19±0.77	~
Anti-parallel β-sheet	25.04±0.57	24.79±0.25	24.37±0.40	24.52±1.36	25.38±0.34	~
Parallel β-sheet	1.04±0.14	2.00±0.22	2.47±0.59	2.23±0.29	1.52±0.29	~
β-turn	22.54±0.23	21.97±0.17	21.55±0.53	21.78±0.37	22.33±0.22	~
others	32.82±0.70	33.32±0.21	33.32±0.73	33.17±0.92	32.59±0.38	~

**The mean value of data in triplicates ± S.E.*

As referred to Table 4.5, the content of secondary structures of SB with or without ultrasound treatment were similar. The results revealed that secondary structures were not altered by ultrasound treatment. There were about 18% α-helix, 25% anti-parallel β-sheet, 2% parallel β-sheet, 22% β-turn and 32% other structures. After thermal treatment, the secondary structures of SB were lost especially for the α-helix structure, from 18.02% to 6.17%. Besides, a blue shift of the negative maximum was observed from 208nm to 198nm. On the contrary, the content of the parallel β-sheet was increased. The content of chemically treated SB could not be calculated as the denaturant GmHCl absorbed strongly under 220nm (Bloemendal & Johnson, 1995).

4.5.4 Surface Hydrophobicity Test

Since the hydrophobic core is to stabilize the conformations of a protein, any change of it could give information on protein stability. Figures 4.11a and 4.11b show the change in surface hydrophobicity (SH) of SB with various treatments. SB without treatment and with ultrasound treatment (amplitude setting of 5%) had similar SH about 760FI/mg/ml at 5min of treatment time. Slightly decrease in SH was found at amplitude settings of 10% (729.74FI/mg/ml) and 20% (718.4FI/mg/ml). The reduction was obviously at 40%, i.e. 508.51FI/mg/ml. At 10min of treatment time, SH decreased significantly at amplitude

setting of 20% (614.45FI/mg/ml) and 40% (299.81FI/mg/ml).

A largely drop of SH was found in chemically denatured SB, i.e. 89.08FImg/ml. The results suggested that the hydrophobic groups were exposed to the surface firstly and let them freely accessible to the solvent. The conformation of SB molecule would become relatively unstable that would further lead to the stacking of exposed hydrophobic groups together in order to obtain a stable conformation (Rumbo *et al.*, 1996). Moreover, the aromatic residue on the surface interacted with other hydrophobic groups and hence protein aggregation would be initiated. It made the assessment of hydrophobic groups become difficult. That could also be explained the results that SH decreased as ultrasound power increased.

On the contrary, SH increased up to 843.59FI/mg/ml for thermally denatured SB. According to Rumbo *et al.* (1996), the protein only unfolded partially and the hidden hydrophobic groups would be exposed for easy assessment.

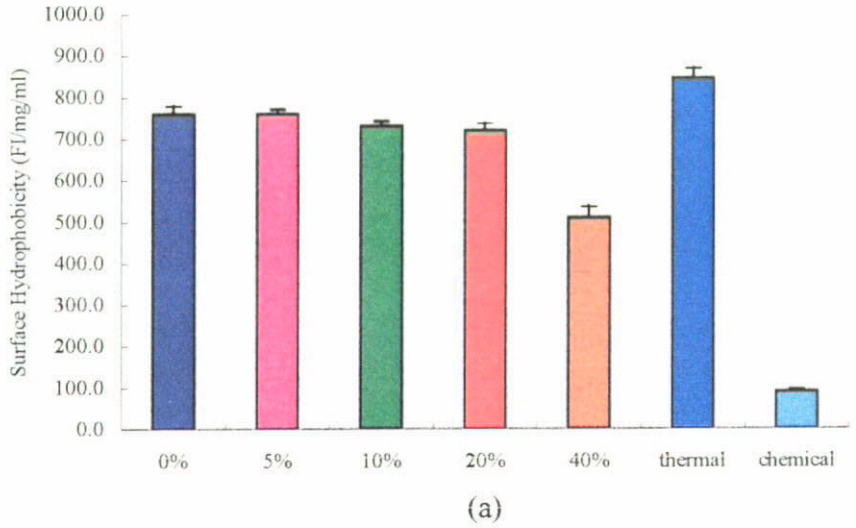

(a)

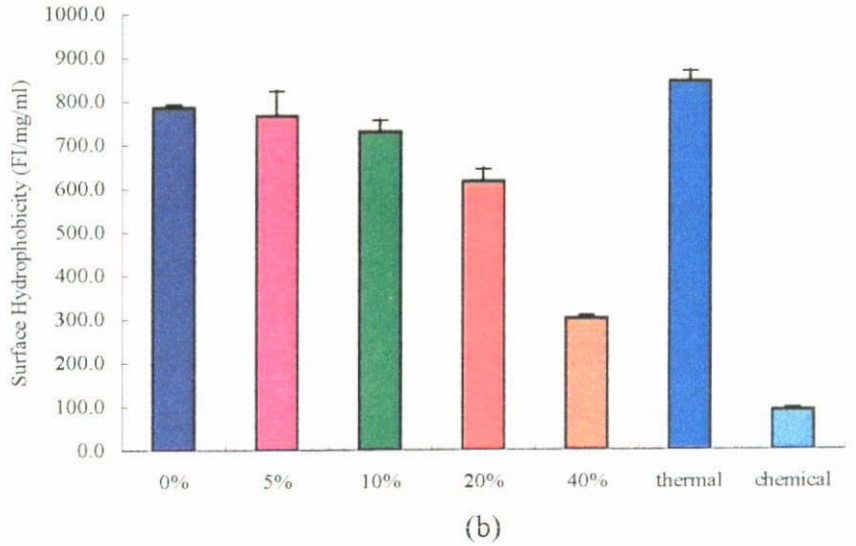

(b)

Figure 4.11 Change in surface hydrophobicity of SB for different amplitude settings and treatment time at (a) 5min and (b) 10min.

Chapter 5. Discussion

5.1 Ultrasound Mechanisms

Ultrasound could induce thermal, chemical, mechanical mixing and cavitation effects into the treated system and hence altered the catalytic activity of SB. The thermal effect of ultrasound to our system was eliminated as the experiments were performed in isothermal condition.

5.1.1 Chemical Effect

A very high temperature, which was generated during the transient cavitation of sonication, could dissociate the bonding of the molecules and hence produce free radicals (Frizzell, 1988). The production of free radicals ($H^{\cdot}$, $OH^{\cdot}$ and $O_2^{\cdot}$) and hydrogen peroxide (H_2O_2) from oxygenated water would alter the bonding in the molecules such as disulphur bonds (Sinisterra, 1992). These radicals did exert chemical effect on enzyme and substrate molecules.

As referred to the results of the SB activities with ultrasound pretreated SB or CLN

(Figure 4.6), ultrasound caused spontaneous hydrolysis of CLN because the enzyme activity increased directly with the ultrasound power when CLN was pretreated. As referred to Suslick (1988), due to the production of free radicals under ultrasound irradiation, amine form of substrate yields aldehydes, alcohols and hydrocarbons; while ester form of substrate gives acids and alcohols as the principle products. CLN as an organic amide substrate follows the same hydrolytic pathway like ester (Wong, 1995); therefore, it can be assumed that CLN followed the similar pathway as the ester attacking by free radicals. This attack favors the hydrolysis of CLN and hence more products were obtained.

However, this situation did not give any advantage to the SB-catalyzed reaction under ultrasound treatment because the key determinant on SB activity was the enzyme molecule. When SB was pretreated by ultrasound alone and then transferred to CLN solution immediately, the activity was promoted at amplitude setting of 5% and reduced at setting of 40%. At high power levels, temperatures and pressures inside the compressed bubbles were sufficient to produce free radicals that would denature the enzymes (Sala *et al.*, 1995).

5.1.2 Effect of Mechanical Mixing

It was suggested that ultrasound might exert a mixing effect on the SB-catalyzed reaction, which in turn enhanced the SB activity. According to the results of effect of mechanical stirring on SB-catalyzed reaction (Figure 4.5), mechanical stirring at low or high speeds could not induce any increase in SB activity at various CLN concentrations. However, the effect of ultrasound treatment on the reaction was different that the activity promoted at low power levels and then gradually decreased at high power levels. The results indicated that the effect of ultrasound on our system could not be fully explained by the mechanical stirring effect. Vulfson *et al.* (1991) demonstrated that ultrasound irradiation could enhance subtilisin activity as compared to mechanical stirring because it favored mass transfer of the reagents to the active site of the enzyme. It was also believed that ultrasound prevented water molecules accumulating on the enzyme surface that let more active sites available for substrate binding.

5.1.3 Effect of Cavitation

Both acoustic microstreaming and transient cavitation are considered as the core mechanism exerted by ultrasound treatment. Their occurrences are mainly determined by

the levels of ultrasound power. Acoustic microstreaming refers to the appearance of strong vibrated currents in confined regions of the sonicated medium, but no bubble or only tiny bubbles are observed. On the other hand, transient cavitation creates a great amount of bubbles which vary their sizes and collapse rapidly. There is a transition state between microstreaming and cavitation.

5.1.3.1 Low Ultrasound Power

The acoustic microstreaming induced by low ultrasound power enhanced the mixing of the enzyme (SB), substrate (CLN) and product (*p*-nitrophenol). The sample medium would become more homogenous. At a microscopic level, it also facilitated the diffusion of substrate to or product away from the active site of the enzyme (Sinisterra, 1992; Barton *et al.*, 1996; Mason *et al.*, 1996; Forment *et al.*, 1998).

Moreover, low ultrasound power also favored the 'lock and key' mechanism during enzyme and substrate binding. As referred to Table 4.2, V_{max} at amplitude setting of 5% was similar to that of without ultrasound, but its K_m was reduced about 50%. The results revealed that the apparent affinity between SB and CLN molecules was increased (Sakakibara *et al.*, 1996). Similar result was reported by Ishimori *et al.* (1981) who

demonstrated K_m of immobilized α-chymotrypsin under ultrasound irradiation was about 50% less than that without treatment.

Since the conformation of the enzyme including active site might be altered during the extraction process in which the enzyme was manufactured, thus the kinetic parameters were changed. Low ultrasound power could make minor conformational change in SB, that in turn would increase the flexibility of active site for CLN binding. As a result, the catalytic efficiency (k_{cat}/K_m) was increased. In 1998, Forment *et al.* explained this small increase in catalytic activity of butyrylcholinesterase was due to the faint conformational change altering the active site reactivity.

5.1.3.2 High Ultrasound Power

At high ultrasound power, vigorous cavitation was created in the sonicated medium and bubbles were oscillated irregularly together with localized increase in temperature and pressure. Such high power also reduces the enzymatic activity by alteration of the secondary structure of the enzyme (Sinisterra, 1992). Under such turbulent chaos, the conformation of SB would not be maintained anymore; hence the catalytic free sulfhydryl group in cysteine residue was destructed (Sala *et al.*, 1995). There was less "lock"

available for the 'lock and key' mechanism because the enzyme was denatured. As a result, both SB activity and catalytic efficiency (k_{cat}/K_m) were decreased.

5.2 Conformational Change of SB Induced by Ultrasound Treatment

5.2.1 Ultraviolet Absorption Spectrometry

The results of UV absorption spectrum show that ultrasound caused the conformational change relating to aromatic residues. A slightly blue shift in wavelengths could be observed from amplitude setting of 5% to 40% in comparison with SB without ultrasound. Such shifts were more pronounced for SB with either thermal or chemical treatment. It could be explained that some of the aromatic residues that were originally buried in the hydrophobic core of the folded native protein were exposed to the solvent during unfolding. During unfolding, the change in the magnitude of the absorbance depended strongly on the environment of the respective chromophores in the native protein (Schmid, 1997). Similar result was showed by Jackman & Yada (1989). They observed a blue shift and reduction of wavelength of UV absorption spectrum during preparation of whey-potato and whey-pea protein at pH 4 to 8.

5.2.2 Fluorescence Emission Spectrometry

The change of the chromophore towards its environment is sensitively detected by fluorescence emission rather that light absorbance. The fluorescence emission spectrometry is an excellent tool to investigate the conformational change of a protein. Both shifts in wavelength and changes in fluorescent intensity indicate protein unfolding (Schmid, 1997).

It is believed that the change in Trp residues was minimum because the change in fluorescence emission spectrum after ultrasound treatment was insignificant. The Trp residues might be buried deeply inside the central core that were difficult to expose for assessment. The results seemed to contradict the findings in UV absorption spectrum. Jackman and Yada (1989) also pointed out such contradiction in both spectra of whey-potato and whey-pea at pH 4 to 8. According to Owusu (1992), UV and fluorescence spectra are sensitive to different classes of Trp residues. There are two classes of Trp residues: high wavelength emitting groups (340-350nm) which assumed to be exposed, and low wavelength emitting groups (300-320) which assumed to be buried (Kronman & Robbins, 1970). Thus, these two spectra were attributed by different classes of aromatic residues.

The red shift in wavelength and increase in FI could be observed for SB in chemical denaturation. As referred to the fluorescence studies of glucose dehydrogenase, a red shift of maximum wavelength to about 360nm accompanied with an increase in FI were found at urea concentration above 2M to 8M (Mendoza-Hernandez *et al.*, 2000).

5.2.3 Circular Dichroism Spectrometry

The near UV region of CD spectrum was confirmed that the aromatic residues of SB were subjected to a different surrounding environment, especially for thermally and chemically denatured SB. The degree of denaturation could be indicated by the degree of zero-approach of this CD band (Schmid, 1997).

According to the findings of the far UV region, secondary structures of SB could not be affected by ultrasound. Significant change in this CD spectrum was found in thermally denatured SB that the wavelength was left shifted and the ellipticity was more approached to zero value in all wavelengths expect from 190 to 200nm. The same pattern of the spectrum was showed by Arroyo-Reyna and Hernandez-Arana (1995) who demonstrated the thermal denaturation of SB. The increase in the β-sheet structure of thermally denatured SB was attributed to the surrender of α-helix structure (Kato & Takagi, 1988).

5.2.4 Surface Hydrophobicity Test

After intensive ultrasound treatment, the hydrophobic amino acid residues that were usually buried in the interior of the molecules were gradually exposed (Kato & Nakai, 1980). The exposed hydrophobic groups of the denatured SB interacted with other hydrophobic groups to form a protein matrix that was stabilized by hydrophobic interactions and caused protein aggregation was initiated (Wagner & Anon, 1990; Marcone & Yada, 1995), that made the assessment of hydrophobic groups became difficult.

Surface hydrophobicity (SH) of SB increased after thermal treatment. Rumbo *et al.* (1996) found that SH of ovalbumin rise as treatment temperature increased because of unfolding the protein and exposing side chains hidden in the native structure.

5.3 Kinetic Model

Some assumptions had to be made in order to develop a hypothesis model of ultrasound induced enzyme kinetics. First, activation and inactivation followed the first-order kinetics. The Arrhenius equation (equation 3 in Section 2.4) was still valid at constant

temperature. Similar way as the replacement of activation energy with the activation volume and pressure (Ludikhuyze *et al.*, 1996), then the power and time could be incorporated into the equation and represented the activation energy. As a result, the activation energy is replaced as.

$$E_a = P_t * t_t \qquad (5)$$

where P_t is the activation power of the system (W/mol) which may have a similar kinetic significance as activation volume; t_t is the treatment time (s).

The revised first-order kinetic model equation is shown as the follows:

$$\frac{dA}{A} = \pm\frac{P_t}{RT} * dt_t \qquad (7)$$

Integration both sides of equation (7) give:

$$\ln\frac{A_a}{A_o} = \pm\frac{P_t}{RT} * \Delta t_t \qquad (8)$$

The activation power can be found as:

Activation $$P_{t,ac} = \frac{\ln A_a / A_o * RT}{\Delta t_t} \quad (9)$$

Inactivation $$P_{t,in} = -\frac{\ln A_a / A_o * RT}{\Delta t_t} \quad (10)$$

where $P_{t,ac}$ is the activation power of the system during activation(W/mol); $P_{t,in}$ is the activation power of the system during inactivation(W/mol); A_a is the activity with ultrasound treatment (μmol/min·mg); A_o is the activity without ultrasound treatment (μmol/min·mg); Δt_t is the treatment time (s); R is gas constant (8.314 J/mol·K); T is the temperature of the reaction (298K).

Table 5.1 shows that the activation power (P_t) changed during ultrasound treatment. The activation power is not kept at constant neither in activation nor inactivation. It is a function of treatment time that it deceases as the treatment time prolongs for all amplitude settings. It is difficult to correlate the activation power with ultrasound power. It is independent of ultrasound power and no function can be concluded.

Table 5.1 Activation power (P_t) found during ultrasound treatment at 960μM CLN.

Treatment	Amplitude Setting			
Time	5%	10%	20%	40%
$P_{t,ac}$ (W) in Activation				
1min	9.488	3.223	~	~
3min	3.142	1.098	~	~
5min	1.739	0.602	~	~
10min	0.766	0.288	~	~
$P_{t,in}$ (W) in Inactivation				
1min	~	~	8.703	21.119
3min	~	~	3.477	7.125
5min	~	~	2.008	4.300
10min	~	~	1.163	2.090

On the contrary, the product of activation power (P_t) and treatment time (Δt_t) is kept at constant for a given system (Table 5.2), which verified the replacement if the activation energy with the activation power and treatment time. The change in the activation power and treatment time is correlated, that P_t increases as Δt_t decreases.

Table 5.2 Product of the activation power (P_t) and treatment time (Δt_t) found during ultrasound treatment.

Treatment	Amplitude Setting			
Time	5%	10%	20%	40%
$P_{t,ac}$*Δt_t (J) in Activation				
1min	9.47	3.20	~	~
3min	9.24	3.06	~	~
5min	9.48	3.14	~	~
10min	9.42	3.28	~	~
$P_{t,in}$*Δt_t (J) in Inactivation				
1min	~	~	8.73	21.12
3min	~	~	9.09	21.37
5min	~	~	9.48	21.50
10min	~	~	10.50	21.37

During ultrasound treatment, both activation and inactivation mechanisms occur simultaneously. The activation and inactivation of the enzyme is depended on which one is dominated. Below 5% of amplitude setting, activation promoted as amplitude setting increased since microstreaming was favored at that stage. The activation was diminished at amplitude settings from 5% to 10%. For amplitude settings of 10% to 20%, inactivation was resulted and it was pronounced as the amplitude setting increased up to 40%. The transient cavitation was predominated at that stage. A critical power zone

should exist for the system. The zone is the transition state between microstreaming and transient cavitation. Activation and inactivation may occur before and after this zone respectively. This zone should be found by experiment. But, the experiment is difficult to carry out as the fine adjustment of amplitude setting in the system is hard to achieve. For our system, the critical power zone was found laid around the amplitude setting of 10% as shown in Figure 5.1 below:

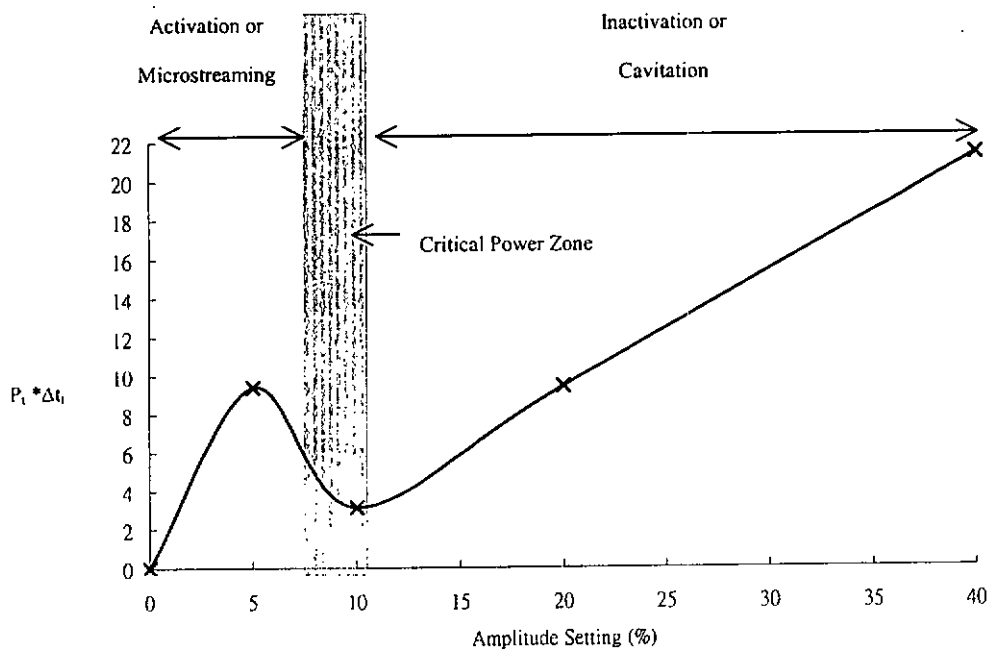

Figure 5.1 Product of the activation power (P_t) and treatment time (Δt_t) found during ultrasound treatment.

Chapter 6. Conclusion and Recommendation

6.1 Conclusion

During ultrasound treatment, energy was delivered from the probe to the medium in which part of it would be absorbed by the medium and the other would be lost to surroundings. Ultrasound power was constantly delivered from the probe. Energy absorption was affected by ultrasound amplitude and treatment time. It was well fitted to a second order polynomial equation with $R^2 > 0.992$.

Apart from mechanically mixing effect, ultrasound might exert the effect of acoustic microstreaming and transient cavitation to SB-catalyzed reaction. The experimental results showed that the SB activity was first promoted at low ultrasound power (amplitude setting <5%) and then gradually decreased at higher power levels (amplitude setting >20%). When the treatment time was less than 5min, the effect of ultrasound on SB activities were similar for the power level at amplitude settings of 30% and 40%. It was also found that at amplitude setting of 5% for 5min, the maximum catalytic activity of SB was about 25% higher than that without treatment, while its activity reduced by about 40% at amplitude setting of 40%. At lower ultrasound power, acoustic microstreaming was favored that facilitated the diffusion of substrate to or product away from the active site of the enzyme. It also enhanced the 'lock and key' mechanism during enzyme and substrate binding. Thus, the increase in the catalytic efficiency was double at amplitude range of 5% to 20%. At higher ultrasound power (amplitude setting of 40%), vigorous cavitation was

created in the sonicated medium that caused alteration of the enzyme's conformation resulting in a 50% decrease in the catalytic efficiency.

Ultrasound would alter both conformations of SB and CLN. But, the change of activity was greatly depended on the conformation change of SB rather than that of CLN. Therefore, only the conformation of SB molecule was analyzed. According to the results of thermally and chemically treated SB, ultraviolet absorption spectrometry, fluorescence emission spectrometry, circular dichroism spectrometry and surface hydrophobicity test were effective to determine the conformational change of SB.

The analytic results indicated that ultrasound induced only a minor conformational change of SB without varying its secondary structures. The major change was caused by the interaction between exposed aromatic residues, which were originally buried in the inner zone of the protein, and their surrounding environments. That altered only the tertiary structure. Moreover, ultrasound also reduced the surface hydrophobicity of SB. These effects were more severe at high ultrasound amplitude (40%). As a result, the activity and catalytic efficiency was dramatically decreased.

A hypothesis model for incorporating the effect of ultrasound into the enzyme kinetics was proposed by introducing the concept of activation power. This kinetic model suggested that the activation energy for the catalytic reaction could be replaced by the activation power and treatment time. A critical power zone should exist for a given system. Ultrasound activation and inactivation may occur before and after this zone respectively.

6.2 Recommendation

It is recommended to measure the change in localized temperature in sonicated medium. The effect of ultrasound on CLN hydrolysis should be confirmed. The detailed changes of the key residues arrangement in the protein molecule caused by ultrasound should be found. Moreover, the effect of ultrasound on activation energy of SB kinetics by conducting the experiment at different temperatures should be investigated. It is also suggested to extend the study of the effect of ultrasound on more hydrolytic enzymes, thus the generics of the kinetic model can be confirmed.

References

Arroyo-Reyna A.; Hernandez-Arana A. & Arreguin-Espinosa R. Circular dichroism of stem bromelain: a third spectral class within the family of cysteinie proteinases. *Biochemical Journal* **1994**, *300*, 107-110.

Arroyo-Reyna A. & Hernandez-Arana A. The thermal denaturation of stem bromelain is consistent with an irreversible two-state model. *Biochimica et Biophysica Acta* **1995**, *1248*, 123-128.

Azhar A. & Hamdy M. K. Sonication effect on potato starch and sweet potato powder. *Journal of Food Science* **1979**, *44*, 801-804.

Barton S.; Bullock C. & Weir D. The effects of ultrasound on the activities of some glycosidase enzymes of industrial importance. *Enzyme and Microbial Technology* **1996**, *18*, 190-194.

Belitz H. D. & Grosch W. *Food Chemistry*; Springer-Verlag Berlin Heidelberg: New York, 1999; pp76.

Beveridge T.; Toma S. J. & Nakai S. Determination of SH- and SS-groups in some food proteins using Ellman's reagent. *Journal of Food Science* **1974**, *39*, 49-51.

Bloemendal M. & Johnson W. C., Jr. Structural Information on Proteins from Circular Dichroism Spectroscopy Possibilities and Limitations. In *Physical Methods to Characterize Pharmaceutical Proteins*; James N. Herron *et al.*, Ed.; Plenum Press: New York, 1995; pp65-100.

Branden C. I. & Tooze J. *Introduction to protein structure*; 2nd Ed.; Garland Pulishing, Inc.: New York, 1999.

Budavari S.; O'Neil M. J.; Smith A. & Heckelman P. E. *The Merck Index: an encyclopedia of chemicals, drugs and biologicals*; Merck & Co., Inc.: USA, 1989; pp1382.

Burdock G. A. *Encyclopedia of Food and Color Additives*; CRC Press, Inc.: USA, 1997; pp299-300.

Cardamone M. & Puri N. K. Spectrofluorimetric assessment of the surface hydrophobicity of proteins. *Biochemical Journal* **1992**, *282*, 589-593.

Compton L. A. & Johnson W. C. Jr. Analysis of protein circular dichroism spectra for secondary structure using a simple matrix multiplication. *Analytical Biochemistry* **1986**, *155*, 155-167.

De Gennaro L.; Cavella S.; Romano R & Masi P. The use of ultrasound in food technology I: inactivation of peroxidase by themosonication. *Journal of Food Engineering* **1999**, *39*, 401-407.

Fersht A. The Basic Equations of Enzyme Kinetics. In *Structure and mechanism in protein science: a guide to enzyme catalysis and protein folding*; W. H. Freeman and Company: New York, 1998; pp98-120.

Frizzell L. A. Biological effects of acoustic cavitation. In *Ultrasounds: its chemical, physical and biological effects*; Suslick K. S., Ed.; VCH Pulishers: New York, 1988; pp287-303.

Froment M. T.; Lockridge O. & Masson P. Resistance of butyrylcholinesterase to inactivation by ultrasound: effects of ultrasound on catalytic activity and subunit association. *Biochimica et Biophysica Acta* **1998**, *1387*, 53-64.

Gallagher J.; Kanekanian A. D. & Evans E. P. Hydrolysis of casein: a comparative study of two proteases and their peptide maps. *International Journal of Food Science and Technology* **1994**, *29*, 279-285.

Goldenberg D. P. Analysis of protein conformation by gel electrophoresis. *In Protein Structure: A Practical Approach*; Creighton T. E., Ed.; Oxford University Press, Inc.: New York, 1997; pp 187-218.

Heinrikson R. L. & Kézdy F. J. Acidic cysteine protease inhibitors from pineapple stem. *In Methods in enzymology v.19, 45*; Lorand L., Ed.; 1976; pp740-742.

Ishimori Y.; Karube I. & Suzuki S. Acceleration of immobilized α-chymotrypsin activity with ultrasonic irradiation. *Journal of Molecular Catalysis* **1981**, *12*, 253-259.

Jackman R. L. & Yada R. Y. Ultraviolet absorption and fluorescence properties of whey-potato and whey-pea protein composition. *Canadian Institute of Food Science and Technology Journal* **1989**, *22(3)*, 252-259.

Jens A. N. *Enzymatic hydrolysis of food proteins*; 1986; pp1-20.

Kato A. & Nakai S. Hydrophobicity determined by a fluorescence probe method and its correlation with surface properties of proteins. *Biochimica et Biophysica Acta* **1980**, 624, 13-20.

Kronman M. J. & Robbins F. M. Buried and exposed groups in proteins. *In Fine Structure of Proteins and Nucleic Acids*; Fasman G. D. & Timasheff S. N. Ed.; Marcel Dekker, Inc.: New York, 1970; pp271.

Laidler K. J. The influence of pressure on the rates of biological reactions. *Arch. Biochemistry & Biophysics* **1951**, 30, 226-236

Lehninger A. L.; Nelson D. L. & Cox M. M. Enzymes. *In Principles of Biochemistry*; 2nd Ed.; Worth Pulishers, Inc.: New York, 1993; pp160-237.

Liang H. H.; Yang R. D. & Kwok K. C. Ultrasonic inactivation of soybean trypsin inhibitiors. *In Food Flavors: Formation, Analysis and Packaging Influences*; Contis E. T. *et al.*, Ed.; 1998; pp621-626.

Lodish H.; Berk A.; Zipursky S.; Maatsudaira P.; Baltimore D. and Darnell J. *Molecular and Cell Biology*; 4th Ed.; W. H. Freeman and Company, New York, 2000; pp87.

Ludikhuyze L.; De Cordt S.; Weemaes C.; Hendrickz M. and Tobback P. Kinetics for heat and pressure-temperature inactivation of *Bacillus subtilis* α-amylase. *Food Biotechnology* **1996,** 10(2), 105-129

Ludwig H. & Greulich K. O. Volume changes during enzyme reactions: the influence of pressure on the action of invertase, dextranase and dextransucrase . *Biophysical Chemistry* **1978,** 8, 163-169.

Mason T. J.; Paniwnyk L. & Lorimer J. P. The uses of ultrasound in food technology. *Ultrasonics Sonochemistry* ***1996,*** *3,* S253-S260.

Marcone M. F. & Yada R. Y. A proposed mechanism for the cryoaggregation of the seed storage globulin and its polymerized form from *Triticum aestivum. Journal of Food Biochemistry* ***1995,*** *18,* 147-163.

Mendoza-Hernandez G.; Miauro F. & Rendon J. L. Aggregation, dissociation and unfolding of glucose dehydrogenase during urea denaturation. *Biochimica et Biophysica Acta* ***2000,*** *1478,* 221-231.

Miller M. W.; Miller D. L. & Brayman A. A. A review of *in vitro* bioeffects of inertial ultransoinc cavitation from a mechanistic perspective. *Ultrasound in Medicine and Biology* ***1996,*** *22(9),* 1131-1154.

Minami Y.; Doi E. & Hata T. Fractionation, purification and some properties of proteolytic enzymes from stem bromelain. *Agricultural and Biological Chemistry* ***1971,*** *35(9),* 1419-1430.

Murachi T. Structure and function of stem bromelain. *In Proteins, structure and function (vol. 2)*; Funatsu M. *et al.*, Ed.; 1976; pp47-101.

Omar S.; Idrus A. Z. & Razak O. A. Extraction and activity of bromelain from pineapple. *Mardi Research bulletin* **1978,** *6(2),* 172-179.

Owusu R. K. The effect of calcium on bovine α-Lactalbumin conformational transitions by ultraviolet difference and fluorescence spectrophotometry. *Food Chemistry* **1992**, *43*, 41-45.

Perry R. H. & Chilton C. H. Chemical Engineers' Handbook (5th Ed.); McGraw-Hill, Inc.: New York, 1973.

Raabe E. & Knorr Dietrich. Kinetics of starch hydrolysis with *Bacillus amyloliquefaciens*-α-amylase under high hydrostatic pressure. *Starch* **1996**, 48, 409-414.

Ritonja A.; Rowan A. D.; Buttle D. J., Rawlings N. D.; Turk V. & Barrett A. J. Stem bromelain: amino acid sequence and implications for weak binding of cystatin. *FEBS-Letters* **1989**, *247(2)*, 419-424.

Rodger A. & Ismail M. A. Introduction to circular dichroism. In *Spectrophotometry and Spectrofluorimetry: a practical approach*; Gore M. G. Ed.; Oxford University Press Inc., New York, 2000; pp99-139.

Rowan A. D.; Buttle D. J. & Barrett A. J. Ananain: a novel cysteine proteinase found in pineapple stem. *Archives of Biochemistry & Biophysics* **1988**, *267(1)*, 262-270.

Rowan A. D.; Buttle D. J. & Barrett A. J. The cysteine proteinases of the pineapple plant. *Biochemical Journal* **1990**, *266*, 869-875.

Rumbo M.; Chirdo F. G.; Fossati C. A. & Anon M. C. Analysis of structural properties and immunochemical reactivity of heat-treated ovalbumin. *Journal of Agricultural and Food Chemistry* **1996**, *44*, 3793-3798.

Sala F. J.; Burgos J.; Condon S.; Lopez P. & Raso J. Effect of heat and ultrasound on microorganisms and enzymes. In *New Methods of Food Preservation*; Gould G. W., Ed.; Blackie Academic & Professional: London, 1995; pp177-204.

Sakakibara M.; Wang D.; Takahashi R.; Takahashi K. & Mori S. Influence of ultrasound irradiation on hydrolysis of sucrose catalyzed by invertase. *Enzyme and Microbial Technology* **1996**, *18*, 444-448.

Schmid F. X. Optical spectroscopy to characterize protein conformation and conformational changes. *In Protein Structure: A Practical Approach*; Creighton T. E., Ed.; Oxford University Press, Inc.: New York, 1997; pp 261-298.

Sinisterra J.V. Application of ultrasound to biotechnology: an overview. *Ultrasonics* **1992**, *30(3)*, 180-185.

Suslick K. S. Homogeneous Sonochemistry. In *Ultrasounds: its chemical, physical and biological effects*; Suslick K. S., Ed.: VCH Pulishers: New York, 1988; pp123-163.

Takahashi N.; Yasuda Y.; Goto K.; Miyake T. & Murachi T. Isolation and characterization of two closely related components, SB1 and SB2. *Journal of Biochemistry* **1973**, *74*, 355-373.

Takeda K.; Shigemura A.; Hamada S.; Gu W; Fang D.; Sasa K. & Hachiya K. Dependence of reaction rate of 5,5'-dithiobis-(2-nitrobenzoic acid) to free sulfhydryl groups of bovine serum albumin and ovalbumin on the protein conformations. *Journal of Protein Chemistry* **1992**, *11(2)*, 187-192.

Thomenius K. E. Estimation of the potential for bioeffects. In *Ultrasonic Exposimetry*; Ziskin M. C. & Lewin P. A., Ed.; CRC Press, Inc.: Florida, 1993; pp371-407.

Vercentt A.; Lopez P. & Burgos J. Inactivation of heat-resistant pectinmethylesterase from orange by manothermosonication. *Journal of Agricultural and Food Chemistry* **1999**, *47*, 432-437.

Vulfson E. N.; Sarney D. B. & Law B. A. Enhancement of subtilisin-catalyzed interesterification in organic solvents by ultrasound irradiation. *Enzyme and Microbial Technology* **1991**, *13*, 123-127.

Wade G. Human uses of ultrasound: ancient and modern. *Ultrasonics* ***2000***, *38*, 1-5.

Wagner J. R. & Anon M. C. Influence of denaturation, hydrophobicity and sulfhydryl content on solubility and water absorbing capacity of soy protein isolates. *Journal of Food Science* **1990**, *55(3)*, 765-770.

Whitaker J. R. & Bender M. L. Kinetics of papain-catalyzed hydrolysis of α-N-benzoyl-L-arginine ethyl ester and α-N-benzoyl-L-argininamide. *Journal of the American Chemical Society* **1965**, *87(12)*, 2728-2737.

Wong W. S. Proteolytic enzymes. In *Food Enzymes: Structure and Mechanism*; Chapman & Hall, New York, 1995; pp125-169.

Yamada F.; Takahashi N. & Murachi T. Purification and characterization of a proteinase from pineapple fruit, fruit bromelain FA2. *Journal of Biochemistry* **1976**, *79*, 1223-1234.

Zeffren E. & Hall P. A. Kinetics II. In *The Study of Enzyme Mechanisms*; John Wiley & Sons, Inc., New York, 1973; pp71-79.

Appendix A. Calculation of Ultrasound Power in the Experimental Media

The dimension of the sonicated chamber was shown as the follows:

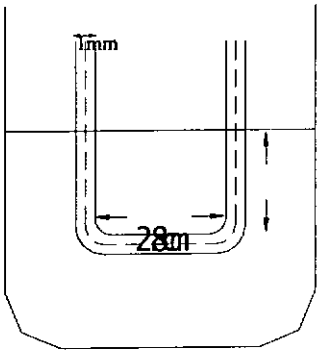

Energy absorbed by the media (E_1) was calculated by the following equation:

$$E_1 = c_p \cdot m \cdot \Delta T$$

where c_p was the specific heat capacity of the substance ($Jg^{-1}°C^{-1}$), m was the mass of the substance (g^{-1}) and ΔT was the change of temperature (°C).

Energy lost from the media (E_2) was calculated by the following equation:

$$E_2 = k \cdot A \cdot \frac{\Delta T}{\Delta x} \cdot \Delta t$$

where k was the thermal conductivity of the Pyrex glass (W/m.K), ΔT was the

temperature difference (K), Δx was the thickness of the Pyrex glass (m), A was the surface area of the sample container (m^2) and Δt was the treatment time (s).

Energy delivered from the probe (E_3) was calculated by the following equation.

$$E_3 = E_1 + E_2$$

Power delivered from the ultrasound system was calculated by the following equation.

$$Power \quad delivered = \frac{E_3}{\Delta t}$$

Appendix B. Calculation of Proteolytic Activity of SB

The concentration of product was calculated by the following equation.

$$c = \frac{A}{\varepsilon l}$$

where c was the concentration of the product (M), A was absorbance at 340nm, ε was the change in molar absorptivity of the substrate (Mcm^{-1}) and l was the pathlength (cm).

Proteolytic activity was determined as follows

$$PA = \frac{cV}{tw}$$

where PA was the proteolytic activity (μmol/mg.min), c was the concentration of the product (M), V was total assay volume(L), t was reaction time (min) and w was the weight of SB (mg).

Pao Yue-Kong Library
PolyU • Hong Kong

Appendix C. Calculation of CD Spectrum

$$[\Theta]_{MRW} = \frac{\Theta \times 100 \times MRW}{c \times l}$$

where $[\Theta]_{MRW}$ was the residue ellipticity (degrees cm^2dmol^{-1}); Θ was the measured ellipticity in degrees; c was the protein concentration in mg/ml; l was the pathlength in cm; MRW was the mean residue weight. The factor 100 was the conversion of the molar concentration to the $dmol/cm^3$ concentration unit.

In amide region

$\Theta = \Theta$ millidegree

MRW = 108 per amino acid residue

$c = 0.2$ mg/ml

$l = 0.1$ cm

$$[\Theta]_{MRW} = \frac{\Theta \times 10^{-3} \times 100 \times 108}{0.2 \times 0.1}$$

$$= \Theta \times 540$$

In aromatic region

$\Theta = \Theta$ millidegree

MRW = 108 per amino acid residue

$c = 0.4$ mg/ml

$l = 1$ cm

$$[\Theta]_{MRW} = \frac{\Theta \times 10^{-3} \times 100 \times 108}{0.4 \times 1}$$

$$= \Theta \times 27$$

The contents of the secondary structures were calculated by the dot product of the inverse vector for different secondary structures and the CD spectrum for SB.

All dot products of α-helix portions for all wavelengths in the amide region were to sum up to yield the fraction of α-helix. The percentage of α-helix was calculated as its fraction over the total content of secondary structures.

The generalized inverses for various secondary structures from 178 to 260nm at 2nm intervals ($\Delta\varepsilon^{-1} \times 10^3$).

wavelength	H	A	P	T	O
178	-0.04	-19.9	-18.87	-13.86	-41.99
180	3.01	-19.09	-13.41	-11.69	-25.26
182	2.2	-14.41	-7.02	-9.23	-12.23
184	-0.24	-8.7	-2.74	-7.08	-6.95
186	-2.69	-3.85	3.23	-5.54	0.58
188	-3.46	-0.85	8.3	-4.27	7.71
190	-3.64	1.39	9.13	-3.18	5.6
192	-4.94	2.54	3.16	-3.43	-12.74
194	-3.07	2.5	-4.25	-2.38	-28.45
196	-0.26	-0.2	-10.33	-2.31	-38.454
198	1.23	-5.6	-9.95	-4.42	-34.12
200	5.81	-12.13	1.58	-5.26	0.11
202	7.05	-17.61	9.8	-7.45	22.31
204	5.24	-17.98	14.15	-8.14	31.28
206	1.28	-16.01	13.66	-8.74	26.54
208	-3.68	-13.17	9.5	-9.58	11.68
210	-7.19	-9.93	3.89	-9.46	-4.19
212	-9.04	-7.64	-0.59	-9.06	-15.73
214	-10.28	-5.94	-3.04	-8.66	-22.15
216	-11.28	-4.25	-4.8	-8.1	-26.65
218	-12.56	-2.07	-6.21	-7.37	-30.98
220	-13.04	-0.27	-7.29	-6.43	-33.52
222	-13.21	1.87	-7.25	-5.11	-33.28
224	-13.52	3.2	-7.63	-4.48	-34.3
226	-13.05	3.24	-6.64	-4.27	-31.51
228	-11.7	3	-4.9	-3.79	-25.98
230	-9.33	1.59	-5.3	-3.57	-23.96
232	-7.25	1	-4.64	-2.93	-19.62
234	-5.95	1.17	-5.15	-2.23	-18.83
236	-4.83	0.96	-5.39	-1.89	-17.97
238	-3.78	0.68	-4.73	-1.57	-15.21
240	-2.91	0.4	-3.82	-1.33	-12.2
242	-1.98	0.04	-2.84	-1.08	-8.8
244	-0.97	-0.28	-1.99	-0.73	-5.53
246	-0.5	-0.27	-1.2	-0.46	-3.29
248	-0.04	-0.4	-0.26	-0.28	-0.69
250	0.15	-0.3	0.17	-0.11	0.54
252	0.02	-0.08	-0.04	-0.04	-0.07
254	-0.04	0.02	-0.12	-0.01	-0.31
256	-0.04	0.02	-0.12	-0.01	-0.31
258	-0.03	0	-0.09	-0.02	-0.24
260	-0.01	-0.05	0.01	-0.04	-0.03

Appendix D. Calculation of Surface Hydrophobicity (SH)

$$SH = \frac{FI_1 - FI_2}{c}$$

where SH was the surface hydrophobicity (ml/mg), FI_1 was FI with ANS, FI_2 was FI without ANS, c was the concentration of SB (mg/ml).

Appendix E. Calculation of Kinetic Parameters of SB

The Lineweaver-Burk equation defines as:

$$\frac{1}{V_o} = \frac{K_m}{V_{max}} \cdot \frac{1}{[S]} + \frac{1}{V_{max}}$$

For enzymes obeying the Michaelis-Menten relationship, a plot of $1/V_o$ versus $1/[S]$ yields a straight line which will have a slope of K_m/V_{max}, a y-intercept of $1/V_{max}$, and a x-intercept of $-1/K_m$.

The turnover number or catalytic constant, k_{cat} was calculated by the following equation.

$$k_{cat} = V_{max} \times 22828/1000$$

where the number 22828 is the molecular weight of SB;

the number 1000 is the conversion factor.

SB Activity **without ultrasound; 1, 3, 5min**

CLN (uM)	1/[s]	Activity(umol/min/mg)			1/v (a)	1/v (b)	1/v (c)
60	0.0167	0.747	0.772	0.759	1.339	1.295	1.318
120	0.0083	1.291	1.241	1.278	0.775	0.806	0.782
180	0.0056	1.519	1.595	1.570	0.658	0.627	0.637
240	0.0042	1.797	1.886	1.835	0.556	0.530	0.545
360	0.0028	1.987	2.025	1.975	0.503	0.494	0.506
480	0.0021	2.165	2.165	2.152	0.462	0.462	0.465

	(a)	(b)	(c)			
R^2	0.994	0.9962	0.9949			
slope	59.982	58.275	58.797			
y-intercept	0.3198	0.3179	0.3209			
x	-0.0053	-0.0055	-0.0055	Ave.	s.d.	s.e.
V_{max}	3.127	3.146	3.116	3.130	0.015	0.009
K_m (uM)	187.561	183.312	183.225	184.700	2.478	1.431
k_{cat} (min^{-1})	71.382	71.809	71.137	71.443	0.340	0.196
k_{cat}/K_m	0.381	0.392	0.388	0.387	0.006	0.003

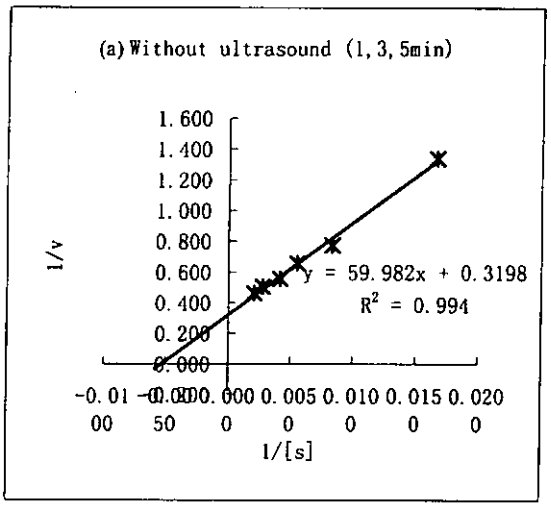

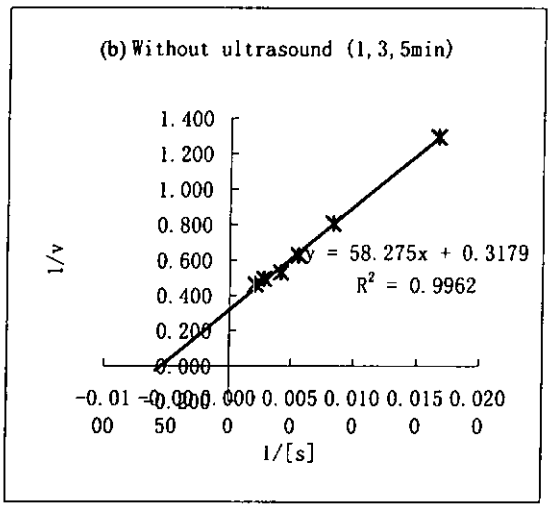

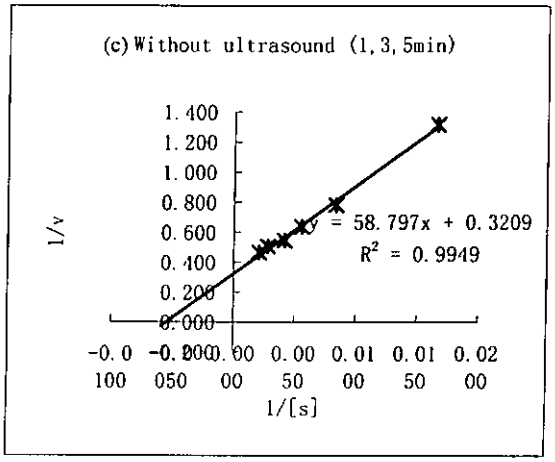

SB Activity **without ultrasound; 10min**

CLN (uM)	1/[s]	Activity(umol/min/mg)			1/v (a)	1/v (b)	1/v (c)
60	0.0167	0.589	0.627	0.608	1.698	1.595	1.645
120	0.0083	1.089	1.146	1.076	0.918	0.873	0.929
180	0.0056	1.443	1.335	1.367	0.693	0.749	0.732
240	0.0042	1.696	1.734	1.614	0.590	0.577	0.620
360	0.0028	1.905	1.905	1.899	0.525	0.525	0.527
480	0.0021	2.038	2.025	2.038	0.491	0.494	0.491

	(a)	(b)	(c)	Ave.	s.d.	s.e.
R^2	0.9917	0.9904	0.9975			
slope	84.141	76.239	79.808			
y-intercept	0.264	0.299	0.2972			
x	-0.0031	-0.0039	-0.0037			
V_{max}	3.788	3.344	3.365	3.499	0.250	0.145
K_m (uM)	318.716	254.980	268.533	280.743	33.576	19.385
k_{cat} (min^{-1})	86.470	76.348	76.810	79.876	5.715	3.300
k_{cat}/K_m	0.271	0.299	0.286	0.286	0.014	0.008

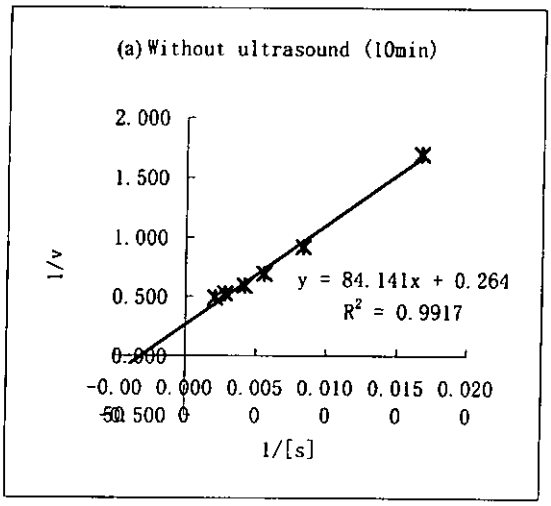

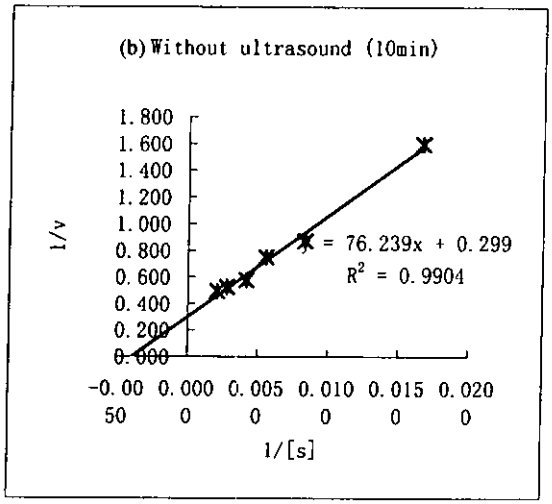

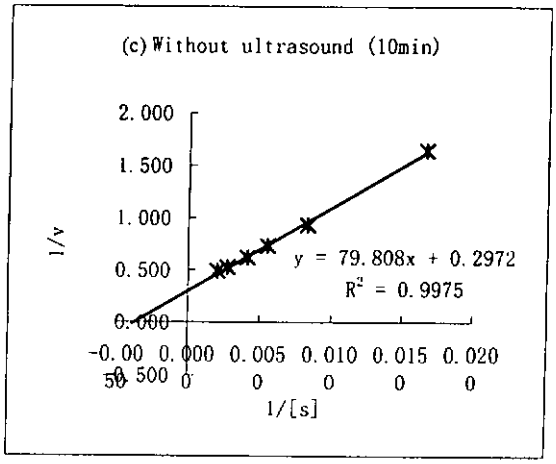

SB Activity **5%; 1min**

CLN (uM)	1/[s]	Activity(umol/min/mg)			1/v (a)	1/v (b)	1/v (c)
60	0.0167	1.177	1.215	1.190	0.850	0.823	0.840
120	0.0083	1.481	1.468	1.494	0.675	0.681	0.669
180	0.0056	1.924	1.886	1.835	0.520	0.530	0.545
240	0.0042	2.203	2.165	2.051	0.454	0.462	0.488
360	0.0028	2.646	2.709	2.747	0.378	0.369	0.364
480	0.0021	2.633	2.722	2.772	0.380	0.367	0.361

	(a)	(b)	(c)	Ave.	s.d.	s.e.
R^2	0.9532	0.924	0.9316			
slope	33.648	32.297	33.152			
y-intercept	0.3207	0.3257	0.3258			
x	-0.0095	-0.0101	-0.0098			
V_{max}	3.118	3.070	3.069	3.086	0.028	0.016
K_m (uM)	104.920	99.162	101.756	101.946	2.884	1.665
k_{cat} (min^{-1})	71.182	70.089	70.068	70.446	0.637	0.368
k_{cat}/K_m	0.678	0.707	0.689	0.691	0.014	0.008

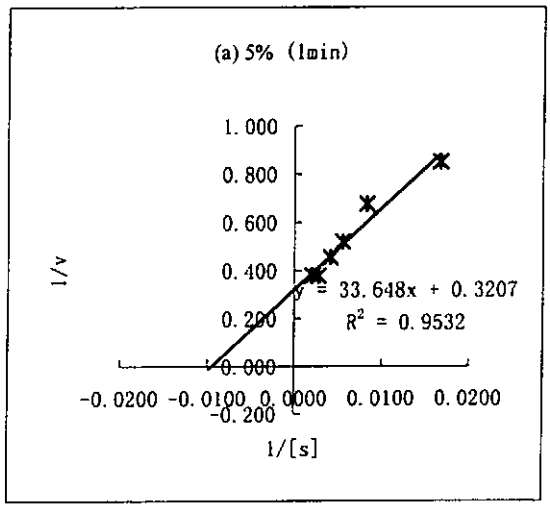

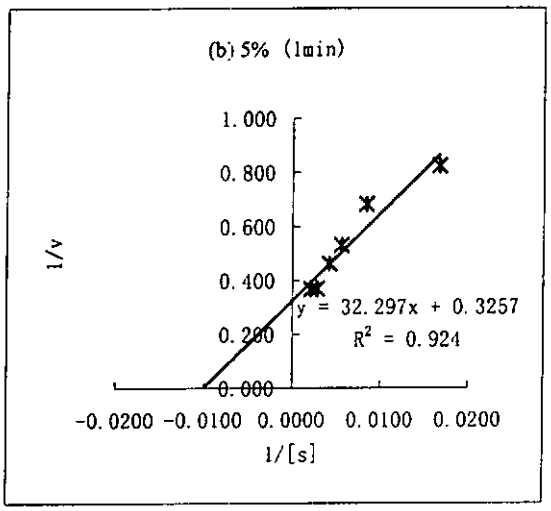

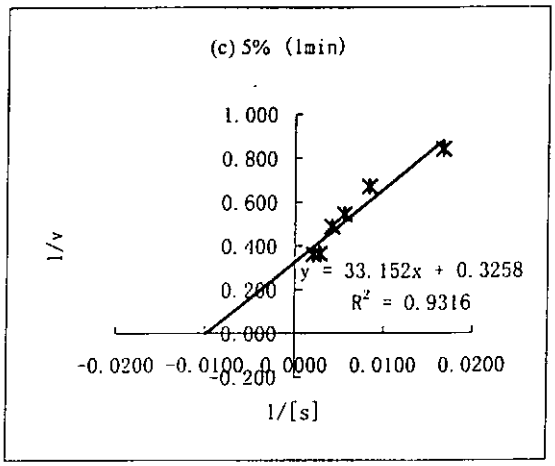

SB Activity **5%; 3min**

CLN (uM)	1/[s]	Activity(umol/min/mg)			1/v (a)	1/v (b)	1/v (c)
60	0.0167	1.177	1.203	1.177	0.850	0.831	0.850
120	0.0083	1.456	1.443	1.405	0.687	0.693	0.712
180	0.0056	1.911	1.848	1.861	0.523	0.541	0.537
240	0.0042	2.152	2.177	2.127	0.465	0.459	0.470
360	0.0028	2.734	2.797	2.696	0.366	0.358	0.371
480	0.0021	2.658	2.722	2.785	0.376	0.367	0.359

	(a)	(b)	(c)	Ave.	s.d.	s.e.
R^2	0.9383	0.911	0.9126			
slope	34.01	33.269	34.509			
y-intercept	0.32	0.3221	0.3221			
x	-0.0094	-0.0097	-0.0093			
V_{max}	3.125	3.105	3.105	3.111	0.012	0.007
K_m (uM)	106.281	103.288	107.138	105.569	2.021	1.167
k_{cat} (min^{-1})	71.338	70.872	70.872	71.027	0.269	0.155
k_{cat}/K_m	0.671	0.686	0.662	0.673	0.012	0.007

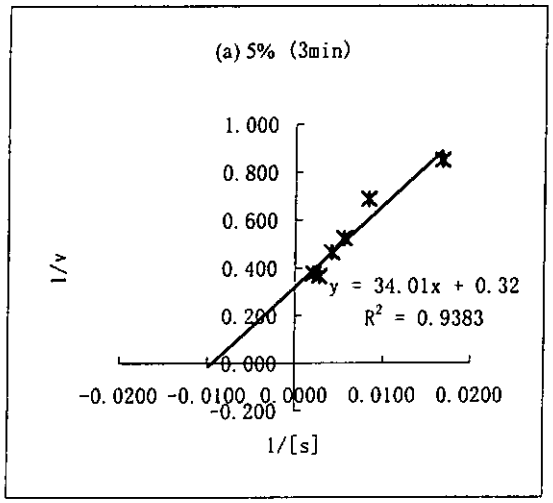

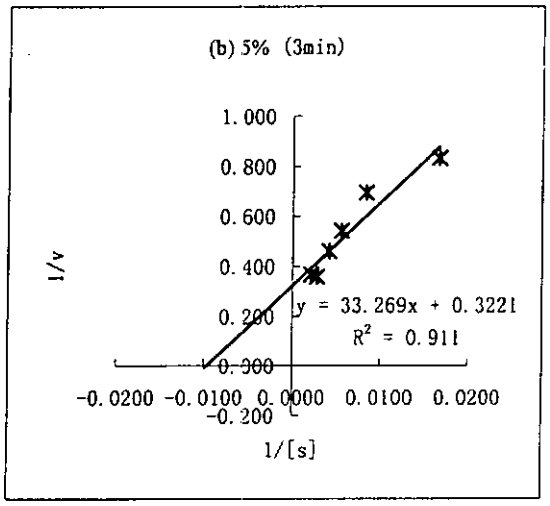

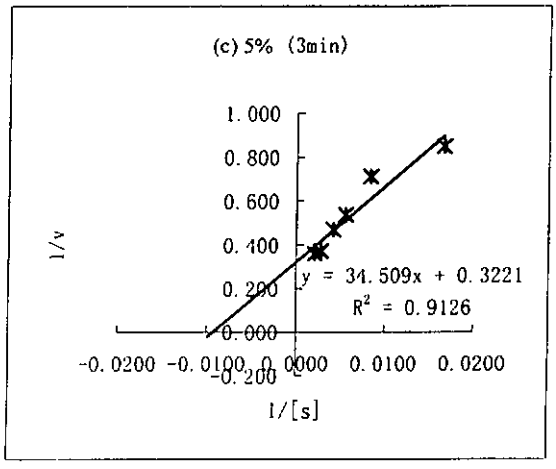

SB Activity **5%; 5min**

CLN (uM)	1/[s]	Activity(umol/min/mg)			1/v (a)	1/v (b)	1/v (c)
60	0.0167	1.203	1.228	1.177	0.831	0.814	0.850
120	0.0083	1.481	1.418	1.418	0.675	0.705	0.705
180	0.0056	1.899	1.848	1.937	0.527	0.541	0.516
240	0.0042	2.241	2.215	2.114	0.446	0.451	0.473
360	0.0028	2.759	2.785	2.722	0.362	0.359	0.367
480	0.0021	2.759	2.747	2.696	0.362	0.364	0.371

	(a)	(b)	(c)			
R^2	0.9336	0.8849	0.9222			
slope	33.403	32.444	34.261			
y-intercept	0.3137	0.3252	0.321			
x	-0.0094	-0.01	-0.0094	Ave.	s.d.	s.e.
V_{max}	3.188	3.075	3.115	3.126	0.057	0.033
K_m (uM)	106.481	99.766	106.732	104.326	3.951	2.281
k_{cat} (min^{-1})	72.770	70.197	71.115	71.361	1.304	0.753
k_{cat}/K_m	0.683	0.704	0.666	0.684	0.019	0.011

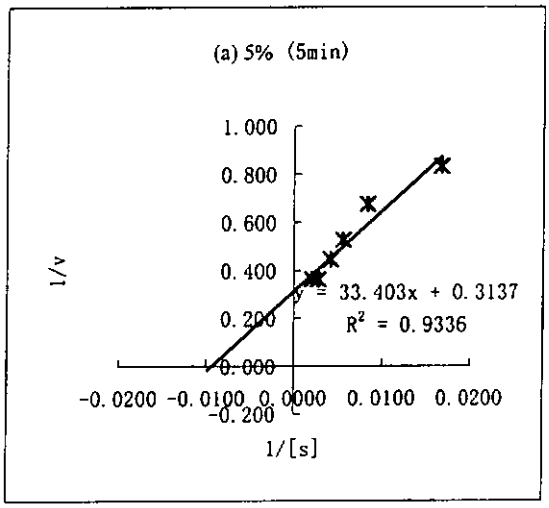

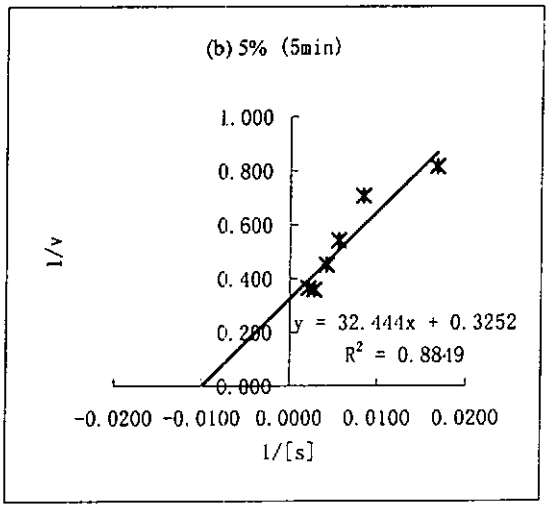

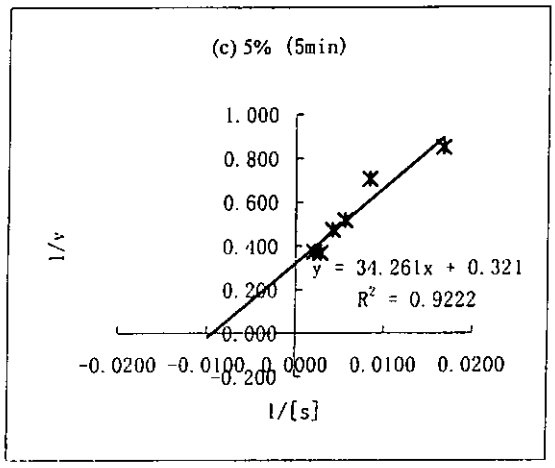

SB Activity **5%; 10min**

CLN (uM)	1/[s]	Activity(umol/min/mg)			1/v (a)	1/v (b)	1/v (c)
60	0.0167	0.829	0.861	0.861	1.206	1.161	1.161
120	0.0083	1.247	1.253	1.266	0.802	0.798	0.790
180	0.0056	1.589	1.741	1.696	0.629	0.574	0.590
240	0.0042	1.835	1.911	1.810	0.545	0.523	0.552
360	0.0028	2.462	2.462	2.430	0.406	0.406	0.412
480	0.0021	2.551	2.525	2.563	0.392	0.396	0.390

	(a)	(b)	(c)	Ave.	s.d.	s.e.
R^2	0.9888	0.9869	0.9868			
slope	56.283	53.78	53.131			
y-intercept	0.2921	0.2884	0.2987			
x	-0.0052	-0.0054	-0.0056			
V_{max}	3.423	3.467	3.348	3.413	0.060	0.035
K_m (uM)	192.684	186.477	177.874	185.678	7.437	4.294
k_{cat} (min^{-1})	78.151	79.154	76.425	77.910	1.381	0.797
k_{cat}/K_m	0.406	0.424	0.430	0.420	0.013	0.007

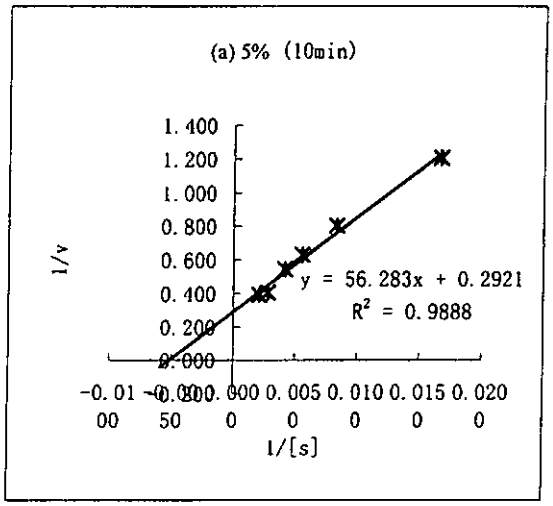

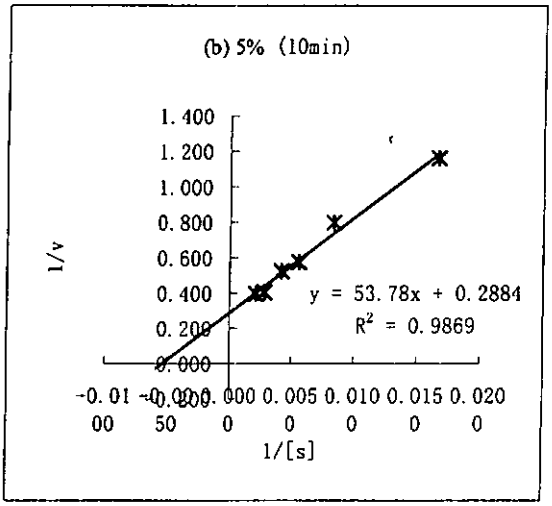

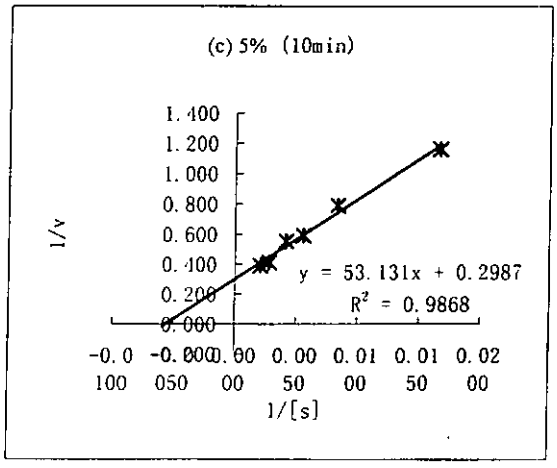

SB Activity **10%; 1min**

CLN (uM)	1/[s]	Activity(umol/min/mg)			1/v (a)	1/v (b)	1/v (c)
60	0.0167	1.127	1.076	1.051	0.887	0.929	0.951
120	0.0083	1.342	1.228	1.253	0.745	0.814	0.798
180	0.0056	1.734	1.620	1.709	0.577	0.617	0.585
240	0.0042	1.924	1.962	1.797	0.520	0.510	0.556
360	0.0028	2.443	2.316	2.215	0.409	0.432	0.451
480	0.0021	2.633	2.405	2.241	0.380	0.416	0.446

	(a)	(b)	(c)	Ave.	s.d.	s.e.
R^2	0.9097	0.8825	0.9257			
slope	34.753	36.649	35.977			
y-intercept	0.3571	0.3779	0.3941			
x	-0.0103	-0.0103	-0.011			
V_{max}	2.800	2.646	2.537	2.661	0.132	0.076
K_m (uM)	97.320	96.981	91.289	95.197	3.388	1.956
k_{cat} (min^{-1})	63.926	60.408	57.924	60.753	3.016	1.741
k_{cat}/K_m	0.657	0.623	0.635	0.638	0.017	0.010

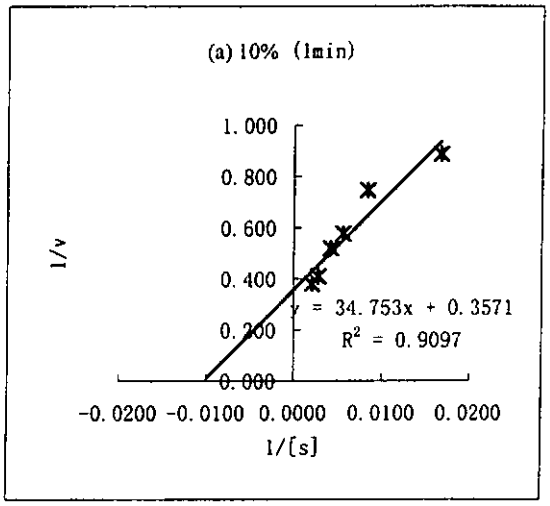

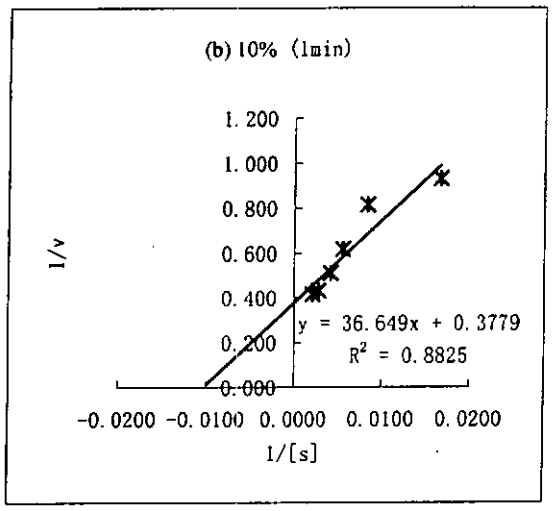

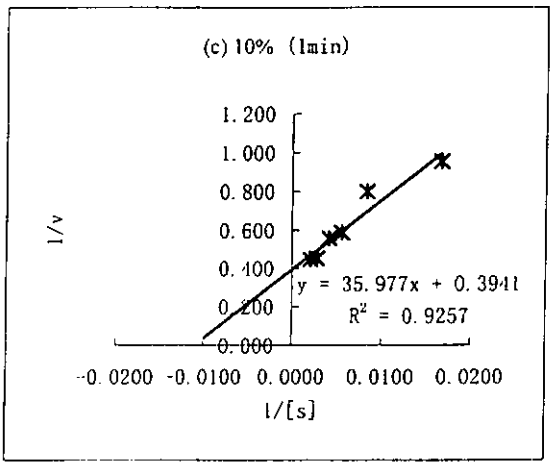

SB Activity **10%; 3min**

CLN (uM)	1/[s]	Activity(umol/min/mg)			1/v (a)	1/v (b)	1/v (c)
60	0.0167	1.139	1.139	1.076	0.878	0.878	0.929
120	0.0083	1.367	1.203	1.228	0.732	0.831	0.814
180	0.0056	1.759	1.696	1.633	0.569	0.590	0.612
240	0.0042	1.975	1.911	1.696	0.506	0.523	0.590
360	0.0028	2.532	2.278	2.190	0.395	0.439	0.457
480	0.0021	2.633	2.367	2.177	0.380	0.422	0.459

	(a)	(b)	(c)	Ave.	s.d.	s.e.
R^2	0.915	0.8203	0.8874			
slope	34.605	32.891	33.366			
y-intercept	0.3482	0.3969	0.4235			
x	-0.0101	-0.0121	-0.0127			
V_{max}	2.872	2.520	2.361	2.584	0.261	0.151
K_m (uM)	99.383	82.870	78.786	87.013	10.905	6.296
k_{cat} (min^{-1})	65.560	57.516	53.903	58.993	5.967	3.445
k_{cat}/K_m	0.660	0.694	0.684	0.679	0.018	0.010

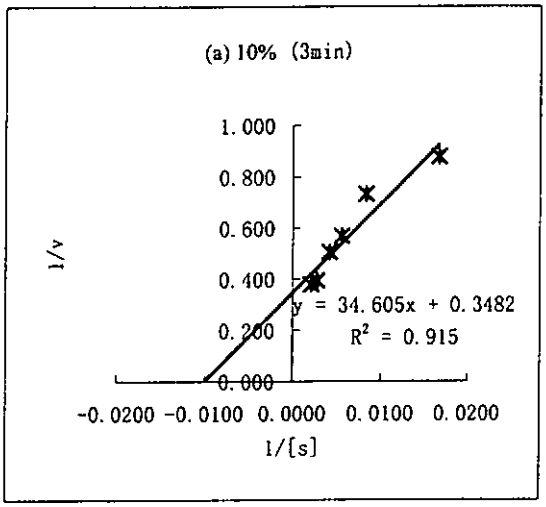

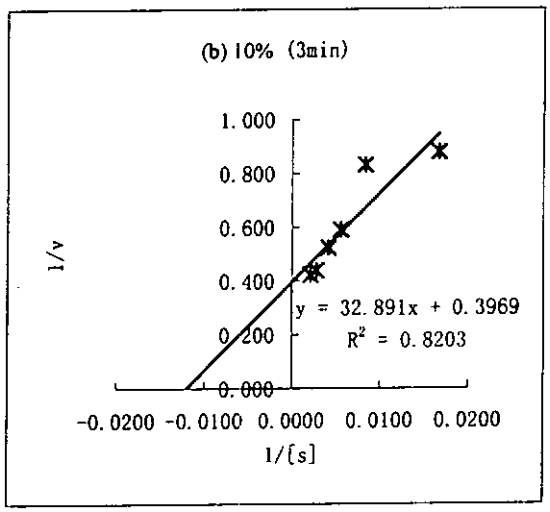

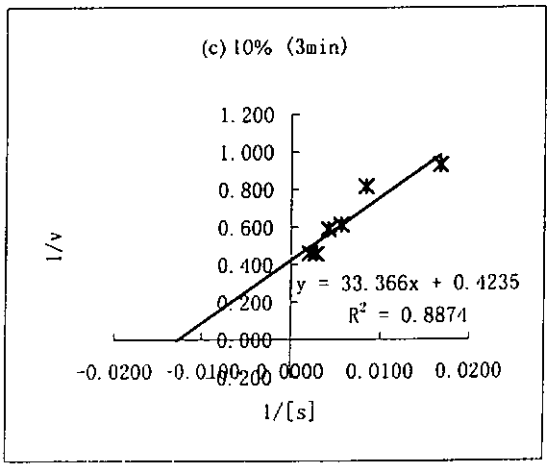

SB Activity **10%; 5min**

CLN (uM)	1/[s]	Activity(umol/min/mg)			1/v (a)	1/v (b)	1/v (c)
60	0.0167	1.114	1.114	1.089	0.898	0.898	0.918
120	0.0083	1.380	1.266	1.241	0.725	0.790	0.806
180	0.0056	1.696	1.759	1.658	0.590	0.569	0.603
240	0.0042	2.025	1.861	1.759	0.494	0.537	0.569
360	0.0028	2.582	2.329	2.177	0.387	0.429	0.459
480	0.0021	2.532	2.405	2.190	0.395	0.416	0.457

	(a)	(b)	(c)	Ave.	s.d.	s.e.
R^2	0.9277	0.8862	0.8941			
slope	35.669	34.129	32.93			
y-intercept	0.346	0.3813	0.418			
x	-0.0097	-0.0112	-0.0127			
V_{max}	2.890	2.623	2.392	2.635	0.249	0.144
K_m (uM)	103.090	89.507	78.780	90.459	12.183	7.034
k_{cat} (min^{-1})	65.977	59.869	54.612	60.153	5.688	3.284
k_{cat}/K_m	0.640	0.669	0.693	0.667	0.027	0.015

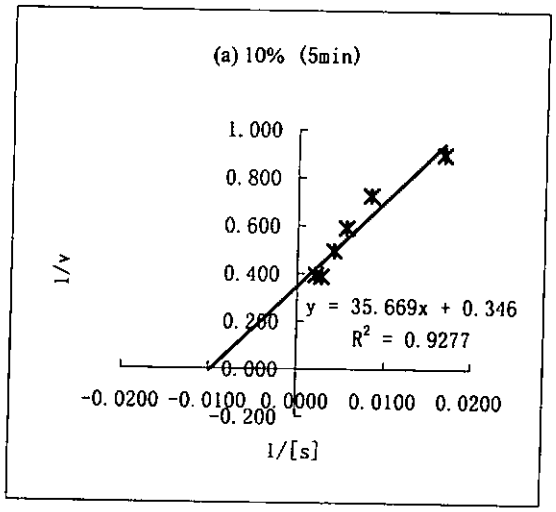

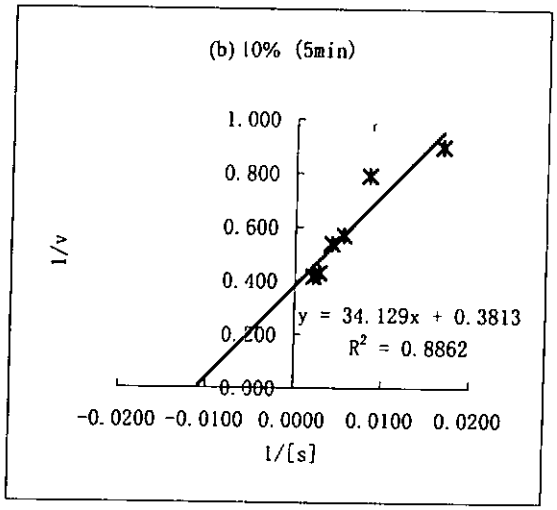

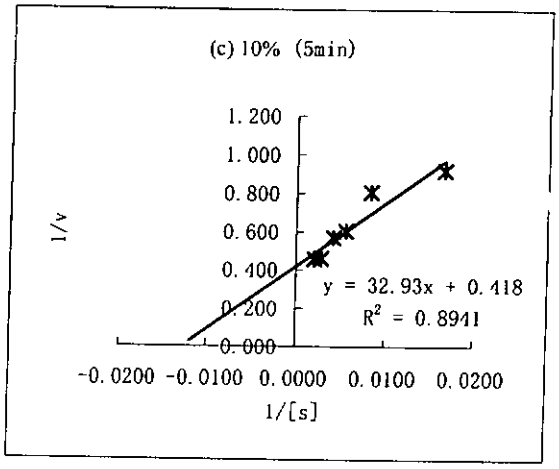

SB Activity **10%; 10min**

CLN (uM)	1/[s]	Activity(umol/min/mg)			1/v (a)	1/v (b)	1/v (c)
60	0.0167	0.823	0.810	0.797	1.215	1.235	1.255
120	0.0083	1.146	1.089	1.133	0.873	0.918	0.883
180	0.0056	1.462	1.519	1.443	0.684	0.658	0.693
240	0.0042	1.652	1.551	1.608	0.605	0.645	0.622
360	0.0028	2.114	2.063	2.038	0.473	0.485	0.491
480	0.0021	2.209	2.146	2.222	0.453	0.466	0.450

	(a)	(b)	(c)	Ave.	s.d.	s.e.
R^2	0.9797	0.9662	0.9843			
slope	52.718	53.415	54.846			
y-intercept	0.3693	0.382	0.3703			
x	-0.007	-0.0072	-0.0068			
V_{max}	2.708	2.618	2.701	2.675	0.050	0.029
K_m (uM)	142.751	139.830	148.112	143.564	4.201	2.425
k_{cat} (min^{-1})	61.814	59.759	61.647	61.074	1.141	0.659
k_{cat}/K_m	0.433	0.427	0.416	0.426	0.009	0.005

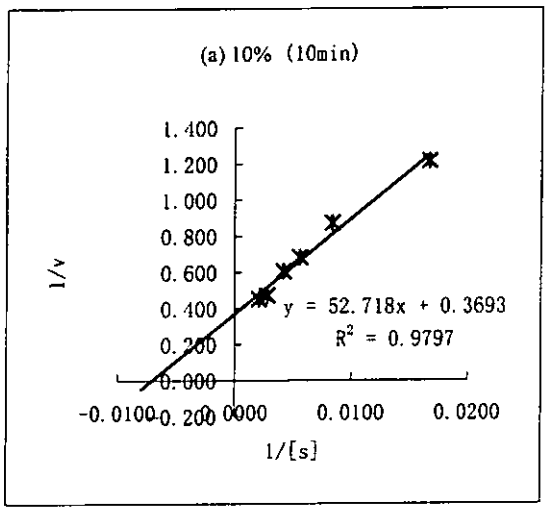

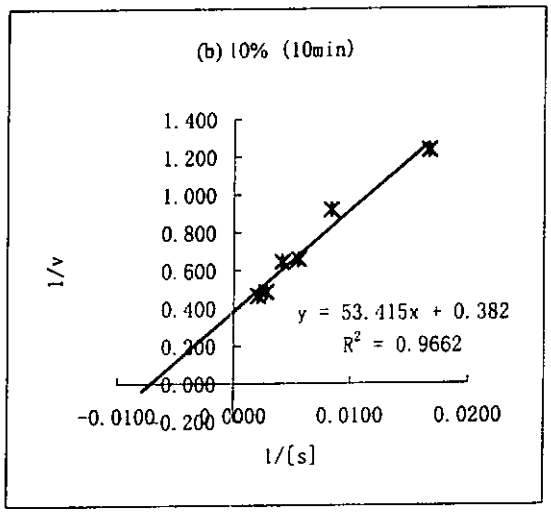

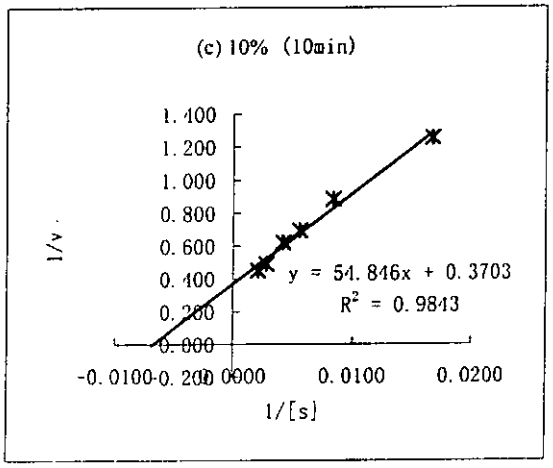

SB Activity **20%; 1min**

CLN (uM)	1/[s]	Activity(umol/min/mg)			1/v (a)	1/v (b)	1/v (c)
60	0.0167	0.911	0.937	0.975	1.098	1.067	1.026
120	0.0083	1.215	1.127	1.038	0.823	0.887	0.963
180	0.0056	1.462	1.405	1.354	0.684	0.712	0.739
240	0.0042	1.620	1.494	1.456	0.617	0.669	0.687
360	0.0028	2.127	1.899	1.646	0.470	0.527	0.608
480	0.0021	1.962	1.734	1.620	0.510	0.577	0.617

	(a)	(b)	(c)	Ave.	s.d.	s.e.
R^2	0.9662	0.9296	0.8457			
slope	42.175	36.24	30.436			
y-intercept	0.4221	0.5007	0.5724			
x	-0.01	-0.0138	-0.0188			
V_{max}	2.369	1.997	1.747	2.038	0.313	0.181
K_m (uM)	99.917	72.379	53.173	75.156	23.496	13.565
k_{cat} (min^{-1})	54.082	45.592	39.881	46.518	7.146	4.125
k_{cat}/K_m	0.541	0.630	0.750	0.640	0.105	0.060

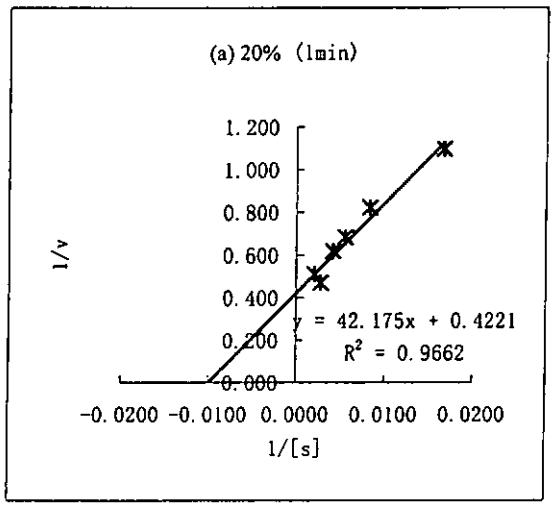

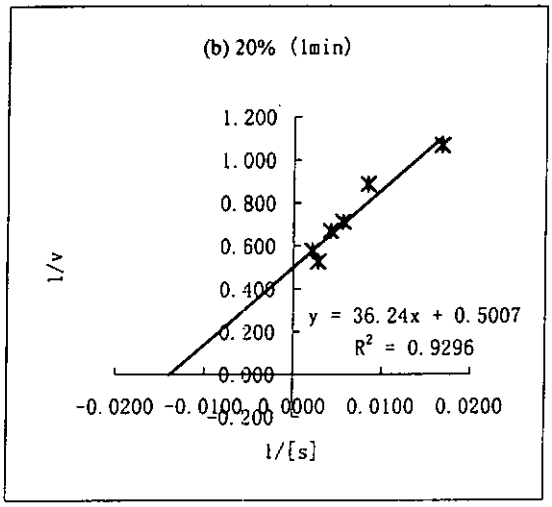

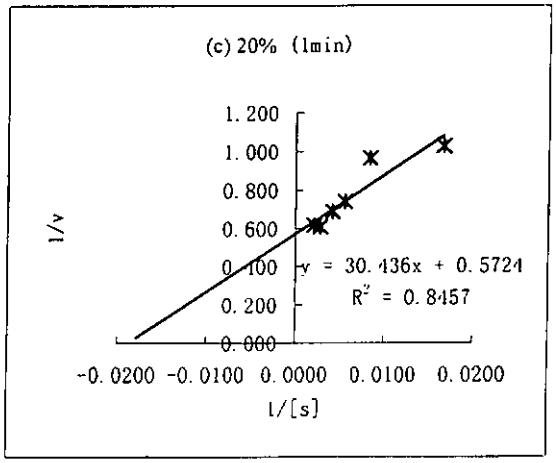

SB Activity **20%; 3min**

CLN (uM)	1/[s]	Activity(umol/min/mg)			1/v (a)	1/v (b)	1/v (c)
60	0.0167	0.924	0.924	0.911	1.082	1.082	1.098
120	0.0083	1.266	1.114	0.987	0.790	0.898	1.013
180	0.0056	1.519	1.443	1.304	0.658	0.693	0.767
240	0.0042	1.671	1.430	1.392	0.598	0.699	0.718
360	0.0028	2.177	1.734	1.481	0.459	0.577	0.675
480	0.0021	2.038	1.785	1.633	0.491	0.560	0.612

	(a)	(b)	(c)	Ave.	s.d.	s.e.
R^2	0.9762	0.9416	0.8654			
slope	42.083	36.232	33.643			
y-intercept	0.4022	0.5125	0.592			
x	-0.0096	-0.0141	-0.0176			
V_{max}	2.486	1.951	1.689	2.042	0.406	0.235
K_m (uM)	104.632	70.697	56.829	77.386	24.593	14.199
k_{cat} (min^{-1})	56.758	44.542	38.561	46.620	9.275	5.355
k_{cat}/K_m	0.542	0.630	0.679	0.617	0.069	0.040

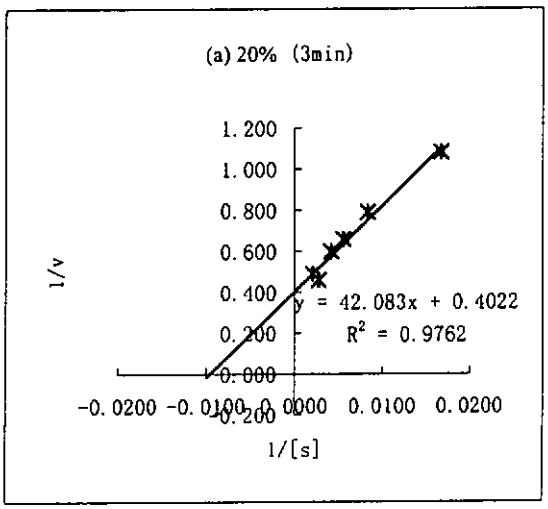

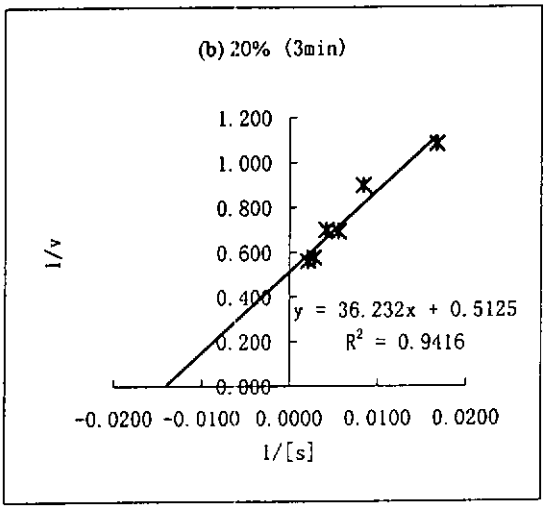

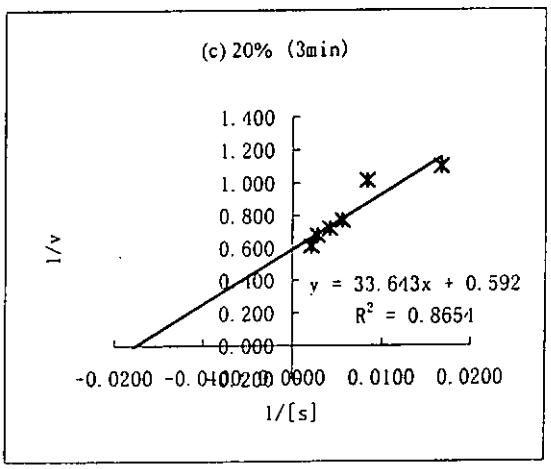

SB Activity **20%; 5min**

CLN (uM)	1/[s]	Activity(umol/min/mg)			1/v (a)	1/v (b)	1/v (c)
60	0.0167	0.949	0.949	0.924	1.054	1.054	1.082
120	0.0083	1.241	1.165	1.000	0.806	0.858	1.000
180	0.0056	1.335	1.405	1.304	0.749	0.712	0.767
240	0.0042	1.734	1.494	1.430	0.577	0.669	0.699
360	0.0028	2.165	1.747	1.418	0.462	0.572	0.705
480	0.0021	2.051	1.823	1.684	0.488	0.549	0.594

	(a)	(b)	(c)			
R^2	0.9207	0.9605	0.8509			
slope	40.055	34.641	32.53			
y-intercept	0.4249	0.5072	0.5933			
x	-0.0106	-0.0146	-0.0182	Ave.	s.d.	s.e.
V_{max}	2.353	1.972	1.685	2.004	0.335	0.193
K_m (uM)	94.269	68.299	54.829	72.466	20.048	11.575
k_{cat} (min^{-1})	53.726	45.008	38.476	45.737	7.651	4.417
k_{cat}/K_m	0.570	0.659	0.702	0.644	0.067	0.039

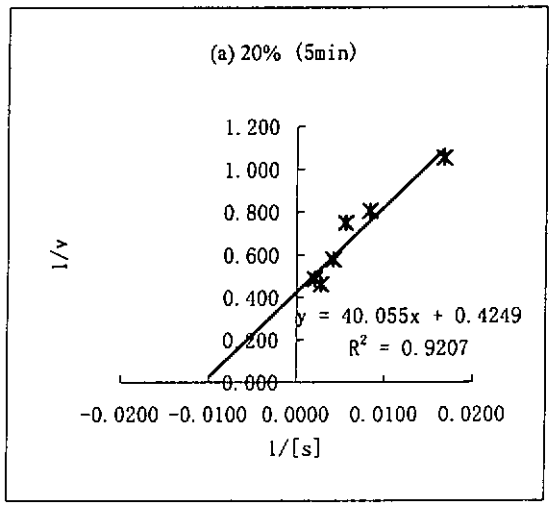

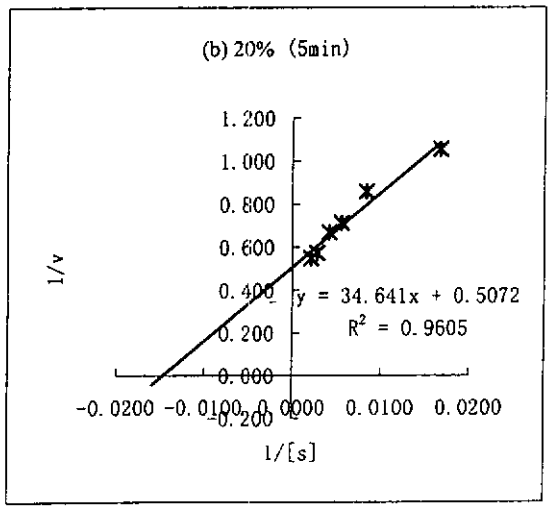

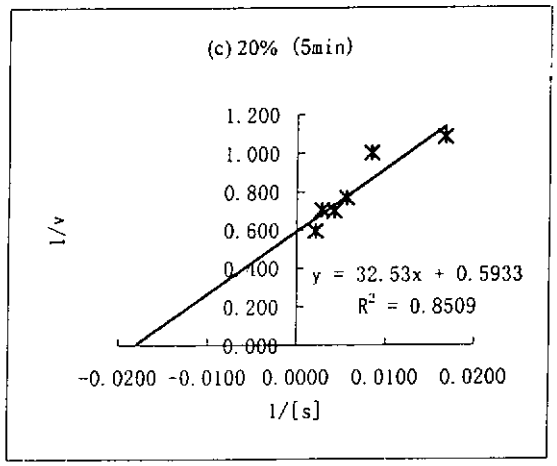

SB Activity **20%; 10min**

CLN (uM)	1/[s]	Activity(umol/min/mg)			1/v (a)	1/v (b)	1/v (c)
60	0.0167	0.709	0.728	0.690	1.410	1.374	1.449
120	0.0083	0.975	0.995	1.000	1.026	1.005	1.000
180	0.0056	1.297	1.278	1.348	0.771	0.782	0.742
240	0.0042	1.361	1.228	1.234	0.735	0.814	0.810
360	0.0028	1.848	1.620	1.513	0.541	0.617	0.661
480	0.0021	1.899	1.835	1.873	0.527	0.545	0.534

	(a)	(b)	(c)	Ave.	s.d.	s.e.
R^2	0.972	0.9609	0.9669			
slope	61.15	54.416	59.118			
y-intercept	0.4315	0.4973	0.476			
x	-0.0071	-0.0091	-0.0081			
V_{max}	2.317	2.011	2.101	2.143	0.158	0.091
K_m (uM)	141.715	109.423	124.197	125.112	16.165	9.333
k_{cat} (min^{-1})	52.904	45.904	47.958	48.922	3.598	2.077
k_{cat}/K_m	0.373	0.420	0.386	0.393	0.024	0.014

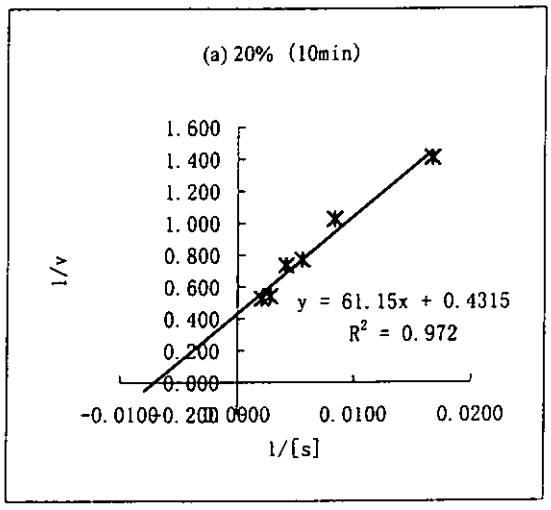

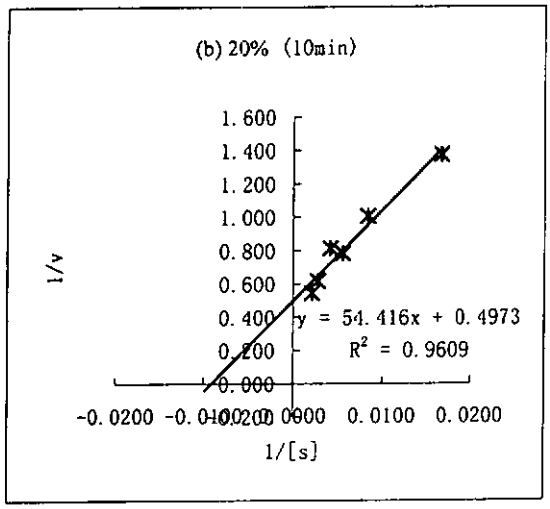

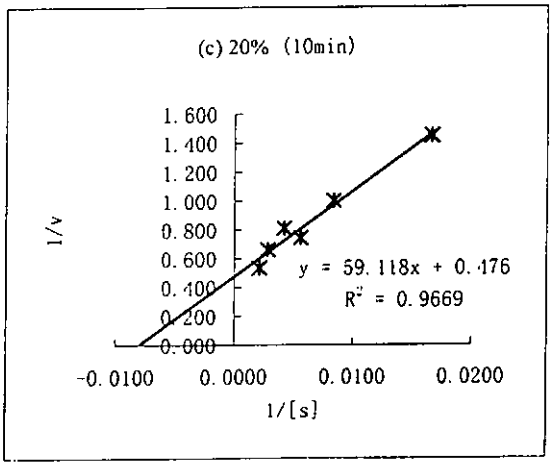

SB Activity **40%; 1min**

CLN (uM)	1/[s]	Activity(umol/min/mg)			1/v (a)	1/v (b)	1/v (c)
60	0.0167	0.418	0.456	0.443	2.392	2.193	2.257
120	0.0083	0.759	0.797	0.747	1.318	1.255	1.339
180	0.0056	1.063	1.000	1.051	0.941	1.000	0.951
240	0.0042	1.241	1.089	1.025	0.806	0.918	0.976
360	0.0028	1.152	1.190	1.253	0.868	0.840	0.798
480	0.0021	1.241	1.380	1.316	0.806	0.725	0.760

	(a)	(b)	(c)	Ave.	s.d.	s.e.
R^2	0.9657	0.9904	0.987			
slope	112.63	99.111	103.94			
y-intercept	0.4453	0.5013	0.4944			
x	-0.004	-0.0051	-0.0048			
V_{max}	2.246	1.995	2.023	2.088	0.138	0.079
K_m (uM)	252.931	197.708	210.235	220.291	28.952	16.716
k_{cat} (min^{-1})	51.264	45.538	46.173	47.658	3.139	1.812
k_{cat}/K_m	0.203	0.230	0.220	0.218	0.014	0.008

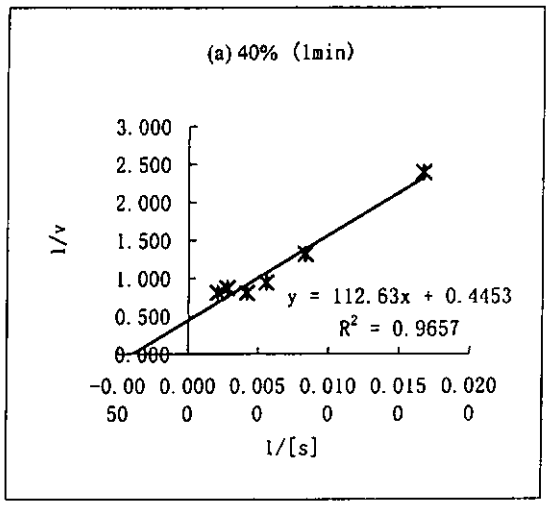

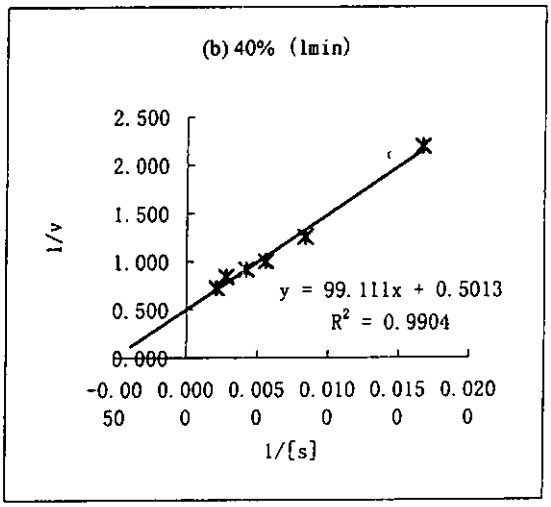

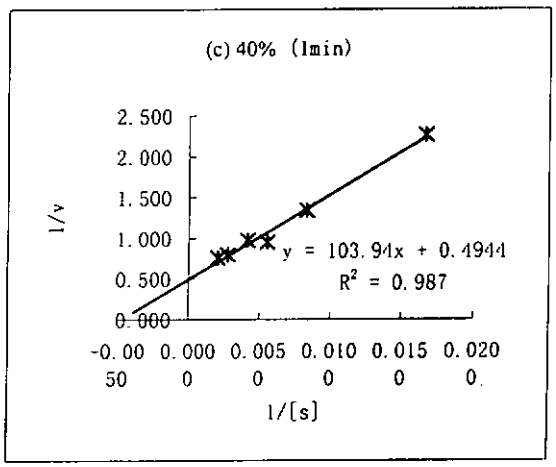

SB Activity **40%; 3min**

CLN (uM)	1/[s]	Activity(umol/min/mg)			1/v (a)	1/v (b)	1/v (c)
60	0.0167	0.468	0.430	0.443	2.137	2.326	2.257
120	0.0083	0.772	0.747	0.722	1.295	1.339	1.385
180	0.0056	1.025	1.076	1.101	0.976	0.929	0.908
240	0.0042	1.253	1.089	1.013	0.798	0.918	0.987
360	0.0028	1.139	1.215	1.266	0.878	0.823	0.790
480	0.0021	1.392	1.304	1.329	0.718	0.767	0.752

	(a)	(b)	(c)	Ave.	s.d.	s.e.
R^2	0.9804	0.9821	0.9797			
slope	97.105	108.88	105.05			
y-intercept	0.4931	0.4653	0.487			
x	-0.0051	-0.0043	-0.0046			
V_{max}	2.028	2.149	2.053	2.077	0.064	0.037
K_m (uM)	196.928	234.000	215.708	215.545	18.537	10.702
k_{cat} (min^{-1})	46.295	49.061	46.875	47.410	1.459	0.842
k_{cat}/K_m	0.235	0.210	0.217	0.221	0.013	0.008

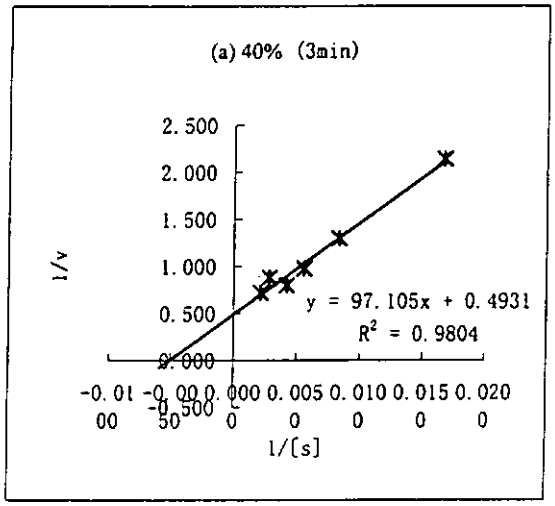

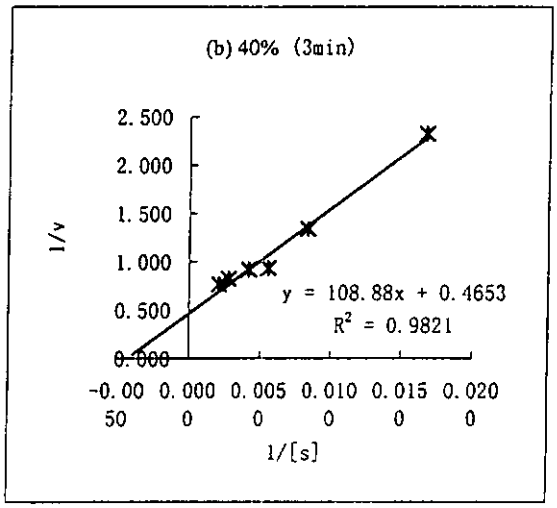

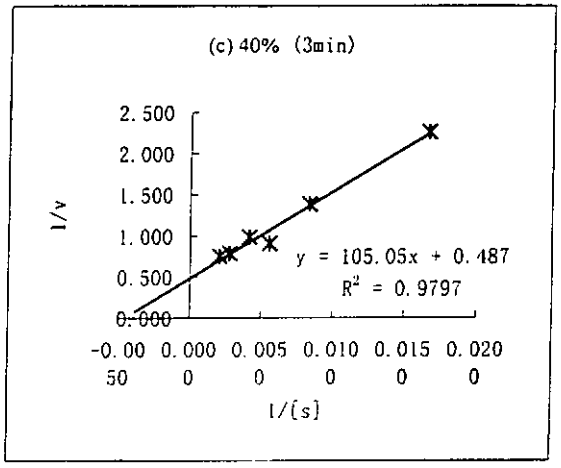

SB Activity **40%; 5min**

CLN (uM)	1/[s]	Activity(umol/min/mg)			1/v (a)	1/v (b)	1/v (c)
60	0.0167	0.481	0.456	0.430	2.079	2.193	2.326
120	0.0083	0.722	0.785	0.772	1.385	1.274	1.295
180	0.0056	1.025	1.013	1.127	0.976	0.987	0.887
240	0.0042	1.253	1.127	1.038	0.798	0.887	0.963
360	0.0028	1.266	1.241	1.177	0.790	0.806	0.850
480	0.0021	1.418	1.380	1.266	0.705	0.725	0.790

	(a)	(b)	(c)	Ave.	s.d.	s.e.
R^2	0.9849	0.9937	0.9657			
slope	96.9	100.85	106.51			
y-intercept	0.4829	0.48	0.4825			
x	-0.005	-0.0048	-0.0045			
V_{max}	2.071	2.083	2.073	2.076	0.007	0.004
K_m (uM)	200.663	210.104	220.746	210.504	10.048	5.801
k_{cat} (min^{-1})	47.273	47.558	47.312	47.381	0.155	0.089
k_{cat}/K_m	0.236	0.226	0.214	0.225	0.011	0.006

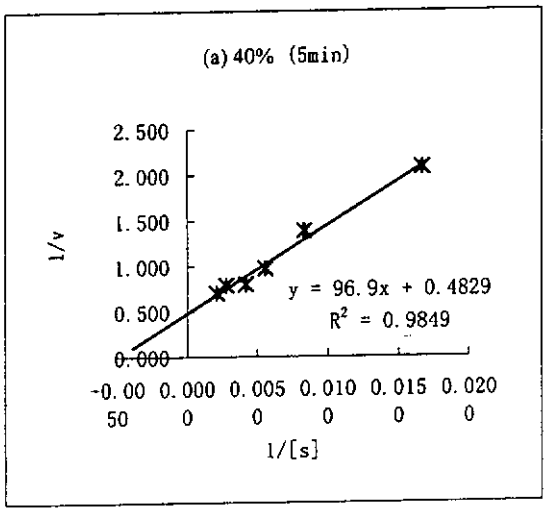

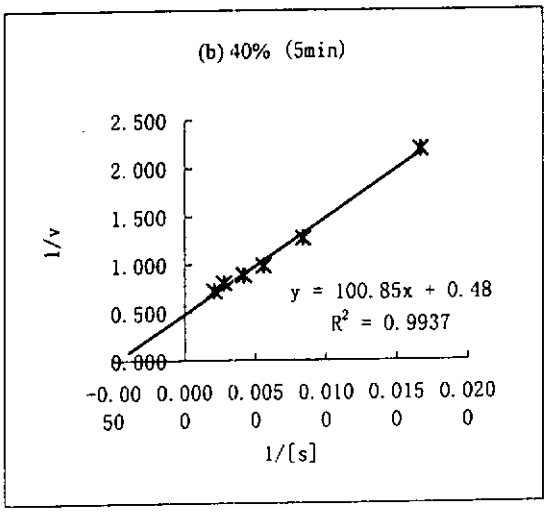

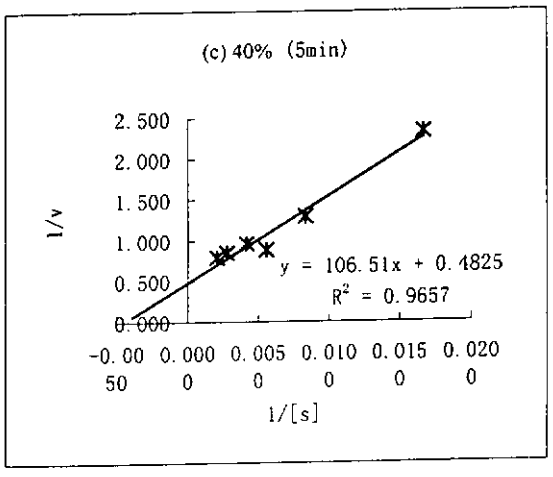

SB Activity **40%; 10min**

CLN (uM)	1/[s]	Activity(umol/min/mg)			1/v (a)	1/v (b)	1/v (c)
60	0.0167	0.297	0.310	0.335	3.367	3.226	2.985
120	0.0083	0.652	0.633	0.671	1.534	1.580	1.490
180	0.0056	0.949	0.937	0.968	1.054	1.067	1.033
240	0.0042	1.057	1.019	0.956	0.946	0.981	1.046
360	0.0028	1.297	1.297	1.266	0.771	0.771	0.790
480	0.0021	1.386	1.411	1.285	0.722	0.709	0.778

	(a)	(b)	(c)	Ave.	s.d.	s.e.
R^2	0.9803	0.9884	0.9805			
slope	184.25	174.8	153.71			
y-intercept	0.1833	0.2358	0.3397			
x	-0.001	-0.0013	-0.0022			
V_{max}	5.456	4.241	2.944	4.213	1.256	0.725
K_m (uM)	1005.18	741.306	452.487	732.992	276.441	159.604
k_{cat} (min^{-1})	124.539	96.811	67.200	96.183	28.674	16.555
k_{cat}/K_m	0.124	0.131	0.149	0.134	0.013	0.007